Imperial College London

Imperial College London

Department of Life Sciences

Thesis submitted in partial fulfilment of the requirements for the degree of Doctor in Philosophy

# Engineering the Membrane Rotor Ring of ATP synthases involved in Photosynthesis

*Author:*
Anthony Cheuk

*Supervisors:*
Prof. Dr. Thomas Meier
& Prof. Dr. Peter Nixon

2023

## Statement of Originality

I, Anthony Cheuk, declare that this work is my own, conducted under the supervision of Prof. Thomas Meier and Prof. Peter Nixon, and that all else is appropriately referenced.

## Copyright Declaration



## Acknowledgements

Firstly, I would like to thank my supervisors, Thomas Meier and Peter Nixon, for the opportunity to research the most fascinating of ancient enzymes and for their support and mentorship throughout. Lab members from both TM and PN labs, past and present, have taught me a great deal and I miss working with them all. I feel very privileged to have worked with and to have seen a complete turnover of the TM lab from Julius, Lisa, Michael, Mong Sing, Craig and Yilmaz when I first started through to the current team of Julia, Ben and Jim. In particular, I would like to thank Julia for all her support with cyanobacterial culturing, biochemical assays and the many polyacrylamide gels she prepared for me. I am also grateful to Ben for all his help with the *cryo*EM side of the project; the many late evenings he spent preparing grids, operating the microscopes and processing

the data were essential for this project.

I must also thank Nora Cronin and Paul Simpson for managing the LonCEM and Imperial CSB electron microscopy facilities, respectively. Thanks to my personal review panel, Morgan Beeby and Bill Rutherford, for their insightful discussions and advice during my early stage assessment and late stage review. I would like to thank Artur Włodarcyzk and Tiago Selão for their guidance with the CRISPR transformation of *Synechococcus sp.* PCC 7002; together with Lifang and Birgitta, they made me feel very welcome during my research visit to Nanyang Technological University.

# Engineering the membrane rotor ring of ATP synthases involved in Photosynthesis

## Abstract

The F-type ATP synthase is a macromolecular machine capable of coupling the proton-motive force with the synthesis of adenosine triphosphate, ATP, the universal energy currency in biology. A key component of the ATP synthase machinery is the $c_n$-ring with a stoichiometry that is constant within a given species but varies across different species, presumably due to the different bioenergetic demands placed on an organism in various environments. The $c_n$-ring stoichiometries of F-type ATP synthases involved in the light dependent reactions of photosynthesis are among the largest known, ranging from $c_{13}$ to $c_{15}$-rings. The recent increase in availability of genome-editing tools paves the way for investigating the importance of large $c_n$-rings for photosynthesis.

In this study, CRISPR-Cas12a genome editing is used to alter the stoichiometry of the $c_n$-ring of the F-type ATP synthase found in the model cyanobacterium, *Synechococcus sp.* PCC 7002, by replacing the endogenous *c*-subunit gene, *atpE*, with the *atpE* gene from *Spirulina platensis* which natively possess a $c_{15}$-ring. The native stoichiometry of the *Synechococcus sp.* PCC 7002 $c_n$-ring was unknown but suspected to be in the range of 13 to 15 subunits. Electron *cryo*-microscopy was used to identify a native $c_{14}$-ring stoichiometry in the wild-type organism and later confirm the formation of a chimeric F-type ATP synthase possessing all the native subunits of the *Synechococcus sp.* PCC 7002 enzyme with the exception of a $c_{15}$-ring from *Spirulina platensis*. Functional comparisons between prepared spheroplasts of the wild-type and mutant strains showed a decreased ATP synthesis rate under high light for the mutant. Furthermore, the mutant strain showed improved growth in alkaline media. These findings highlight the potential for targeting $c_n$-ring stoichiometries to improve photosynthesis.

# Table of Contents

# List of Figures

# List of Tables

# Chapter 1

# Introduction

## 1.1 Bioenergetics

All living organisms on Earth are a complex collection of biochemical reactions and these reactions require energy. As a discipline, bioenergetics emerged from the desire to understand how energy could be made available to living organisms. Bioenergetics aims to unveil the complex mechanisms that take light energy or energy released from the oxidation of substrates and couples it to thermodynamically unfavourable reactions such as the movement of ions across membranes against electrochemical gradients. The coupling of an electrochemical gradient across a membrane to the synthesis of adenosine 5'-triphosphate (ATP) is known as the chemiosmotic theory and lies at the core of bioenergetics (Mitchell 1961). The chemiosmotic theory relies on the presence of membranes with two distinct ion pumps. The first pump establishes a proton gradient by using an energy source to pump protons across the membranes, in mitochondria and respiring bacteria this energy is sourced from an electron transport chain while in pho-

tosynthetic organisms light energy is exploited. The second ion pump uses the energy stored in the form of an ion gradient to make ATP.

ATP is the universal energy currency in biology. The exergonic cleavage of the anhydride bond between the second and third phosphates gives ADP and a free phosphate and releases energy that can be coupled to a wide variety of cellular processes (Fig. 1.1). A few notable examples include anabolic/catabolic reactions, ion transport and mechanical work. The biochemical properties of ATP make it a suitable short-term energy carrier in biology as enzymes can easily catalyse the hydrolysis of the anhydride bond but in the absence of the correct enzymes, hydrolysis of this anhydride bond is chemically slow. The energy released from the hydrolysis of ATP is considerably high ($\Delta G^{0'}$ = -32.3 kJ/mol) and can be even greater under cellular conditions ($\Delta G^{0} \sim$ -50 kJ/mol). Owing to the many essential uses of ATP, the average human body consumes its body weight in ATP every single day (Phillips and Milo 2009).

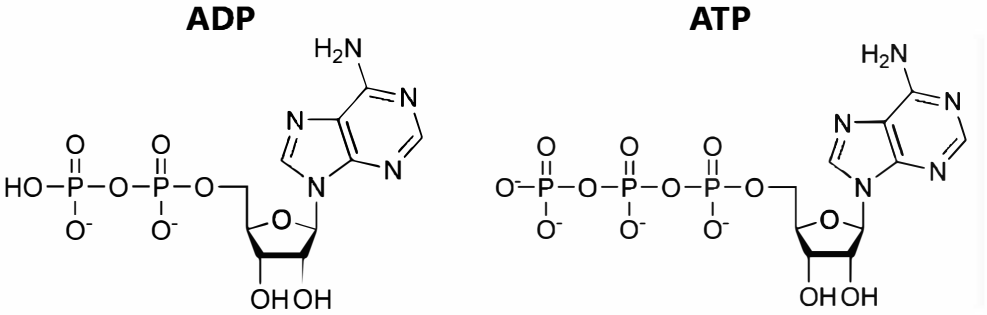


**Figure 1.1: Structure of ADP and ATP**

Chemical structure of adenosine diphosphate and adenosine triphosphate. In ATP, three phosphates ($\alpha$, $\beta$, $\gamma$) are bound in a row by two ester bonds and then a final anhydride bond. The first phosphate $\alpha$ forms a 5'-ester bond to a ribose sugar and adenine group. The cleavage of the anhydride bond, between the second and third phosphate, is exergonic and releases energy that can be coupled to a wide variety of cellular reactions.

## 1.2 Rotary ATPases

Although some ATP synthesis is catalysed by soluble enzymes, the major supplier of ATP across all three domains of life on Earth, are a group of membrane-embedded rotary ATPases. These macromolecular machines are multi-subunit enzyme complexes capable of coupling an ion-motive force (*imf*) with the synthesis of ATP from ADP and inorganic phosphate ($P_i$) through a rotary mechanism (Abrahams et al. 1994; Boyer 1997; Noji et al. 1997). The catalysis of this reaction is reversible in principle but *in vivo* the biochemical environment of each enzyme constrains the reaction in one direction only.

From here on the rotary enzymes primarily functioning in the synthesis direction, coupling the free energy available from an *imf* to synthesise ATP, will be referred

to as ATP synthases; while those primarily functioning in the hydrolysis direction, hydrolysing ATP and using the energy released to pump ions across the membrane in the opposite direction, will be referred to as ATPases. As per the chemiosmotic theory (Mitchell 1961), the driving force for ATP synthesis is an *imf* of either protons or $Na^+$ ions (Dimroth 1997), the *imf* is a function of both transmembrane electric potential ($\Delta\psi$) and transmembrane proton/sodium ion gradient ($\Delta$pH/$\Delta$p$Na^+$). The side of the membrane from which the protons are pumped is usually referred to the N-side (negative) and the side of the membrane to which the protons are pumped is referred to as the P-side (positive). ATP synthases play a central role in cellular respiration and photosynthesis and to this day remain an active area of study due to their key role in bioenergetics, their involvement in a number of diseases and their potential as drug targets for novel antibiotics (Dautant et al. 2018; Demmer et al. 2022; Preiss et al. 2015).

$$pmf = \Delta\psi + \left(\frac{2.3RT}{F}\right)\Delta pH \tag{1.1}$$

**Equation for proton-motive force.** Where *pmf* = proton-motive force, $\Delta\psi$ = transmembrane electric potential, $R$ = gas constant, $T$ = absolute temperature, $F$ = Faraday's constant and $\Delta$ pH = transmembrane proton gradient. The proton-motive force has two variable components, $\Delta\psi$ and $\Delta$ pH, both of which contribute towards the overall *pmf* driving ATP synthesis.

Different types of ATP synthases and ATPases have been classified based on their different functions and the cellular environment in which they are found. A-type ATP synthases are present in archaea (Grüber et al. 2014; Vonck et al. 2009). V-type ATPases are found in eukaryotes where they consume ATP in order to pump protons and maintain vacuolar pH (Futai et al. 2019; Rawson

et al. 2015; Tan et al. 2022; Zhao et al. 2015). F-type ATP synthases can be found embedded in inner mitochondrial membranes, thylakoid membranes and bacterial cytoplasmic membranes where they act as the cell's primary source of ATP. The evolution of F-, A- and V-type ATPases/ATP synthases involves a number of gene duplication events and at least two reversals in primary function from a progenitor proton-pumping ATPase to a proton-driven ATP synthase and then back into a proton-pumping ATPase (Cross and Müller 2004). The N-type ATPase was first identified through a bioinformatics search which identified genes encoding similar subunits to an F-type ATP synthase but arranged in a unique order in the operon and with two additional genes of unknown function (Dibrova et al. 2010; Schulz et al. 2017).

### 1.2.1 A Brief History of ATP synthase Research

After the chemiosmotic theory proposed by Peter Mitchell was established in the 1970s work turned towards understanding the catalytic mechanism of the ATP synthase. Some early ATP synthase research focused on the ATP synthase from *Bacillus* PS3, a thermophilic bacterium isolated from a Japanese hot spring (Yoshida et al. 1975). Other groups also investigated the *E. coli* and bovine mitochondrial ATP synthases (Walker et al. 1982). Paul Boyer was able to combine the subunit stoichiometry of $F_1$ and catalytic role of the $\beta$-subunits reported by Masasuke Yoshida and Yasuo Kagawa (Yoshida et al. 1979) and further investigate a previously proposed rotational catalytic model for ATP synthesis (Gresser et al. 1982).

By the 1990s, the crystal structure of the $\alpha_3\beta_3\gamma$ of $F_1$ could be used alongside Boyer's "binding change mechanism" to describe the rotational catalytic mechanism (Fig. 1.4). Further experiments during the 90s added to the proposed mechanism; cross-linking one of the $\beta$-subunits to the $\gamma$-subunit showed that the asymmetric $\gamma$-subunit was capable of causing conformational changes in $\beta$-subunits during catalysis (Duncan et al. 1995). Introducing mutations to one of the $\beta$-subunits resulted in a complete loss of catalysis (Kaibara et al. 1996). A famous and elegant experiment directly observed the rotation of the $\gamma$-subunit under an optical microscope by attaching actin filaments to the $\gamma$-subunit of an $F_1$-ATPase (Noji et al. 1997). This directly showed, for the first time, the counterclockwise and ATP-dependent rotation of the central stalk. The direction of this rotation was consistent with the direction proposed by the crystal structure of $F_1$-ATPase which contained an ATP, ADP and an empty catalytic binding site (Abrahams et al. 1994).

A short time later, the first crystal structure of the membrane rotor ring (*c*-ring) was solved (Meier et al. 2005b), revealing the coming together of individual *c*-subunits into an hourglass-shaped ring. In this case, the membrane rotor ring came from *Ilyobacter tartaricus* and was composed of 11 *c*-subunits, each with $Na^+$-binding sites. However since then, many other *c*-rings have been solved with a range of stoichiometries and either proton or sodium ion binding capabilities (Pogoryelov et al. 2009; Preiss et al. 2010; Saroussi et al. 2012; Schulz et al. 2017).

In recent years, as discussed in the previous chapter, the "resolution revolution" in single-particle electron *cryo*-microscopy has allowed the structure of a number of complete ATP synthases to be determined. Remarkably, the overall ATP synthase architecture and rotational catalytic mechanism is conserved throughout all living organisms. Furthermore, conserved homology with flagellar proteins suggests this enzyme is as ancient as the last universal common ancestor (LUCA) (Matzke et al. 2021). Crucially and most relevant to this project, this series of intact ATP synthase structures began with the chloroplast $cF_1F_o$-ATP synthase from spinach chloroplasts (Hahn et al. 2018). This provided key insights into the proton translocation pathway around $cF_o$ and a redox regulation mechanism via the $\gamma$-subunit which is unique to $cF_1F_o$ (Hahn et al. 2018; Yang et al. 2020).

### 1.2.2 Proton-driven ATP synthesis

Crucial to the chemiosmotic theory, is the interconversion of proton motive force into Gibbs energy ($\Delta G$) which is used for ATP synthesis. The proton motive force (*pmf* or $\Delta p$) is the sum of two thermodynamically equivalent parameters (Eq. 1.1): the transmembrane electrical potential ($\Delta\psi$) and the transmembrane pH gradient ($\Delta$pH). In mitochondria, the *pmf* is built up across the inner mitochondrial membrane by the respiratory chain complexes while in chloroplasts the primary source of *pmf* arises from photons interacting with the photosynthetic electron transport chain found in the thylakoid membrane.

$$E = hv \tag{1.2}$$

**Energy in a single photon.** Where $E$ = energy of a photon; $h$ = Planck's constant, 6.62 x $10^{-34}$ Js; $v$ = frequency of radiation, ($s^{-1}$).

The above equation (Eq. 1.2) describes the energy supplied by a single photon. One mole of photons can be referred to as an Einstein and the frequency of the light radiation can be calculated by dividing the speed of light ($c$) by the wavelength of light in nm ($\lambda$). Therefore, Eq. 1.3 gives the energy supplied by one mole of photons. For example, the energey associated with the absorption of a single Einstein of red light with wavelength 600 nm = 200 kJ/mol.

$$\Delta G = Nhv = Nh.c/\lambda \tag{1.3}$$

**Gibbs Free Energy of 1 mole of photons.** Where $\Delta G$ = Gibbs Free Energy; $h$ = Planck's constant, 6.62 x $10^{-34}$ Js; $v$ = frequency of radiation ($s^{-1}$); $N$ = Avogadro's constant (6.02 x $10^{23}$); $c$ = the velocity of light and $\lambda$ = the wavelength of radiation (nm).

## 1.3 The F-type ATP synthase

The simplest form of F-type ATP synthase, found in bacteria and chloroplasts, is approximately $\sim 550$ kDa and consists of eight or nine different types of subunits in the following stoichiometry: $\alpha_3\beta_3\gamma\delta\epsilon ab_2c_{8\text{-}17}$ (Junge and Nelson 2015; Kühlbrandt 2019; Walker 2013). This complex can be subdivided into

a water-soluble, catalytic head known as the $F_1$ subcomplex which is composed of subunits $\alpha_3\beta_3\gamma\delta\epsilon$; and a membrane-embedded subcomplex, $F_o$, composed of subunits $ab_2c_{8\text{-}17}$. These two subcomplexes, $F_1$ and $F_o$, are connected via a central stalk and a peripheral stalk with the central stalk attached to the membrane rotor ring in $F_o$ known as the $c_n$-ring .

It should be noted that the architecture of mitochondrial F-type ATP synthases ($mtF_1F_o$) is more complex, with additional subunits and the ability to form dimers with two equivalent ATP synthase units operating in tandem Fig. 1.2. The dimerisation of F-type ATP synthases in mitochondria is essential in cristae formation at the inner mitochondrial membrane (Hahn et al. 2016; Kühlbrandt 2019; Murphy et al. 2019; Spikes et al. 2020). In the classical cristae formation rows of ATP synthase dimers allow the inner mitochondrial membrane to fold into its characteristic shape. More complex assemblies of dimers such as in *Toxoplasma* can shape the inner mitochondrial membrane into a unique curved apical morphology (Mühleip et al. 2021).

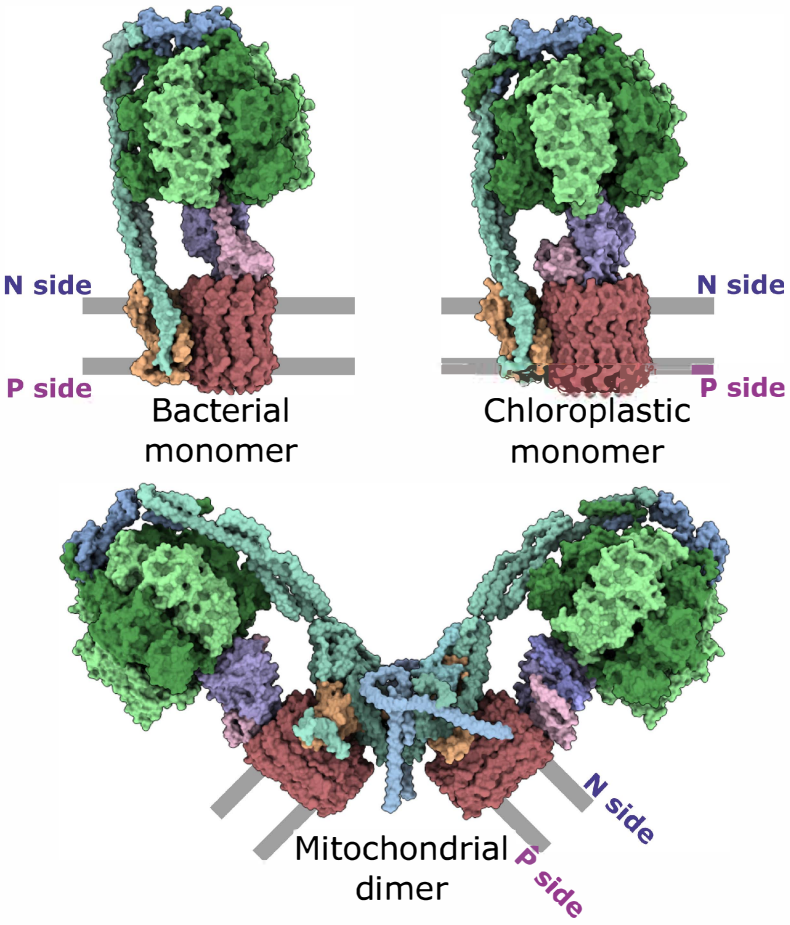


**Figure 1.2: Structures of Monomeric and Dimeric ATP synthases**
Bacterial monomer (*Acinetobacter baumannii*, PDB ID: 7P3N) (Demmer et al. 2022), chloroplastic monomer (*Spinacia oleracea*, PDB ID: 6FKF) (Hahn et al. 2018) and mitochondrial dimer (*Saccharomyces cerevisiae*, PDB ID: 6B8H) (Guo et al. 2017). The $F_1F_o$-ATP synthase found in bacteria and chloroplast are monomeric while mitochondrial ATP synthase possess additional subunits allowing dimerisation and sometimes larger assemblies which can significantly alter the morphology of the inner mitochondrial membrane. The membranes are approximately 4 nm in diameter.

Just as the overall architecture of F-type ATP synthases is conserved throughout biology so too is the overall mechanism of catalysis (Fig. 1.3). In this mechanism

terms such as rotor and stator, traditionally associated with mechanical motors, are remarkably applicable. In both ATP synthesis and hydrolysis, rotary catalysis occurs in three steps of $\sim 120^\circ$ each. These three rotary states represent local energy minima and are observed as probabilistic resting positions as the $F_o$-subcomplex rotates around $360^\circ$ relative to $F_1$ (Abrahams et al. 1994; Noji et al. 1997). A peripheral stalk acts as the stator preventing futile co-rotation of $F_1$ when $F_o$ is rotating.

During ATP synthesis, protons driven by a transmembrane proton-motive force, flow through a half-channel in the *a*-subunit and sequentially bind to the *c*-ring. This sequential binding causes rotation of the *c*-ring and upon almost completing a full $360^\circ$ rotation the bound proton encounters a conserved arginine residue in the *a*-subunit and is released through another half-channel in *a*-subunit that is exposed to the other side of the membrane. As the *c*-ring is tightly but non-covalently bound to the central stalk ($\gamma\epsilon$), the asymmetric central stalk rotates with the *c*-ring and transfers the torque generated in $F_o$ to the $F_1$-domain. In $F_1$, the rotating $\gamma$-subunit causes conformational changes in the catalytic $\beta$-subunits where ATP is synthesised. The peripheral stalk, also known as the outer stalk, consists of two single helix *b*-subunits that attach to the $F_1$-domain via a $\delta$-subunit and extend down to $F_o$ and attach to the *a*-subunit. The peripheral stalk acts as a stabilising stator element and prevents futile co-rotation of $F_1$ with $F_o$ (Meier et al. 2011).

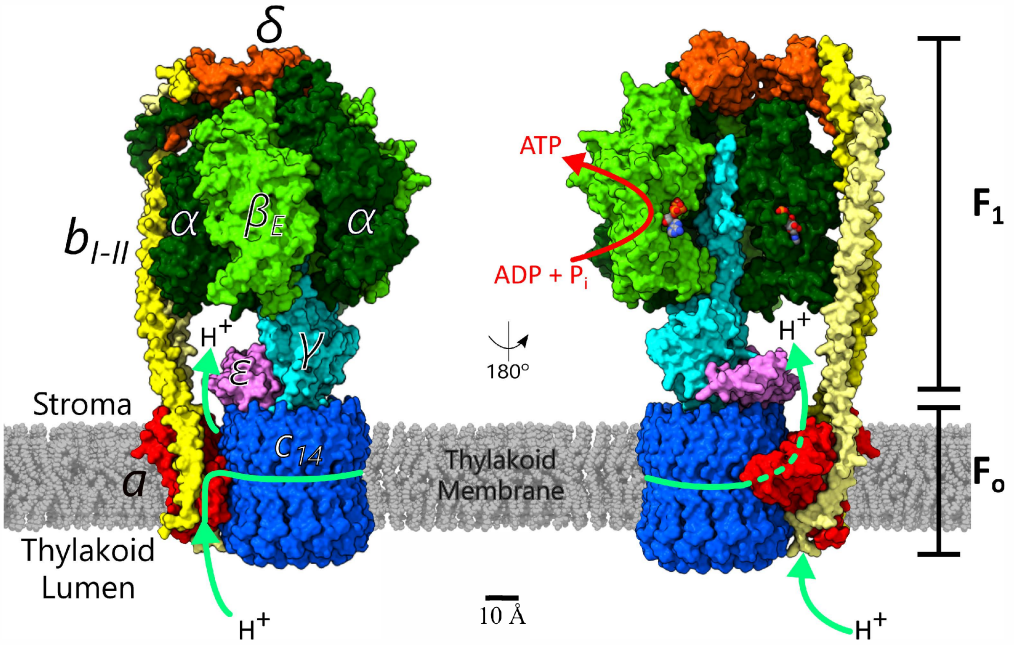


**Figure 1.3: The cF$_1$F$_o$ ATP synthase from spinach chloroplast.** The F$_1$F$_o$-ATP synthase found in the thylakoid membranes of chloroplasts is similar in architecture to the bacterial ATP synthase. This enzyme can be subdivided into a water-soluble F$_1$-domain and a membrane-embedded F$_o$-domain. During ATP synthesis, protons flow from the thylakoid lumen through a half-channel in *a*-subunit binding sequentially to the *c*-ring causing the ring to rotate. Upon almost completing a full $360^\circ$ rotation the proton encounters a conserved arginine residue in the *a*-subunit, the charge of this arginine residue induces the proton to be released through a separate half-channel in *a*-subunit exposed to the stroma. The torque generated by the rotation of the *c*-ring is transferred to F$_1$-domain via the central stalk consisting of $\gamma$-subunit and $\epsilon$-subunit. Each of the three catalytic $\beta$-subunits catalyses the synthesis of one ATP molecule per rotation.

### 1.3.1 F$_1$ subcomplex

The F$_1$ subcomplex is the soluble portion of the ATP synthase enzyme and possesses the three catalytic sites where ATP synthesis and hydrolysis occur. The globular subcomplex is approximately 8 nm in diameter and 11 nm in height and is composed of a hexamer of alternating $\alpha$- and $\beta$-subunits, and a central

stalk composed of a $\gamma$-subunit and $\epsilon$-subunit. The three $\alpha$ and three $\beta$-subunits each contain a Walker A motif (GxxxxGK[T/S] also known as the P-loop) capable of binding to the $\beta$-phosphate of nucleotides like ATP (Abrahams et al. 1994). However only the binding sites at the three $\beta$-subunits are functionally active catalytic sites of ATP synthesis and hydrolysis. The top of the hexamer is attached to a peripheral stalk by a $\delta$-subunit. A central stalk extends into the $\alpha_3\beta_3$-hexamer and co-rotates with the $F_o$ motor which induces the necessary conformational changes for ATP synthesis. This rotary mechanism of catalysis was first proposed by Paul Boyer and is known as the '*binding change mechanism*' (Boyer 1997).

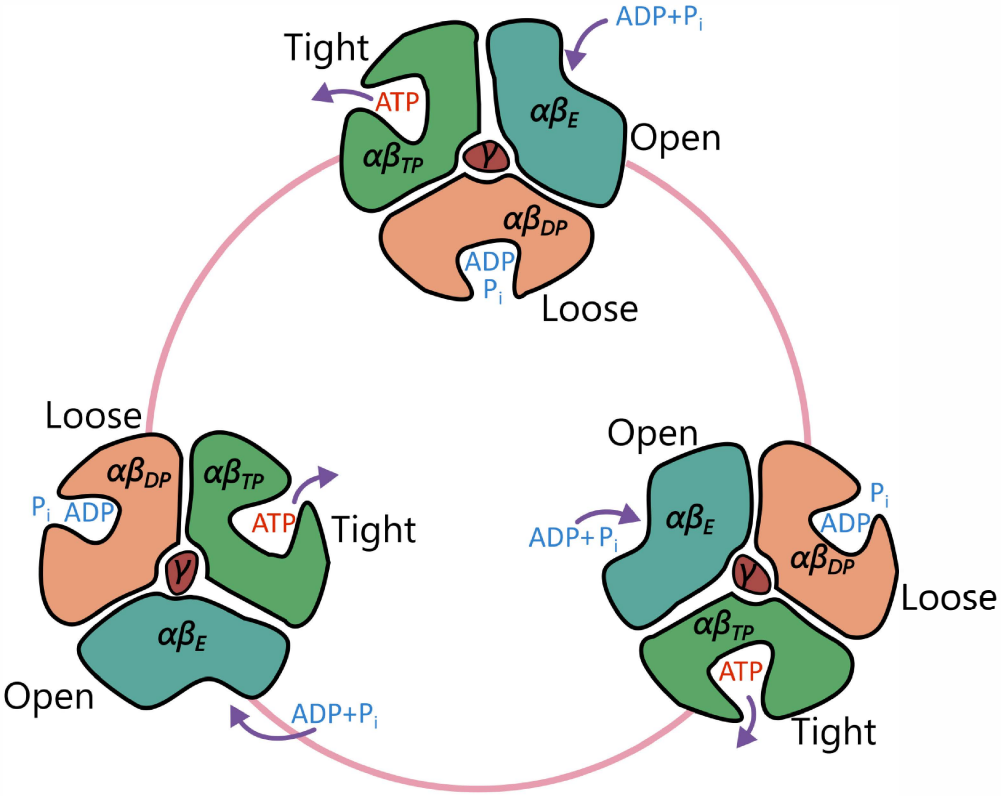


**Figure 1.4: The Binding Change Mechanism**
During catalysis, the three $\beta$-subunits can be described as either "tight, "open" or "loose", as they are either bound to ATP ($\beta_{TP}$, tight), empty ($\beta_E$, open) or bound to ADP + $P_i$ ($\beta_{DP}$, loose). For his pioneering work on the binding change mechanism for ATP synthesis, Paul Boyer was awarded the 1997 Nobel Prize in Chemistry alongside John Walker and Jens Skou.

In the binding change mechanism (Fig. 1.4), the rotation of the asymmetric $\gamma$-subunit causes conformational changes in the hexamer of alternating $\alpha$ and $\beta$-subunits. During catalysis, each of the three Walker A motifs at the $\beta$-subunits are either bound to ATP ($\beta_{TP}$, empty ($\beta_E$) or ADP + $P_i$ ($\beta_{DP}$); these are described as "tight, "open" or "loose" respectively. Upon an approximately $120°$C rotation of the central stalk $\gamma$-subunit the $\beta$-subunit transition from the "tight"

state to the "open" state is associated with an approximate increase in $K_d$ of ATP from $10^{-12}$ to $10^{-2}$ M (Cross 2000), therefore releasing the bound ATP.

A recent paper discusses the possibility of an alternative model to the binding change model (Nakano et al. 2023). Here, the $F_1F_o$-ATP synthase from *Geobacillus stearothermophilus* was purified and structurally characterised by *cryo*EM at different time points to capture the intermediate states of rotation. In this model, ATP hydrolysis occurs simultaneously at all three catalytic sites alongside a $80^\circ$ rotation, and the remaining $40^\circ$ rotation is induced by the release of intramolecular strain accumulated in the initial $80^\circ$ rotation.

### 1.3.2 Central and Peripheral Stalks

The central stalk consists of a $\gamma$- and an $\epsilon$-subunit that tightly but non-covalently associates with the *c*-ring so that the central stalk rotates with the *c*-ring. The $\gamma$-subunit extends into the $\alpha_3\beta_3$-hexamer so that co-rotation of the central stalk with the *c*-ring induces the necessary conformational changes for catalysis in $F_1$. A number of different regulatory mechanisms involving the central stalk have been discovered and variations exist among different organisms. Some bacterial species possess an $\epsilon$-subunit that can extend into the $F_1$ hexamer and inhibit ATP hydrolysis (Demmer et al. 2022).

### 1.3.3 $F_o$ subcomplex

The membrane-embedded $F_o$ subcomplex is so called because it is sensitive to inhibition by the antibiotic, oligomycin (Kagawa and Racker 1966). For ATP synthases, the rotation of the $F_o$ subcomplex generates the torque required for ATP synthesis in $F_1$, while in ATPases the hydrolysis of ATP in $F_1$ induces rotation of $F_o$ which pumps ions across the membrane in the opposite direction. The key components of $F_o$ include the *c*-ring which rotates as ions sequentially bind and the *a*-subunit which funnels ions towards and away from the *c*-ring. The *a*-subunit lies outside and adjacent to the *c*-ring and forms two water accessible half-channels, each leading to opposite sides of the membrane (Fig. 1.5). In this way ions are able to be channeled to and from the *c*-ring and sequential proton-binding and dissociation leads to rotation of the *c*-ring. Two membrane hairpins in the *a*-subunit made of four helices wrap horizontally beside the ring and a conserved positively charged arginine residue spatially and electrostatically separates the sites of proton association and dissociation (Allegretti et al. 2015; Hahn et al. 2018).

The *c*-ring is a highly conserved hourglass-shaped cylinder and is composed of a number of *c*-subunits. Each *c*-subunit monomer is a hairpin of two transmembrane $\alpha$-helices of approximately 8 kDa in size and oligomerise to form the *c*-ring. The N-terminal $\alpha$-helix orientates towards the centre while the C-terminal $\alpha$-helix, containing the highly conserved ion-binding glutamate or aspartate residue, forms the outside of the ring (Meier et al. 2005b; Pogoryelov et al. 2009; Preiss et al. 2010; Saroussi et al. 2012).

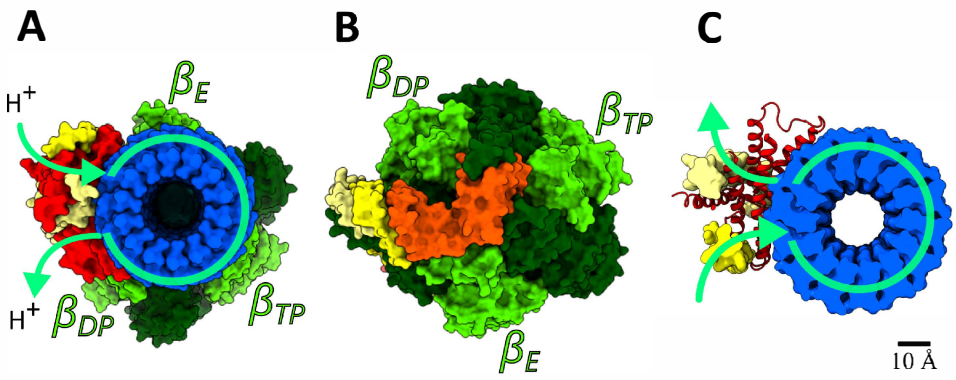


**Figure 1.5: Bottom and top views of $cF_1F_o$ ATP synthase from spinach chloroplast.**
**A**: The $cF_1F_o$-ATP synthase seen from below (lumenal N-side). The proton translocation pathway is indicated in cyan. **B**: The $cF_1F_o$-ATP synthase seen from above (stromal P-side). The three catalytic $\beta$-subunits can be seen forming a hexamer with three alternating $\alpha$-subunits. The three nucleotide binding sites can be described as being tight, open or loose dependent on whether it is bound to ATP, empty or bound to ADP (tight = bound to ATP ($\beta_{TP}$), open = empty ($\beta_E$), loose = bound to ADP ($\beta_{DP}$)). **C**: View from the stromal P-side of the enzyme but with a cut-through to show *a*-subunit (red) helices and proton translocation pathway (green) around the *c*-ring (blue).

### 1.3.4 Membrane rotor ring stoichiometries

The stoichiometry of a given $c_n$-ring is constant for each type of rotary ATPase/synthase in a given species but can vary across different species (Meier et al. 2005b; Müller et al. 2001a; Pogoryelov et al. 2009; Preiss et al. 2010). Currently, the known range of $c_n$-ring stoichiometries for F-type ATP synthases spans $c_8$ (*Bos taurus*) (Watt et al. 2010) to $c_{15}$-ring (*Spirulina platensis*) (Pogoryelov et al. 2009), however a $c_{17}$-ring has been observed in a N-type ATPase from the pathogenic bacterium, *Burkholderia pseudomallei* (Schulz et al. 2017). In this organism, the N-type ATPase is thought to act exclusively in the ATP

hydrolysis direction where it is able to pump protons out of the cell to escape macrophage degradation.

It has been observed that the $c_n$-ring stoichiometry is determined solely by the primary structure of the *c*-subunit and remains constant within a given species but variable across different species (Meier et al. 2011; Müller et al. 2001a; Pogoryelov et al. 2007; Preiss et al. 2010) (Fig. 1.6). The notion of the *c*-subunit primary structure determining *c*-ring stoichiometry is supported by the formation of functional chimeric enzymes upon introduction of an exogenous *c*-subunit gene and maintaining the stoichiometry of the source organism (Laubinger et al. 1990; Suzuki et al. 2007). Another piece of evidence is that point mutations targeting a glycine motif (GxGxGxGxG) in the N-terminal helix of the *c*-subunit can lead to shifts in stoichiometry (Pogoryelov et al. 2012; Preiss et al. 2013). Furthermore, heterologous expression of a variety of *c*-rings in *Escherichia coli* cells yield native i.e. non *E. coli* stoichiometries (Meier and Dimroth 2002; Meier et al. 2005a, 2007).

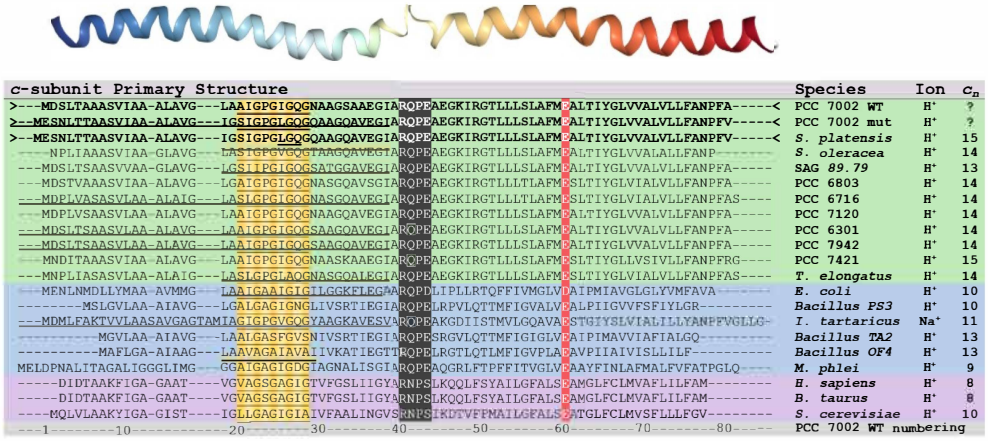


**Figure 1.6: Multiple sequence alignment of c-subunits**
Each *c*-subunit consisting of approximately 70-80 amino acid residues is a hairpin of two transmembrane $\alpha$-helices joined by a loop (RQPE/D or sometimes in mitochondria RNPS), highlighted in grey. Upon oligomerisation the N-terminal helix is arranged in the centre of the *c*-ring and contains a glycine motif (GxGxGxGxG), highlighted in yellow. Meanwhile the C-terminal helix is found on the outside of the *c*-ring and contains the ion-binding glutamate or aspartate residue.

With each *c*-subunit binding to one proton at a time and the *c*-ring stoichiometry varying across different species but the $F_1$ catalytic $\beta$-subunits remaining constant (three), tightly coupled $F_1F_o$-ATP synthases have a key parameter known as the *ion-to-ATP* ratio. A full $360^\circ$ rotation of the *c*-ring is coupled to the synthesis/hydrolysis of three ATP molecules (one by each of the $\beta$-subunits so that the *ion-to-ATP* ratio is equal to the number of *c*-subunits in the *c*-ring ($n$) divided by three. This ratio can be viewed as the "bionergetic cost" of making a single molecule of ATP for a given organism (Watt et al. 2010). Clearly, this ratio has implications on the thermodynamic efficiency of energy-transducing membranes (Silverstein 2014). Therefore, the *c*-ring stoichiometry and resultant *ion-to-ATP* ratio is a potential bio-engineering target for tinkering with bioenergetics.

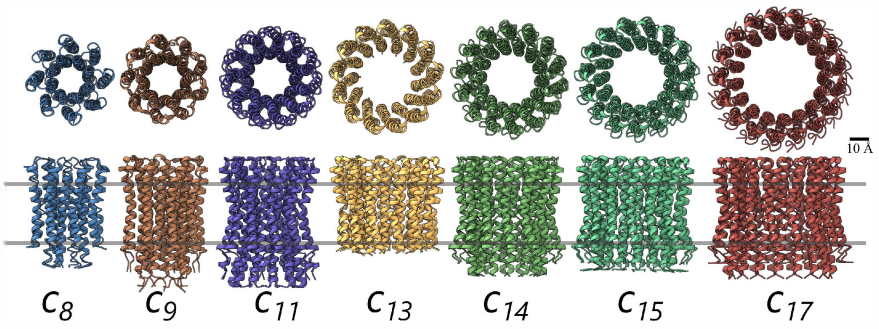


**Figure 1.7: Examples of different $c_n$-ring stoichiometries**
Top and side views (Top view from $F_1$ perspective). From left to right: *Bos taurus* mitochondria ($c_8$), *Mycobacterium phlei* ($c_9$), *Ilyobacter tartaricus* ($c_{11}$), *Bacillus pseudofirmus* OF4 ($c_{13}$), *Pisum sativum* chloroplast ($c_{14}$), *Spirulina platensis* ($c_{15}$), *Burkholderia pseudomallei* N-type ATPase ($c_{17}$).

## 1.4 Photosynthesis

Virtually all life on Earth is directly or indirectly powered by sunlight. The direct users of this light are plants, algae and photosynthetic bacteria such as cyanobacteria. These photoautotrophic organisms are able to store solar energy by capturing quanta of visible light and converting it into chemical forms of energy by a series of reactions, collectively known as photosynthesis. It is estimated that 0.1 % of total solar energy reaching the Earth is converted into chemical energy for life on Earth by phototrophs, this is approximately 7 x $10^{16}$ g of carbon fixed into chemically useful forms such as sugars annually (Phillips and Milo 2009). In the case of oxygenic phototrophs, the electrons are sourced from water molecules and ultimately result in glucose. The photosynthetic reactions

can be divided into two sets of reactions, firstly, the light-dependent reactions of photosynthesis and secondly, the carbon-fixation reactions.

### 1.4.1 The Light Dependent Reactions

In the light-dependent reactions of photosynthesis, light energy is used to split water molecules releasing electrons ($e^-$) for the reduction of nicotinamide adenine dinucleotide phosphate ($NADP^+$) and protons ($H^+$) which contribute to the *pmf* driving ATP synthesis. The two products, NADPH and ATP, are essential substrates for the Calvin-Benson-Bassham (CBB) cycle where carbon fixation occurs. There are five main membrane protein complexes involved in the light dependent reactions: photosystem II (PSII), cytochrome $b_6f$, photosystem I (PSI), ATP synthase and NAD(P)H dehydrogenase-like (NDH) complex (Ferreira et al. 2004; Hahn et al. 2018; Jordan et al. 2001; Kurisu et al. 2003; Laughlin et al. 2019; Naschberger et al. 2022; Pan et al. 2020; Shikanai 2016).

The primary electron donor in PSII is a chlorophyll molecule ($P_{680}$) facing the luminal side of the thylakoid membrane (Barber 2003; Nixon et al. 2010). Upon illumination, an electron from $P_{680}$ is excited and quickly transferred towards the stromal side of the PSII complex. The excited electron is passed through a series of redox reactions via pheophytin before reaching the electron acceptor, plastoquinone. The addition of electrons reduces plastoquinone into plastoquinol which is then released into the membrane matrix. Meanwhile, the $P_{680}{}^+$ cation is reduced by a redox active tyrosine residue. The redox active state of the tyrosine

is regenerated by a Mn ion cluster that accumulates oxidising equivalents from the photolysis of water (Saito et al. 2011).

Similar to the respiratory electron transport chain, the redox reactions of the photosynthetic electron transport chain are coupled to the generation of a proton motive force (*pmf*) by the pumping of protons across a membrane. In linear electron transport (LET), water-splitting in photosystem II and the translocation of protons ($H^+$) across the thylakoid membrane by cytochrome $b_6f$ via the quinone (Q) cycle are the main contributors of the *pmf* which is a function of both transmembrane electric potential ($\Delta\psi$) and transmembrane proton gradient ($\Delta$pH). The carbon fixation reactions consume ATP and NADPH to complete the CBB cycle and fix $CO_2$ into glucose.

### 1.4.2 ATP synthase from photosynthetic organisms

The F-type ATP synthases found in photosynthetic organisms are driven by electrochemical proton gradients generated across thylakoid membranes during the light dependent reactions of photosynthesis. The unique features of the photosynthetic ATP synthases are reviewed in (Cheuk and Meier 2021) but can be summarised in two main features, a larger-than-average transmembrane rotor ring and a unique redox regulation loop in the $\gamma$-subunit. In both chloroplasts and cyanobacteria the architecture of F-type ATP synthase more closely resembles the bacterial enzyme over the mitochondrial enzyme. As such, they are composed of eight or nine different subunits and lack the dimer-specific subunits

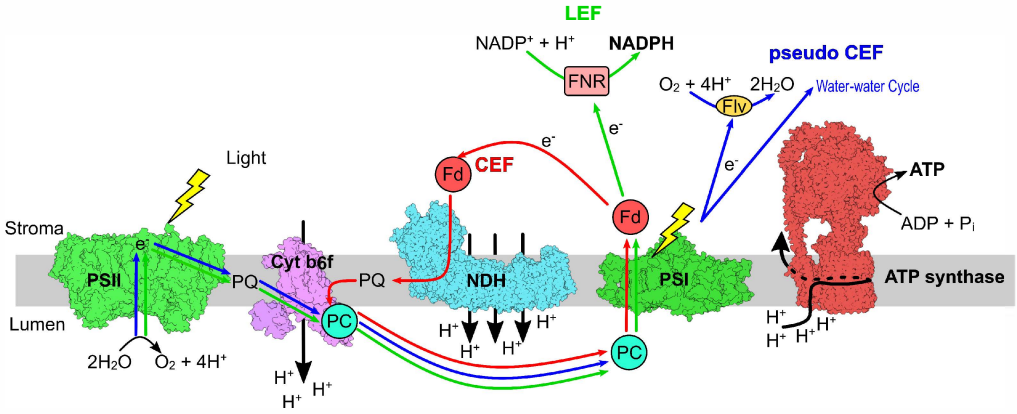


**Figure 1.8: Schematic of the light-dependent reactions.**
The photolysis of water molecules releases electrons for the reduction of NADPH and protons that contribute to the *pmf*. In LET, a series of redox reactions carries excited electrons via the two photosystems, cytochrome $b_6f$, plastocyanin (PC) and ferredoxin (Fd) before being transferred to $NADP^+$ which is reduced to NADPH. The redox reactions are coupled to the pumping of protons into the thylakoid lumen contributing to the *pmf* driving ATP synthesis.

found in $mtF_1F_o$, therefore form monomers only. The stoichiometry of the membrane rotor ring or *c*-ring found in photosynthetic ATP synthases are the largest known ranging from 13 to 15 *c*-subunits. It is noted that a bacterial *c*-ring with 17 subunits exists, however this is found in an N-type ATPase and only functions in the ATP hydrolysing and proton pumping direction (Schulz et al. 2017).

Additionally, $F_1F_o$-ATP synthases from chloroplasts possess a redox loop in the $\gamma$-subunit that is modulated by thioredoxin allowing regulation of activity in response to light and dark conditions (Hahn et al. 2018). This has been confirmed by treating the spinach enzyme with an uncompetitive inhibitor, tentoxin, to obtain structures of both the active and inactive redox states (Yang et al. 2020). Relative to non-photosynthetic bacteria, cyanobacteria also possess an insertion

resembling the chloroplast redox loop however the cyanobacterial insertion loop is missing the two cysteine residues responsible for the redox behaviour. The exact nature of the regulation in cyanobacterial ATP synthase is not clear but it is thought to involve the $\epsilon$-subunit (Akiyama et al. 2019; Hisabori et al. 2013; Kondo et al. 2021; Murakami et al. 2018). As with other methods of regulating ATP synthase the purpose is to prevent wasteful ATP hydrolysis and is especially important in photosynthetic organisms during periods of low light or darkness. Recently, an additional method of regulating ATP synthase was discovered in cyanobacteria, in the form of a small amphipathic peptide called *Atp*$\theta$ (Song et al. 2022). Although the exact mechanism of *Atp*$\theta$ inhibition is not yet known, inhibition through small peptides is not unique to cyanobacteria; for example the mitochondrial IF1 peptide is known to inhibit mitochondrial ATP synthase (Gu et al. 2019; Mühleip et al. 2020).

### 1.4.3 Synechococcus sp. PCC 7002

Cyanobacteria are bacteria capable of growing photoautotrophically, using light as their primary energy source. They share a common ancestor with chloroplasts and can be good model organisms for studying photosynthesis (Vries and Archibald 2017). Cyanobacteria also possess unique specialised microcompartments known as carboxysomes which concentrate $CO_2$ around the carbon-fixing enzyme ribulose 1,5-bisphosphate carboxylase/oxygenase (RuBisCO) and improves the efficiency of carbon fixation (Tabita 1994). Another research area involving cyanobacteria is engineering them to produce high-value products such

as isoprenes and commodity chemicals (Ducat et al. 2011).

*Synechococcus sp.* PCC 7002 is euryhaline and unicellular cyanobacterium originally isolated from the fish pens of Magueyes Island, Puerto Rico (Baalen 1962). *Synechococcus sp.* PCC 7002 can grow over a wide range of salinities and is tolerant of high light irradiation (Ludwig and Bryant 2011). The genome of *Synechococcus sp.* PCC 7002 has also been sequenced and the ability to transform this organism by homologous recombination make it an attractive model for studying many aspects of photosynthesis.

## 1.5 Project Aims

This work aims to investigate the evolutionary advantage of having relatively high $c_n$-ring stoichiometries ($c_{13}$ to $c_{15}$) in the F-type ATP synthases of photosynthetic organisms. Starting with the photosynthetic model organism, *Synechococcus sp.* PCC 7002, mutations will be introduced to the *atpE* gene encoding the *c*-subunit to alter the *c*-ring stoichiometry. The effect of the altered $c_n$-ring stoichiometry will be assessed on a molecular and cellular level. This work seeks to understand why the higher $c_n$-ring stoichiometry is advantageous in photosynthetic systems and whether engineering *c*-ring stoichiometries is a viable approach to improve the efficiency of photosynthesis.

# Chapter 2

# Materials & Methods

This chapter contains an overview of the materials and methods used throughout the project. More detailed and specific methods can be found in their relevant chapters.

## 2.1 Materials

### 2.1.1 Reagents

Unless otherwise stated, all reagents used in this work were purchased from Sigma-Aldrich, Merck or VWR International.

### 2.1.2 Primers

Primers were ordered from either Microsynth AG (Balgach, SG, Switzerland) or Integrated DNA Technologies (Coralville, Iowa, USA).

| Primer | Sequence (5'-3') | $T_m$(°C) |
|---|---|---|
| A0749-His-1F | AAGCCCAATTTCGTAACTTATTTCAA | 63 |
| A0749-His-2R | GCTACATGATGATGATGATGATGCATGCTTCTCTATTATCGATTGGT | 68 |
| A0749-His-3F | GCATCATCATCATCATCATGTAGCTACACAAGAAAAAACTTTAGGTA | 68 |
| A0749-His-4R | TCGTTCATCTGACCGTACACGA | 63 |
| A0749-His-Check | GATAATAGAGAAGCATGCATCATCATCATCATCA | 67 |
| A0749-His-Seq-R | GACTTGGTTGTCGCCGAGCA | 67 |

**Table 2.1: Primers**

A list of the primers used in this project. Sequences are given in 5'-3' direction and the melting temperature ($T_m$) calculated using the New England BioLabs Tm Calculator. Primers were ordered from either Microsynth AG (Balgach, SG, Switzerland) or Integrated DNA Technologies (Coralville, Iowa, USA)

### 2.1.3 Plasmids

| Plasmid | Size (kb) | Description |
|---|---|---|
| pt7c_7002F | 2.7 | pt7-7 with AmpR and *atpE* from *Synechococcus sp.* 7002 |
| pt7c_SP | 2.7 | pt7-7 with AmpR and *atpE* from *Spirulina platensis* |
| pGEM-T-His | 4.6 | 6x Histidine-tag to N-terminal of 7002 $F_1F_o$ $\beta$-subunit |
| pSW102-trcE* | 11.0 | Cas12a nuclease with theophylline-induced riboswitch |
| pSW104-psbA2 | 11.0 | Cas12a nuclease with psbA2 constitutive inducer |
| pE001 | 4.1 | Background plasmid with no recovery template |
| pE002_A21G | 4.8 | *atpE* gRNA and A21G recovery template |
| pE003_G23A | 4.8 | *atpE* gRNA and G23A recovery template |
| pE004_G27A | 4.8 | *atpE* gRNA and G27A recovery template |
| pE005_G23/27A | 4.8 | *atpE* gRNA and G23/27A recovery template |
| pE006_SP_c15 | 4.8 | *atpE* gRNA and *Spirulina* recovery template |
| pE007_SAG_c13 | 4.8 | *atpE* gRNA and *Synechococcus* 89.79 recovery template |

**Table 2.2: Plasmids**

A list of the plasmids used and obtained throughout the course of this project. The sizes of the plasmids are given in kilo base pairs.

Two equivalent strains of wild-type *Synechococcus sp.* PCC 7002 were from the PN lab with one strain from Imperial College London, United Kingdom, and the other from Nanyang Technological University, Singapore.

### 2.1.4 Bacterial Strains

The following table shows a list of bacterial strains used or obtained over the course of this project:

| Strain name | Species | Description |
|---|---|---|
| BL21 pt7c-7002F | *E. coli* BL21 | Transformed with pt7c-7002F plasmid |
| BL21 pt7c-SP | *E. coli* BL21 | Transformed with pt7c-SP plasmid |
| *Syn* WT | *Synechococcus* 7002 | Wild-type *Synechococcus sp.* PCC 7002 |
| *Syn* WT-His | *Synechococcus* 7002 | *Syn* WT transformed with pGEM-T-His |
| *Syn* E* | *Synechococcus* 7002 | Conjugated with pSW102-pVZ322-trcE* |
| *Syn* psbA2 | *Synechococcus* 7002 | Conjugated with pSW104-pVZ322-psbA2 |
| *Syn* SP | *Synechococcus* 7002 | Genome-edited with *atpE* gene from *S. platensis* |
| *Syn* SP-His | *Synechococcus* 7002 | *Syn* SP transformed with pGEM-T-His |

**Table 2.3: Bacterial Strains**

A list of the bacterial strains used and obtained throughout the course of this project. The *Synechococcus sp.* PCC 7002 strains originated from the *Syn* WT from the PN lab and the *Escherichia coli* BL21 competent cells were made by Mong Sing Lai from the TM lab. All of the *Synechococcus sp.* PCC 7002 strains have been flash frozen in MAD media with 5 % DMSO for long-term storage in a $-70^{\circ}$C freezer. *E. coli* strains were frozen in LB media + 20 % glycerol.

### 2.1.5 Growth Media & Antibiotics

Ampicillin, chloramphenicol, gentamycin or spectinomycin were added as appropriate to liquid media and plates to a final concentration of 50 $\mu$g/mL. *Escherichia coli* was grown in LB media at $37^{\circ}$C with 250 rpm shaking while *Synechococcus sp.* PCC 7002 was grown in liquid modified A-D7 (MAD) media (Włodarczyk et al. 2020) at $30^{\circ}$C with 100 rpm shaking under constant white light (200 $\mu$E $m^{-2}$ $s_{-1}$).

| Stock | Reagent | Concentration (mM) |
|---|---|---|
| **D7 micronutrients** | $H_3BO_3$ | 46 |
| (1000 x) | $MnCl_2.4H_2O$ | 9 |
| | $ZnSO_4.7H_2O$ | 0.77 |
| | $Na_2MoO_4.2H_2O$ | 5.2 |
| | $CuSO_4.5H_2O$ | 0.32 |
| | $CoCl_2.6H_2O$ | 0.17 |
| **$A^+$** | KCl | 805 |
| (100 x) | $NaNO_3$ | 1200 |
| | $CaCl_2.2H_2O$ | 250 |
| | $Na_2EDTA$ | 65 |
| | $KH_2PO_4$ | 37 |

**Table 2.4: Stock solution Reagents**
Reagents and concentrations used to prepare D7 micronutrients (1000 x) and $A^+$ (100 x) stocks. These stock solutions were diluted to 1 x concentrations when preparing the final modified A-D7 (MAD) media.

Modified A-D7 media was prepared by making a 1000 x stock of **D7 micronutrients** and a 100 x stock of **$A^+$**. D7 micronutrients and $A^+$ were then added (1 x final concentration) to 300 mM NaCl, 20 mM $MgSO_4.7H_2O$, 8.3 mM Tris-HCl (pH = 8.2), 80 mM $NaNO_3$, 1 mM $KH_2PO_4$ and then autoclaved. After autoclaving the media was allowed to cool and 0.24 mM $FeCl_3.6H_2O$ and 8 ng/L Vitamin B12 was added. For agar plates the modified A-D7 media was prepared as above but supplemented with sterile 12 g/L agar and 3.125 g/L $Na_2S_2O_3$ after autoclaving.

### 2.1.6 Column Materials and Prepacked Columns

Ni-NTA gravity column was prepared using Chelating Sepharose Fast Flow resin (GE Healthcare) and charged with $NiCl_2$. Two size exclusion columns were used

over the course of this project: a Superose 6 Increase 3.2/300 (Cytiva) and a Superdex 200 10/300 GL (Cytiva).

### 2.1.7 Benchtop centrifuges and ultracentrifuges

| Centrifuge | Supplier | x g |
|---|---|---|
| 5804 R Benchtop | Eppendorf | 1 - 20,000 |
| 5920 R Benchtop | Eppendorf | 1 - 4,000 |
| Optima XPN Ultracentrifuge | Beckman | 1 - 802,400 |
| Optima Max-TL | Beckman | 1 - 657,000 |

**Table 2.5: Centrifuges and Ultracentrifuges**
Benchtop centrifuges and ultracentrifuges were routinely used throughout this project. For the Optima XPN Ultracentrifuge Ti70 and Ti45 (Beckamn) rotors and tubes were used depending on the volumes required.

### 2.1.8 ÄKTA purification system

For size exclusion chromatography and anion exchange chromatography the ÄKTA Pure protein purification system was used (Cytiva). The instrument was stored at $4^{\circ}$C in either a refrigerated cabinet or room. Samples were injected using up to 2 mL glass syringes (Cytiva).

## 2.2 Molecular Biology Methods

### 2.2.1 Escherichia coli Transformation

DH5$\alpha$ or BL21 competent cells were incubated with 2 ng plasmid DNA on ice for 10 mins. The cells were then heat shocked by incubating at $42^{\circ}$C for 45 seconds and then placed onto ice for 5 minutes. 1 mL of fresh LB media was added to the tube and the cells were allowed to recover for an hour at $37^{\circ}$C. Then 100 $\mu$L of cells was spread onto LB agar plates supplemented with suitable antibiotics. The plates were incubated at $37^{\circ}$C overnight and single colonies appear the next day.

### 2.2.2 Plasmid DNA isolation from E. coli

For molecular cloning projects, highly pure plasmids for sequencing, restriction digests and PCR were isolated from *Escherichia coli* by growing suitably transformed DH5$\alpha$ overnight at $37^{\circ}$C. Around 5 mL of cell culture was harvested by centrifugation at 12,000 rpm for 2 mins and plasmids were purified using the GeneJET Plasmid Miniprep Kit (Thermo Scientific).

### 2.2.3 Extraction of Synechococcus sp. PCC 7002 genomic DNA

*Synechococcus sp.* PCC 7002 was grown in liquid modified A-D7 media to an $OD_{730} = 0.8$. 20 mL of liquid culture was used to extract genomic DNA (gDNA) using the *Quick*-DNA Fungal/Bacterial Miniprep kit from Zymo Research following the manufacturer's instructions. The extracted gDNA was stored at $-20^{\circ}$C.

### 2.2.4 Polymerase Chain Reaction (PCR)

Polymerase chain reaction (PCR) was used to amplify DNA fragments; the reactions used the Phusion High-Fidelity DNA polymerase in HF buffer (New England BioLabs) or Q5 polymerase in Q5 Reaction Buffer (New England BioLabs). Primers were used at a final concentration of 10 $\mu$M. Reactions underwent the following programme in a peqSTAR Thermocycler (VWR International):

| Step | Temperature (°C) | Time | |
|---|---|---|---|
| Initial Denaturation | 98 | 30 s | |
| Denaturation | 98 | 7s | 32 x cycles |
| Annealing | 60 - 65 | 15 s | |
| Extension | 72 | 30 s/kb | |
| Final Extension | 72 | 10 mins | |
| Hold | 4 | - | |

**Table 2.6: PCR Conditions**
Unless otherwise stated these PCR conditions were used to amplify DNA during cloning and genotyping steps.

### 2.2.5 DNA Concentration Determination

DNA concentrations were measured using a NanoDrop 2000/2000c Spectrophotometer (Thermo Scientific). The absorbance at 260 nm and 280 nm were recorded after blanking with nuclease-free water.

### 2.2.6 Transformation of Synechococcus sp. PCC 7002

*Synechococcus sp.* PCC 7002 was transformed as described in (Nixon et al. 1992). Briefly, plasmid DNA at a concentration of 40 $\mu$g/mL was added to 0.5 mL of exponentially growing cells ($OD_{730}$ between 0.6 and 1.0) concentrated to $OD_{730} = 2.5$ and incubated in light for 6 hrs at $31^{\circ}$C, with occasional agitation. Afterwards, 200 $\mu$L of transformation mix was plated onto nitrocellulose filter paper and placed onto a A-D7 agar plate with no selective antibiotic. After 2 days in light and at $31^{\circ}$C, the nitrocellulose filter was transferred onto a selection plate with the appropriate antibiotic.

### 2.2.7 Restriction Enzyme Digests

Diagnostic restriction digests were performed by adding restriction enzymes (New England Biolabs) and the appropriate buffer mix (CutSmart or 2.1 buffer). The reactions were incubated at $37^{\circ}$C for 1 hour before adding DNA Gel Loading Dye (New England BioLabs) and running on DNA agarose gels.

### 2.2.8 DNA Agarose gels

Agarose gels were prepared by dissolving 1-1.2 % (w/v) agarose in TAE buffer (40 mM Tris-acetate, 1 mM EDTA, pH = 8.2) and then adding GelGreen DNA stain (Biotium, USA). After casting the gel and adding the samples, 120 V voltage was applied for 35 mins and then the gel was visualised with a blue light reader.

### 2.2.9 DNA Sequencing

DNA plasmids, fragments and other samples for DNA sequencing were submitted to Source BioScience (Nottingham), according to their online instructions.

## 2.3 Biochemical Methods

### 2.3.1 Growth of Synechococcus sp. PCC 7002

*Synechococcus sp.* PCC 7002 was grown in modified A-D7 (MAD) liquid media at $31^{\circ}$C (Włodarczyk et al. 2020) under constant white-light illumination at 100 $\mu$E m$^{-2}$ s$^{-1}$. When growing on agar plates the MAD media was supplemented with 1.2 % agar and 2 g/L $Na_2S_2O_3$.

### 2.3.2 Bacterial Cryo Stocks for Long-term storage

For cryo-storage, $\sim 20$ mL of liquid cultures of *Synechococcus* in exponential growth phase ($OD_{730} \sim 0.6$ to 0.8) were centrifuged at 3,000 rpm for 15 mins at $4^{\circ}$C. The cell pellet was resuspended in 1 mL fresh MAD media + 5 % DMSO. This was briefly vortexed before flash freezing in liquid nitrogen and stored at $-70^{\circ}$C.

To recover frozen cultures, an inoculating loop was used to scrape a loop of the cryo-stock into a sterile Eppendorf. 0.1 mL of fresh MAD media was added and the whole suspension spread onto a sterile MAD agar plate and left at low light for 48 hours before increasing the light to 100 $\mu$E m$^{-2}$.

### 2.3.3 Thylakoid Membrane Preparation

9 L liquid cultures of *Synechococcus* were grown to an $OD_{730} \sim 0.8$ in modified A-D7 media. Cells were pelleted by centrifugation at 3000 rpm for 20 mins at $4^{\circ}$C and resuspended in 200 mL of KPN buffer (40 mM K-phosphate pH = 8.0, 100 mM NaCl, 2 mM $MgCl_2$). Cells were lysed by four passages through a cell disruptor (Constant Systems Ltd.) at 25 kpsi. Unbroken cells and cell debris were removed by centrifugation at 16,000 rpm for 30 mins at $4^{\circ}$C (F21S-8x50Y rotor). The supernatant was immediately ultracentrifuged at 45,000 rpm for 1 hour at $4^{\circ}$C (Ti45 rotor). The pellet containing thylakoid membranes was washed by re-suspending in $\sim 25$ mL of Resuspension Buffer (20 mM Tricine-NaOH pH = 8.0, 200 mM sucrose, 5 mM $MgCl_2$, 0.1 mM $Na_2$-ATP) with a glass homogeniser. The sample was ultracentrifuged again at 55,000 rpm for 1 hour at $4^{\circ}$C (Ti70 rotor). The pelleted thylakoid membranes were resuspended in 8 - 12 mL of Resuspension Buffer to a final chlorophyll *a* concentration [Chl *a*] of 500 $\mu$g/mL and flash frozen in liquid nitrogen ($LN_2$) and stored at $-80^{\circ}$C.

Membrane yields were calculated and normalised by measuring [Chl *a*] as follows: 5 $\mu$L of membrane fractions were added to 995 $\mu$L methanol and left to stand for 5 mins at room temperature. Precipitated material was removed by centrifugation at 15,000 rpm for 2 mins. The $OD_{666}$ and $OD_{750}$ were measured and the following formula used to calculate [Chl *a*]:

$$[Chl\ a]\ \mu g/mL = (OD_{666} - OD_{750}) \times 12.61 \times 200 \quad (2.1)$$

### 2.3.4 Protein Concentration Determination

Protein concentrations of samples were determined using a bicinchoninic acid (BCA) assay (Smith et al. 1985). Known concentrations of bovine serum albumin (BSA) in sample specific buffers were used to create a standard curve for the copper-based, colorimetric BCA assay.

### 2.3.5 Sodium Dodecyl Sulfate Polyacrylamide Gel Electrophoresis (SDS-PAGE)

For SDS-PAGE analysis, protein samples were solubilised in SDS loading buffer and loaded onto 13.4 % or 16 % (w/v) polyacrylamide gels following the Schägger system (Schägger 2006). Electrophoresis was run for 2 hours at room temperature with a constant 30 mA current per gel. Gels were stained with Coomassie Instant*Blue* or by silver-staining (Nesterenko et al. 1994).

### 2.3.6 Clear-Native Polyacrylamide Gel Electrophoresis (CN-PAGE)

A cathode buffer (50 mM Tricine, 15 mM Bis-Tris-HCl (pH = 7.5), 0.01 % DDM and 0.03 % deoxycholate (DOC)) and an anode buffer (50 mM Bis-Tris-HCl (pH

$= 7.5$) were prepared. Sample buffer was made by supplementing cathode buffer with 0.1 % DDM, 12 % glycerol and 0.01 % bromophenol blue. To load samples, 10 $\mu$L of sample buffer was added to 15 $\mu$L of sample and the 25 $\mu$L mixture was loaded onto NativePAGE 3-12 % Bis-Tris gradient gels (Invitrogen). Samples were run at 100 V for 25 mins followed by 280 V for 30 mins.

### 2.3.7 Immunoblot (Western blot) Analysis

Protein samples were run on SDS-PAGE gels and blotted onto polyvinylidene fluoride (PVDF) membranes using an iBlot 2 Dry Blotting System (ThermoFisher Scientific). PVDF membranes were blocked with Blocking buffer (Tris-buffered saline (pH $= 7.6$) $+$ 5 % (w/v) skimmed-milk powder) overnight at $4^{\circ}$C. The blocked membranes were incubated with primary antibody (Agrisera) in Blocking buffer for 1 hour at room temperature followed by incubating with secondary antibody in Blocking buffer for 1 hour at room temperature. The PVDF membrane was then washed with TBS-T and visualised using Clarity western ECL substrate (Bio-Rad).

### 2.3.8 Trichloroacetic Acid (TCA) Treatment of c-rings

As the *c*-ring samples are SDS-stable they typically run as oligomers on SDS-PAGE gels; to identify bands corresponding to *c*-ring oligomers the samples were also treated with TCA to dissociate them into monomeric *c*-subunits. Protein samples were treated with 5x volume of 15 % (w/v) TCA and incubated on ice

| Antibody | Supplier | Catalogue Number |
|---|---|---|
| Anti-*c*-subunit | Agrisera | AS09 591 |
| Anti-$\beta$-subunit | Agrisera | AS10 1590 |
| Anti-Rabbit IgG HRP conjugated | Promega | W4011 |

**Table 2.7: Primary and Secondary Antibodies**
The antibodies listed here were diluted in TBS-Tween20 + 5 % (w/v) milk and used to incubate protein covered PVDF membranes for western blot analysis. The supplier and corresponding catalogue numbers are also listed. The two ATP synthase specific antibodies bound to the *c*-subunit and the $\beta$-subunit and the secondary antibody was conjugated with horse radish peroxidase for image development.

for 5 mins. The mixture was centrifuged at 23,000 rpm for 5 mins at $4^{\circ}$C and the supernatant removed. The pellet was resuspended in 1x SDS loading buffer and turned a yellow colour due to the acidity. 1 $\mu$L aliquots of 0.5 M NaOH were added until the bromophenol blue colour was restored. Samples were then loaded directly onto gels for SDS-PAGE analysis.

## 2.4 Bioinformatic Methods

### 2.4.1 Synechococcus sp. PCC 7002 DNA Sequences

The genome of *Synechococcus sp.* PCC 7002 and DNA sequences of specific genes were obtained from CyanoBase `http://genome.microbedb.jp/cyanobase/GCA_000019485.1`. The complete genome is also available as NCBI Reference Sequence: NC_010475.1. The *atpE* gene encoding the *c*-subunit of the F-type ATP synthase in *Synechococcus sp.* PCC 7002 is found in the chromosomal DNA at the locus: 768144 to 768389 and has the GeneView ID: SYN-

PCC7002_A0738.

### 2.4.2 Multiple Sequence Alignment of c-subunits

The primary structures of *c*-subunits from a variety of organisms were obtained from UniProt.org database and aligned using AliView alignment viewer and editor software (Larsson 2014). Only *c*-subunits from *c*-rings with known stoichiometries were used in the alignment with the exception of *Synechococcus sp.* PCC 7002 F-type ATP synthase *c*-ring, which was unknown at the start of this project. Known *c*-ring stoichiometries are obtained from existing literature and have been determined by methods such as X-ray crystallography, atomic-force microscopy (AFM) and electron *cryo* microscopy (Meier et al. 2005b, 2007; Pogoryelov et al. 2009; Preiss et al. 2010; Saroussi et al. 2012).

### 2.4.3 Homology Modelling

A homology model of the *Synechococcus sp.* PCC 7002 $F_1F_o$-ATP synthase was generated using the SWISS-MODEL Expasy web-server. The homology model used the spinach chloroplast $cF_1F_o$-ATP synthase structure as a template (PDB ID: 6FKF) (Hahn et al. 2018), performing a pairwise sequence alignment with individual subunits from *Synechococcus sp.* PCC 7002 and spinach chloroplast ATP synthase. The web-server then provided a .pdb file of the generated homology model and was viewed in either PyMol or ChimeraX.

# Chapter 3

# Genome Editing of *Synechococcus sp.* PCC 7002

## 3.1 Introduction

### 3.1.1 Genome-Editing by Homologous Recombination

The genome of *Synechococcus sp.* PCC 7002 can be transformed through homologous recombination by introducing exogenous DNA with a minimum homologous sequence length of approximately 250 bp (Kufryk et al. 2002; Ruffing et al. 2016). Typically a DNA construct is created containing the desired mutation with a selectable marker in between an upstream and a downstream flanking sequences, homologous to the target site in the genome (Pope et al. 2020). The efficiency of homologous recombination transformation, the fast growth rate and tolerance to a wide range of salinities, temperature and light make *Synechococcus sp.* PCC 7002 an attractive chassis strain for industrial applications.

Similar to other cyanobacterial strains, like *Synechocystis* 6803, *Synechococcus* 7002 possesses approximately 3 to 4 copies of its chromosome and endogenous plasmids (Nixon et al. 1992; Pope et al. 2020). The exact number of copies of genetic material can be dependent on certain growth conditions such as salinity and the growth phase at a given time point. Given that cyanobacteria possess several copies of their chromosome, the genomes of transformants must be checked for complete segregation where all copies of the chromosome are accurately mutated and no wild-type sequences remain.

### 3.1.2 CRISPR-Cas Systems

In 2012, the lab groups of Doudna and Charpentier published a paper in *Science* giving details of an adaptive immune system found in archaea and bacteria used to defend against invasive phages, viruses and plasmid DNA (Jinek et al. 2012). The adaptive immune system contained genomic elements of clustered regularly interspaced short palindromic repeats (CRISPR) and an associated effector endonuclease (Cas), and was named CRISPR-Cas. The paper highlighted the potential to exploit this protective system for genome-editing through programmable RNA-guided endonucleases. The endonuclease identified in this paper was Cas9 but other CRISPR-Cas endonucleases have been identified since (Bayat et al. 2018; Zetsche et al. 2015). The result has been the classification of six primary classes of CRISPR-Cas systems: classes I-VI. Classes I, III and IV feature Cas proteins that are multisubunit complexes, while classes II, V and VI are

single-subunit effectors (Koonin et al. 2017; Shmakov et al. 2017).

### 3.1.3 CRISPR-Cas12a

Initially, CRISPR genome-editing techniques have not been used extensively on the genomes of cyanobacteria due to the apparent toxicity of the Cas9 nuclease to cyanobacteria (Wendt et al. 2016). However, Cas12a endonuclease, isolated from *Francisella novicida*, is a less toxic alternative for microbial organisms (Ungerer and Pakrasi 2016). Cas12a (also known as Cpf1) is a type V-A endonuclease from the class II family of CRISPR systems. It is a large protein of around 1,300 amino acid residues and 150 kDa in size and has some key differences compared to the more famous Cas9 (Safari et al. 2019). Crystal and *cryo*EM structures have helped to provide mechanistic insights into how the cleavage of target DNA is achieved and the role of the protospacer adjacent motif (PAM) sequence (Swarts and Jinek 2019; Zhang et al. 2019).

Unlike Cas9 which requires both CRISPR RNA and trans-activating crRNA (crRNA and tracrRNA) to act as the guide RNA (gRNA), Cas12a only requires a single crRNA of approximately 42 nucleotides (nts) to target a particular DNA sequence. Cas12a also makes a staggered cut with a 5'-overhang of about 5 nts compared to blunt end cuts made by Cas9. Additionally, the PAM sites recognised by Cas9 and Cas12a are different; Cas12a recognises a 5'-YTN-3' (5'-CTN-3' or 5'-TTN-3') sequence while Cas9 recognises a 5'-NGG-3' sequence. Genome-editing of cyanobacterium by CRISPR-Cas12a has been demonstrated

in *Synechococcus sp.* PCC 2973 with point mutations, knock-out and knock-in mutations yielding markerless mutant strains (Ungerer and Pakrasi 2016). Therefore, Cas12a is a powerful tool for genome engineering and transcriptional disruption.

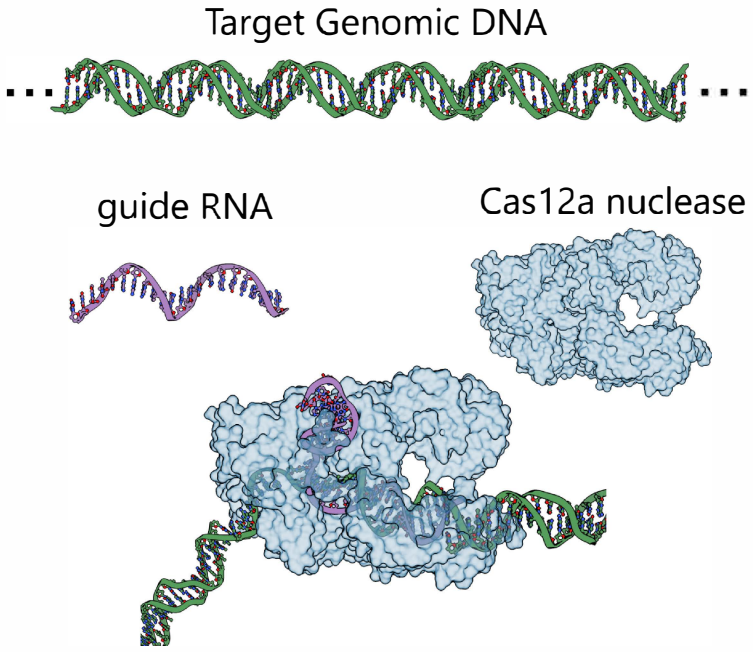


**Figure 3.1: Cas12a effector protein**
The Cas12a effector protein belongs to the class II of CRISPR-Cas systems and is a single-subunit effector. The guide RNA of approximately 42 nucleotides allows the Cas12a nuclease to be targeted to specific sequences in the target genome.

### 3.1.4 CRISPR-Cas12a Genome-Editing of Synechococcus sp. PCC 7002

In this study, CRISPR-Cas12a was used to engineer the $c_n$-ring of the F-type ATP synthase in *Synechococcus sp.* PCC 7002. The experiments were conducted

at Nanyang Technological University, Singapore and were supervised by Artur Włodarcyzk and Tiago Selão, postdocs working in the labs of Peter Nixon and Birgitta Norling.


**Figure 3.2: Desired mutations in Synechococcus sp. PCC 7002 atpE gene**
A multiple sequence alignment of the N-terminal helix of the *c*-subunits from *Synechococcus sp.* PCC 7002, Spinach chloroplasts, SAG 89.79 and *Spirulina platensis*. The mutations to be introduced target the glycine motif (A21G, G23A, G27A, G23/27A - marked by an asterisk) or replace the whole *atpE* gene with the gene from SAG 89.79 or *Spirulina platensis*.

The point mutations selected target the glycine motif found in the N-terminal helix of the *c*-subunit. This is based on observations from previous experiments where it was possible to alter the stoichiometry of the *c*-ring with site-directed mutagenesis of this motif (GxGxGxGxG in *I. tartaricus* or AxAxAxAxA in *B. pseudofirmus* OF4). The motif faces the centre of the *c*-ring and the tight-packing makes it the most narrow point of the central hole. Fig. 3.3 shows some of the key residues involved in tight packing and hydrogen bonding between adjacent *c*-subunits in spinach chloroplast $cF_1F_o$-ATP synthase ($c_{14}$-ring) and the *Spirulina platensis* $F_1F_o$-ATP synthase.

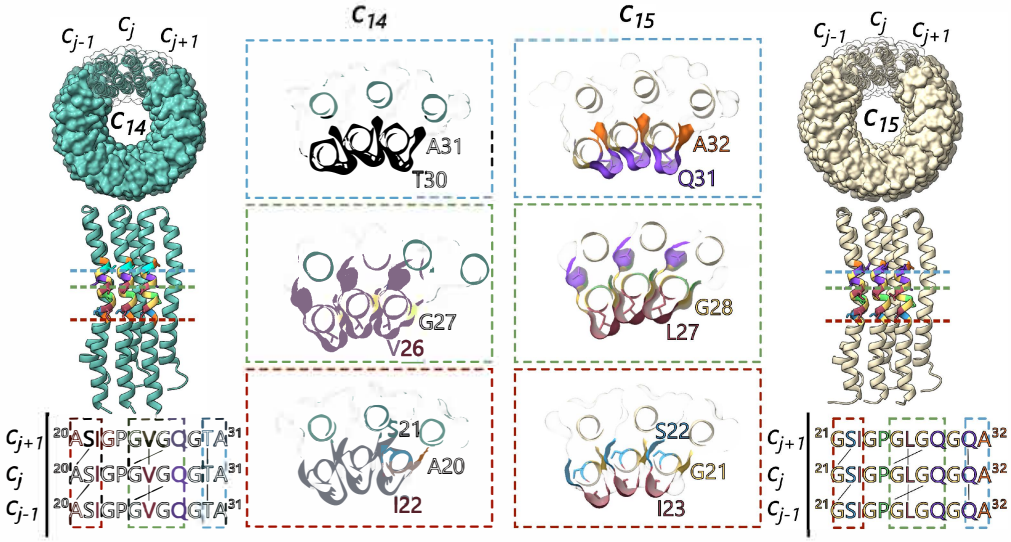


**Figure 3.3: Contacts made by glycine motif in adjacent c-subunits**
The crystal structures of $c_{14}$-ring from spinach chloroplasts and $c_{15}$-ring from *Spirulina platensis* (Pogoryelov et al. 2009; Vlasov et al. 2019). Cross-sections parallel to the membrane are shown at the levels of the coloured dotted lines and residues of the glycine motif are colour-coded with any hydrogen bonds between adjacent subunits indicated with black lines.

## 3.2 Materials & Methods

### 3.2.1 Synechococcus sp. PCC 7002 strains

| Strain name | Species | Description |
|---|---|---|
| *Syn* WT | *Synechococcus* 7002 | Wild-type *Synechococcus sp.* PCC 7002 |
| *Syn* E* | *Synechococcus* 7002 | Conjugated with pSW102-trcE* |
| *Syn* psbA2 | *Synechococcus* 7002 | Conjugated with pSW104-psbA2 |
| *Syn* SP | *Synechococcus* 7002 | CRISPR genome-edited with *atpE* gene from *Spirulina platensis* |

**Table 3.1: Synechococcus sp. PCC 7002 Strains**
A list of the cyanobacterial strains used and obtained throughout the course of this project. *Syn* WT was the starting wild-type strain and was conjugated with either pSW102-trcE* or pSW104-psbA2 plasmids, yielding *Syn* E* and *Syn* psbA2 strains respectively.

### 3.2.2 CRISPR-Cas12a Constructs and DNA sequences

For the constructs used for the CRISPR-Cas12a transformation of *Synechococcus sp.* PCC 7002, two promoters for the Cas12a endonuclease were tested; one was the constitutively active promoter called psbA2 and the second was a theophylline-inducible riboswitch called trcE* (Nakahira et al. 2013; Shibato et al. 1998). These promoters and the coding sequence for Cas12a nuclease were inserted into a pVZ322 cloning vector (NCBI:txid88232) and conjugated into wild-type *Synechococcus sp.* PCC 7002 to give the strains *Syn* E* and *Syn* psbA2.

**Plasmids for CRISPR-Cas12a Transformation**

| Plasmid | Size (kb) | Description |
|---|---|---|
| pSW102-trcE* | 11.0 | Cas12a nuclease with theophylline-induced riboswitch |
| pSW104-psbA2 | 11.0 | Cas12a nuclease with psbA2 constitutive inducer |
| pE001 | 4.1 | Background plasmid with no recovery template |
| pE002_A21G | 4.8 | *atpE* gRNA and A21G recovery template |
| pE003_G23A | 4.8 | *atpE* gRNA and G23A recovery template |
| pE004_G27A | 4.8 | *atpE* gRNA and G27A recovery template |
| pE005_G23/27A | 4.8 | *atpE* gRNA and G23/27A recovery template |
| pE006_SP_c15 | 4.8 | *atpE* gRNA and *Spirulina* recovery template |
| pE007_SAG_c13 | 4.8 | *atpE* gRNA and *Synechococcus* 89.79 recovery template |

**Table 3.2: Plasmids for CRISPR-Cas12a Transformation**
A list of the plasmids used and obtained throughout the course of this project. The DNA for constructing the recovery templates were made by gene synthesis, Twist Bioscience (USA). Primers for cloning were purchased from Microsynth SG (Switzerland).

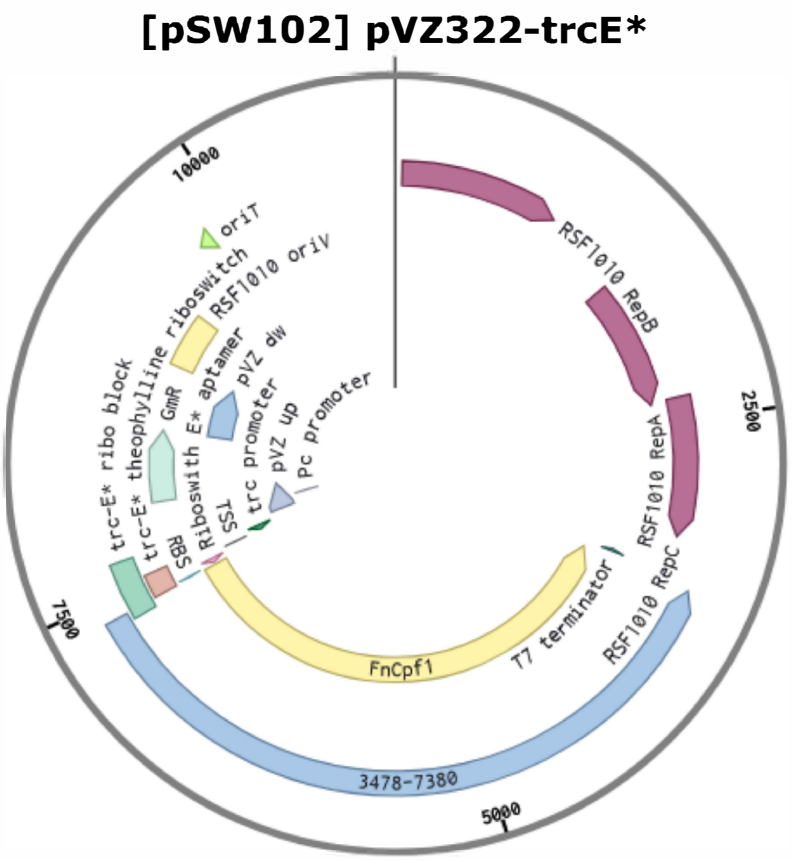


**Figure 3.4: pSW102 plasmid conjugated into Synechococcus sp. PCC 7002**

The gene encoding Cas12a from *Francisella novicida* (aka FnCpf1) was added to either a psbA2 constitutive promoter or a trcE* riboswitch promoter in a pVZ322 cloning vector. These constructs were conjugated into wild-type *Synechococcus sp.* PCC 7002. With these promoters, the production of Cas12a effector nuclease could be induced constitutively (psbA2) or with the addition of theophylline (trcE*).

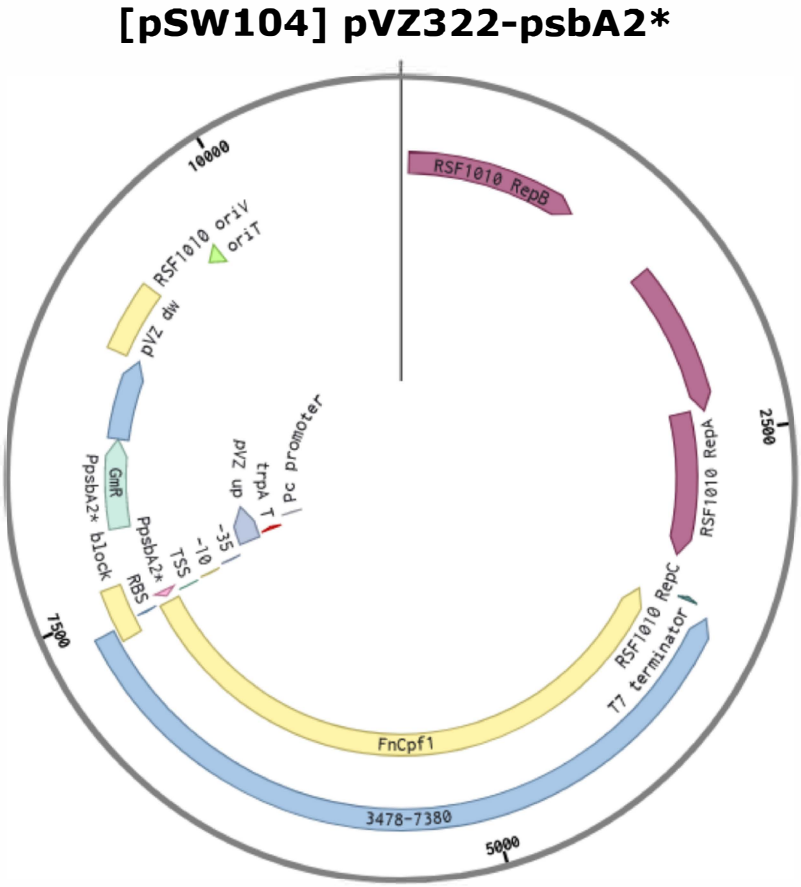


**Figure 3.5: pSW104 plasmid conjugated into Synechococcus sp. PCC 7002**

The gene encoding Cas12a from *Francisella novicida* (aka FnCpf1) was added to either a psbA2 constitutive promoter or a trcE* riboswitch promoter in a pVZ322 cloning vector. These constructs were conjugated into wild-type *Synechococcus sp.* PCC 7002. With these promoters, the production of Cas12a effector nuclease could be induced constitutively (psbA2) or with the addition of theophylline (trcE*).

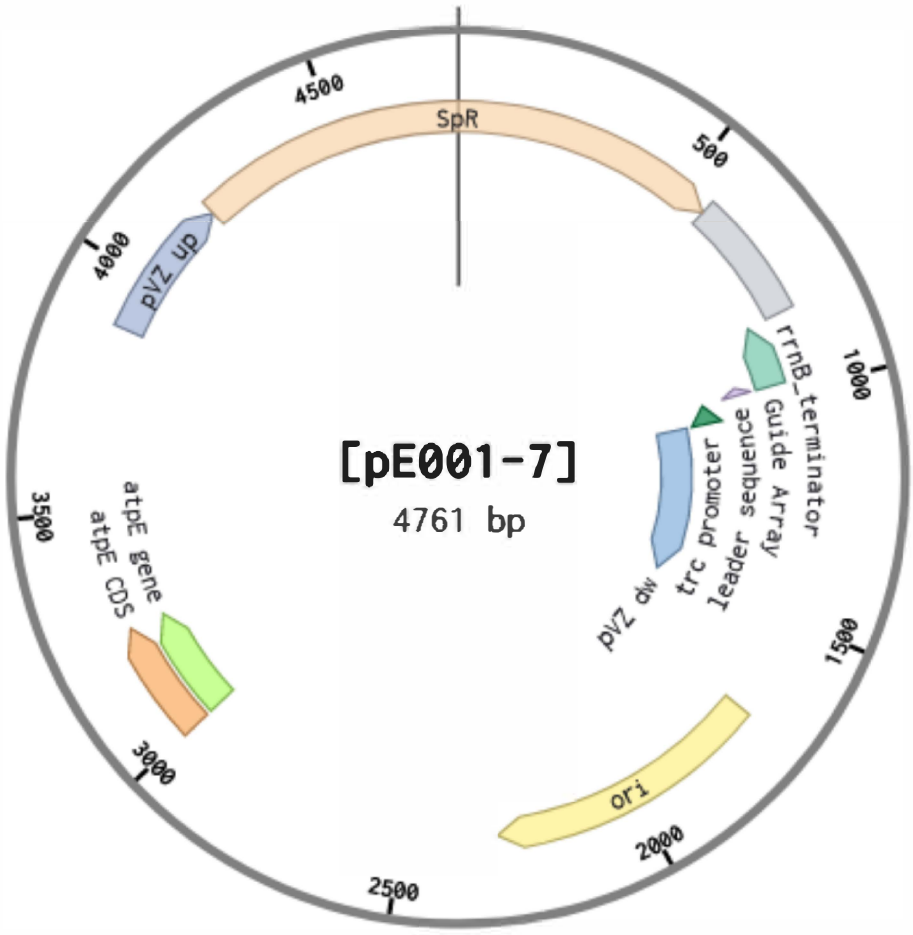


**Figure 3.6: pE001-7 plasmids transformed into Synechococcus sp. PCC 7002**

A guide array targeted the Cas12a nuclease to the *atpE* gene in *Synechococcus sp.* PCC 7002. Meanwhile, a recovery template featuring the mutated or substituted *atpE* genes was also introduced allowing transformation.

### Primers for Genotyping

Primers were ordered from either Microsynth AG (Balgach, SG, Switzerland) or Integrated DNA Technologies (Coralville, Iowa, USA).

| Primer | Sequence (5'-3') | $T_m$(°C) |
|---|---|---|
| mut-F3 | AAATTATGGACAGCTTAACT | 60 |
| mut-R3 | GATGGTGAGGGCTTC | 60 |
| wt_mut-F2 | GTAGATGGTTAAAGCTTC | 55 |
| atpE_wt-R3 | TTGCTGTTGGTCTTG | 55 |
| atpE_wt-F | GGTGAGCTGCCTTTAAAT | 60 |
| Spir-R | GGGCATCGGTTCTATTG | 60 |
| SAG-R | GTTAGCCGTGGGATT | 60 |
| wt_SAG-R | TATTGCTGCTGCTCT | 57 |
| wt_Spir-R | CTCTTGCTGTTGGTC | 57 |

**Table 3.3: Primers for Genotyping**

A list of the primers used for genotyping and checking segregation of CRISPR-Cas12a mutants. Sequences are given in 5'-3' direction and the melting temperature ($T_m$) calculated using the New England BioLabs Tm Calculator. Primers were ordered from either Microsynth AG (Balgach, SG, Switzerland) or Integrated DNA Technologies (Coralville, Iowa, USA)

### 3.2.3 CRISPR-Cas12a Transformation of atpE gene

For the purposes of altering the stoichiometry of the *Synechococcus sp.* PCC 7002 F-type ATP synthase *c*-ring, a number of point mutations were selected (A21G, G23A, G27A and G23+27A) targeting the glycine motif in the N-terminal helix of the *c*-subunit. Additionally two exogenous *atpE* genes were selected to be substituted into the *Synechococcus* genome in place of the native *atpE* gene. Both sources are from photosynthetic cyanobacteria; the first was from SAG 89.79 and the second was from *Spirulina platensis* which have a $c_{13}$ and $c_{15}$-ring respectively. For the CRISPR-Cas12a transformations, all the mutations used the same guide array to target the native *atpE* gene but used unique recovery templates in order to introduce the desired mutations or substitutions and silently mutate any PAM sites to prevent further cleavage by Cas12a.

Starting with the *Syn* E* and *Syn* psbA2 background strains growing in liquid media under gentamycin selection, the cultures were diluted to $OD_{730} \sim 0.2$. Then 300 ng of linear recovery template was added to 1 mL of culture and left to incubate overnight in a growth chamber ($38^{\circ}$C, 1 $\%$ $CO_2$). The following day, 500 ng of pE002-7 plasmid was added and left to incubate overnight. The full 1 mL of transformation culture was plated on A-D7 agar plates supplemented with 25 $\mu$g/mL spectinomycin for *Syn* psbA2 and an additional 0.1 mM theophylline for *Syn* E* (theophylline-induced riboswitch) (Nakahira et al. 2013). Single colonies appeared after 5 days, this was followed by 2 rounds of restreaking onto fresh selection plates; finally colony PCR was used for genotyping and checking segregation.

## 3.3 Results

### 3.3.1 Colony PCR of Transformants

#### Transformant Selection

After the addition of recovery template and addition of pE002-7 plasmids, the transformation cultures were plated onto M-AD7 agar supplemented with 25 $\mu$g/mL spectinomycin (+ 0.1 mM theophylline for *Syn* E*). The number of single colonies visible on each plate after one round of selection are indicated in Table 3.4.

| Syn E* | Single Colonies | Syn psbA2 | Single Colonies |
|---|---|---|---|
| -ve ctrl | 0 | -ve ctrl | 0 |
| A21G | 70 | A21G | 4 |
| G23A | 38 | G23A | 3 |
| G27A | 5 | G27A | 3 |
| G23/27A | 40 | G23/27A | 1 |
| *Spirulina* | 6 | *Spirulina* | 1 |
| SAG 89.79 | 2 | SAG 89.79 | 1 |

**Table 3.4: Single Colony Count of Transformations**
The number of single colonies after one round of selection on spectinomycin (+ theophylline for *Syn* E* transformants) M-AD7 agar plates. Negative controls (-ve ctrl) included the same transformation protocol but without the addition of any recovery template sequences. A lower number of transformants grow on the psbA2 plates

#### Single Colony Genotyping

Single colonies appeared after one day and were picked for genotyping. Primer pairs were designed for colony PCR to distinguish between wild-type sequences

and mutant sequences. The following primer pairs were used with the annealing temperatures indicated in Table 3.3:

- **mut-F3 + mut-R3** to detect A21G, G23A, G27A and G23/27A mutants
- **wt_mut-F2 + atpE_wt-R3** to detect wild-type against point mutants
- **atpE_wt-F + Spir-R** to detect *Spirulina atpE* mutants
- **atpE_wt-F + SAG-R** to detect SAG 89.79 *atpE* mutants
- **atpE_wt-F + wt_Spir-R** to detect wild-type against *Spirulina* mutants
- **atpE_wt-F + wt_SAG-R** to detect wild-type against SAG 89.79 mutants

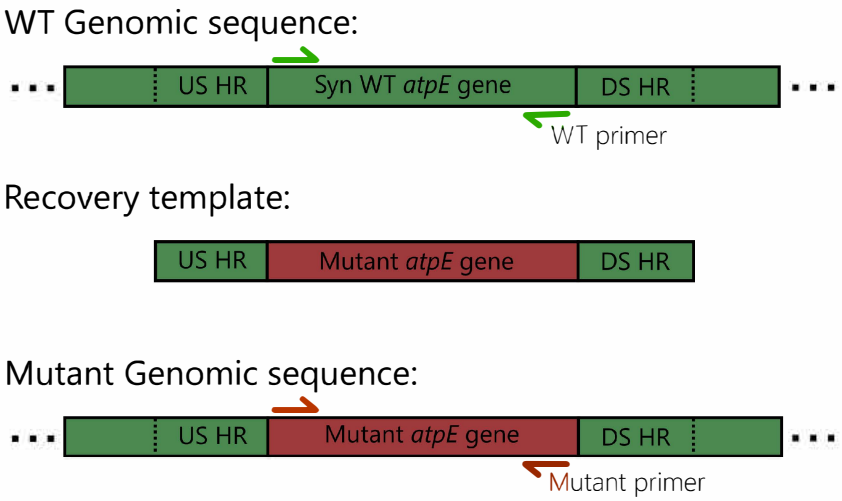


**Figure 3.7: Schematic of Primer binding sites in WT and mutant genomes**
The primer pairs were designed so that at specific annealing temperatures only the wild-type or mutant sequences would be amplified. Each single colony was tested with both pairs of primers to assess the state of segregation of each transformation.

For all transformants, single colonies were picked from selection plates and added to 10 $\mu$L of dd$H_2O$. 0.2$\mu$L of the suspended colonies was used as the template for colony PCR reactions. Colony PCR reactions with the primer pairs indicated above showed the state of genetic segregation in the transformants. As *Synechococcus sp.* PCC 7002 has several copies of its genome, a primer pair binding to the wild-type sequence and a separate primer pair binding to the mutant sequence were used to assess whether all copies of the genome were transformed successfully. The PCR reactions were loaded onto 1 % agarose gels and run for 45 minutes at 100 V.

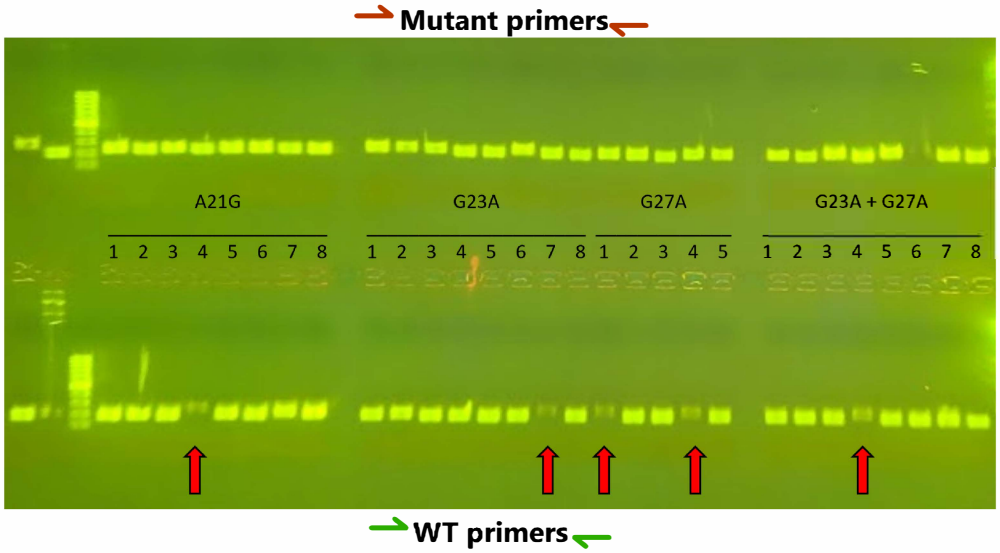


**Figure 3.8: DNA gel of point mutation colony PCR**
Single colonies of the single and double point mutation transformants were picked and used as templates for colony PCR. Positive controls used the pE002 plasmid as template as this contained the recovery template with the mutant sequence, and the negative control used a *Syn* WT colony as template.

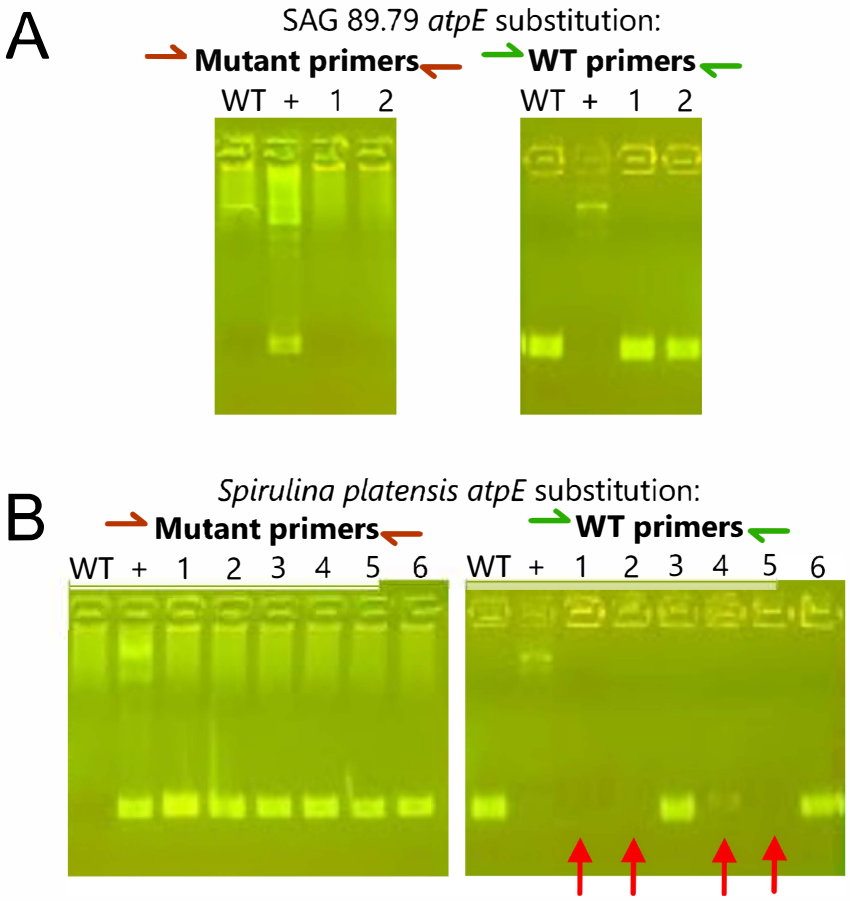


**Figure 3.9: DNA gel of SAG 89.79 and Spirulina mutant colony PCR** Single colonies of the single and double point mutation transformants were picked and used as template for colony PCR. Positive controls used the pE006 and pE007 plasmids as template containing the recovery template with the mutant sequences, and the negative control used a *Syn* WT colony as template. Fully segregated mutants with the *Spirulina atpE* gene substitution are indicated with red arrows.

The DNA gel Fig. 3.8 shows the colony PCR products for the point mutations on the *atpE* gene with the WT (bottom lanes) and mutant (top lanes) primer pairs. Single colonies appearing on the selection plates possess at least one copy of the mutant sequence. However the bottom lanes also show that the wild-type sequence remains in at least one copy of the genome. The colonies with

red arrows appear to have very low yields of wild-type PCR products and were selected for further analysis by DNA sequencing. DNA sequencing results from these PCR products confirm the partial segregation with wild-type sequence still present, this manifests in an ambiguous sequencing trace at the silently mutated PAM sites and at the point mutation sites Fig. 3.10.


**Figure 3.10: DNA sequencing trace of A21G mutant colony PCR**
An example sequencing trace of a partially segregated A21G *atpE* mutant. The PAM site at amino acid position 3 contains a mixed population of both the $_{1}$ATGGACA**GC**$_{9}$ wild-type sequence and the $_{1}$ATGGACA**CT**$_{9}$ mutant sequence. Similarly with the A21G point mutation site, both the wild-type and mutant sequences are present.

Colony PCR of the *Spirulina* and SAG 89.79 transformants, Fig. 3.9, reveal that the SAG 89.79 *atpE* substitution did not give any segregated mutants while four of the six colonies on the *Spirulina atpE* substitution plate were fully segregated. The transformed *atpE* genes were confirmed through sequencing (Source BioScience, Nottingham).

## 3.4 Discussion

### 3.4.1 Fn-Cas12a promoter choice

Two promoters for the *Francisella novicida* Cas12a nuclease tested in this study were the constitutively active psbA2 promoter and the trcE* theophylline-induced riboswitch (Englund et al. 2016; Nakahira et al. 2013). As CRISPR/Cas12a genome editing has not been tested extensively, the purpose of selecting two different promoters was to assess whether a constitutively active promoter leading to a constantly present Cas12a nuclease would increase the transformation efficiency. The theophylline-induced riboswitch system only expresses Cas12a nuclease in the presence of theophylline.

The transformations and subsequent colony PCR experiments suggest that a background presence of the Cas12a nuclease with the psbA2 promoter hinders transformation efficiency compared to inducing Cas12a with theophylline after adding the guide array and recovery template DNA. The energetic and metabolic burden of constitutively synthesising Cas12a and having an unnecessary endonuclease present in the cell may provide a selection pressure that guides *Synechococcus sp* PCC 7002 to develop strategies for minimising the energetic burden and limiting the Cas12a's ability to access and cleave DNA. For example, the organism may be able to export the Cas12a nuclease through the general secretory pathway (Sec) or the twin-arginine translocation (Tat) system (Frain et al. 2019; Russo and Zedler 2020; Tsirigotaki et al. 2017). These adaptations are less likely to occur if the Cas12a nuclease is controlled by an inducible riboswitch and only present during the short window of the CRISPR transformation. Overall, it

is not clear why the transformation with the trcE* promoter had a higher efficiency than the psbA2 promoter in this particular case but it is likely that the background levels of Cas12a in the organism and the timings of these levels can affect transformation efficiency.

### 3.4.2 Glycine motif on atpE gene in Synechococcus sp. PCC 7002

In a previous study the importance of the glycine motif in the *c*-subunit of ATP synthase was investigated by using site-directed mutagenesis to mutate glycine residues into larger residues such as alanine in the bacterium *Ilyobacter tartaricus* (Pogoryelov et al. 2012). *Ilyobacter tartaricus* was originally isolated from the canal waters of Venice and possesses a $Na^+$-binding F-type ATP synthase with 11 *c*-subunits in its *c*-ring (Meier et al. 2005b; Neumann et al. 1998). In (Pogoryelov et al. 2012), a number of point and double point mutations were targeted to the glycine motif ($^{25}$GIGPGVGQG$^{33}$) (Fig. 3.11), and out of these a mutant with a G25A substitution and separate mutant with G29A and a $c_{12}$-ring was observed. Here it was shown that the G25A mutation removes a site of hydrogen bonding between the inner and outer helices and the G29A mutation disrupts the spacing at the inner helices. Both mutations were individually able to increase *c*-ring stoichiometry.

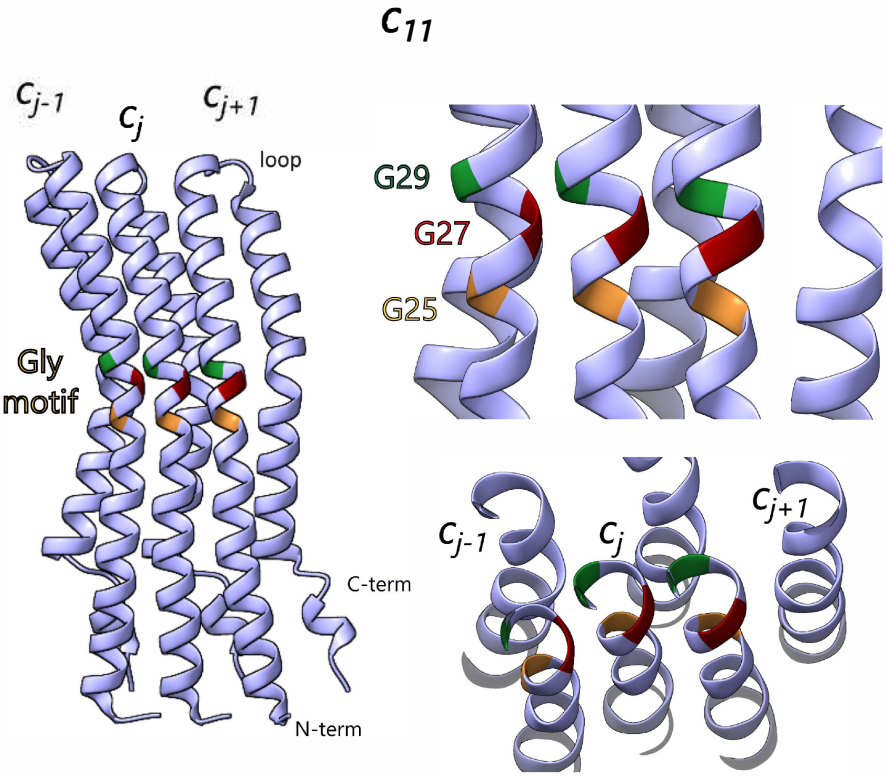


**Figure 3.11: Targeting the Glycine motif to change c-ring stoichiometry** This figure depects three adjacent *c*-subunits from a $c^{11}$-ring. The $c^{11}$-ring from *Ilyobacter tartaricus* can increase in stoichiometry when substituting alanines for glycines at the glycine motif found in the N-terminal alpha-helix. G25 is coloured yellow, G27 is coloured red and G29 is coloured green.

In a separate study, a decrease in *c*-ring stoichiometry was demonstrated in the alkaliphilic *Bacillus pseudofirmus* OF4 which has a relatively large $c_{13}$-ring and mostly alanine residues at the site of the glycine motif ($^{14}$AVAGAIAVA$^{22}$). Here, a A16/20G double mutant yielded a $c_{12}$-ring and a X-ray crystallographic structure at 4.1 Å, revealed a tighter packing of the inner helices in the mutant ring (Preiss et al. 2013). With these two studies in mind, the glycine motif was once again targeted but in a photosynthetic organism, *Synechococcus sp.* PCC 7002.

The point mutations targeting the glycine motif (A21G, G23A, G27A, G23/27A) in the *c*-subunit of *Synechococcus sp.* PCC 7002 did not give rise to fully segregated mutants. Colony PCR and sequencing of any single colonies appearing on selection plates after CRISPR-Cas12a transformation show that the wild-type *atpE* sequence remains in at least one copy of the genome. A possible reason is that the point mutations attempted in *Synechococcus sp.* PCC 7002 yielded unstable *c*-rings that had a deleterious effect on the function of the F-type ATP synthase and therefore the survival of the organism. As the F-type ATP synthase in *Synechococcus sp.* PCC 7002 is so essential for both photosynthesis and respiration an unstable *c*-ring would have a very strong selective pressure against it. This selection pressure would have been acting against the selection pressure of having a Cas12a nuclease targeting the wild-type *atpE* gene and only partially segregated mutants were observed.

### 3.4.3 Introducing exogenous atpE genes into Synechococcus sp. PCC 7002

The SAG 89.79 *atpE* substitution into *Synechococcus sp.* PCC 7002 was unable to generate fully segregated or even partially segregated mutants. While the transformation with the *Spirulina platensis atpE* gene produced 4 fully segregated mutants. A similar observation was recently made in tobacco chloroplast transformations (Yamamoto et al. 2023). In this paper, we collaborated with Hiroshi Yamamoto and Toshiharu Shikanai from Kyoto University, Japan, who

kindly sent wild-type and mutant tobacco seeds to London where we could isolate the *c*-rings and show *c*-ring band shifts on SDS-PAGE (Fig 3A - *Plant Physiology* 2023, kiad143).

The mutations targeting the *c*-subunit gene in tobacco chloroplasts, aimed to make similar mutations to match the SAG 89.79 and *Spirulina platensis* glycine motifs, produced an albino plant for SAG 89.79 and a fully segregated mutant for *Spirulina platensis*. Again, this is an indication that a functional F-type ATP synthase is not being formed in the mutants with *c*-subunits similar or identical to the *c*-subunit found in SAG 89.79. For higher plants, such as tobacco this affects the ATP synthase involved in photosynthesis and not respiration but the effect is still dramatic and the albino mutants are unable to produce seeds. In contrast, a *Synechococcus sp.* PCC 7002 mutant with a malfunctioned ATP synthase would have both photosynthesis and respiration severely hindered and may be unable to survive.

From this point onwards, only the wild-type *Synechococcus sp.* PCC 7002 (*Syn* WT) and the *Synechococcus sp.* PCC 7002 mutants expressing the *Spirulina platensis c*-subunit (*Syn* SP)were studied further. All four fully segregated mutant colonies isolated from the CRISPR/Cas12a transformation were confirmed by sequencing and cryo-preserved by flash-freezing with 5 % DMSO in liquid nitrogen and storing at $-70^{\circ}$C.

# Chapter 4

# Structural Characterisation of Synechococcus sp. PCC 7002 $F_1F_o$-ATP synthase

## 4.1 Introduction

Following its successes in the field of chemistry, X-ray crystallography turned towards biology and the structure of proteins. It is now over six decades since the first protein structure, sperm whale myoglobin, was determined by X-ray crystallography (Kendrew et al. 1958) and today the Protein Data Bank holds over 200,000 structures in its collection. The ability to determine the precise locations of individual atoms in proteins has provided countless insights into life at the molecular level and helped to deepen our mechanistic understanding of biology. Significant advances in electron microscopy for biological samples include a reliable method to vitrify samples in liquid ethane (Dubochet et al.

1982), a maximum-likelihood approach to determine relative orientations from large datasets (Sigworth 1998), direct-electron detectors reducing the effect of beam-induced motion (Elmlund and Elmlund 2015; Wu et al. 2016),

Due to its essential role in bioenergetics, the F-type ATP synthases from bacterial, chloroplast and mitochondrial sources have been studied for over 60 years with many structural and biochemical methods (Junge and Nelson 2015; Kühlbrandt 2019; Stewart et al. 2013; Walker 2013). The earliest partial structures obtained were determined by X-ray crystallography and limited by which components of ATP synthase were crystallisable, of particular note are the $\alpha_3\beta_3\gamma$ subunits of $F_1$ (Abrahams et al. 1994) and the membrane rotor ring (Meier et al. 2005b). Owing to its size of at least 500 kDa and a significant membrane-embedded $F_o$ region, a completely intact ATP synthase has eluded crystallisation.

### 4.1.1 The "Resolution Revolution"

In recent years, the "resolution revolution" brought about by technological and computational advances in single-particle electron *cryo*-microscopy (*cryo*EM) (Kühlbrandt 2014), have allowed the structures of many key membrane complexes and supercomplexes in bionergetics to be determined (Kampjut and Sazanov 2020; Laughlin et al. 2019; Naschberger et al. 2022; Zhu et al. 2016). New statistical methods and algorithms to improve the maximum-likelihood alignments and 3D variance bootstrapping (Lyumkis et al. 2013; Zhang et al. 2008) have coupled with the the new generation of direct-electron detectors to push the

field to higher and higher resolutions with a wider range of samples. The previous detectors were charge-coupled detectors (CCDs) which convert electrons into photons which can be detected, while direct-electron detectors can detect the electrons directly and more rapidly reducing blur from beam-induced motion. Previously, *cryo*EM worked best for large proteins larger than 200 kDa as the requirement to keep electron doses low to preserve the integrity of biological samples limited the signal-to-noise ratio. This lower size limit has shifted in recent years with structures of smaller proteins such as a 3.8 Å structure of the 93 kDa isocitrate dehydrogenase, 2.8 Å structure of lactate dehydrogenase (145 kDa) (Merk et al. 2016) and a 3.2 Å structure of haemoglobin (64 kDa) (Khoshouei et al. 2017). As of 2020, single-particle *cryo*-EM reached atomic resolution with a 1.22 Å structure of mouse apoferritin and also showed the technique was capable in the field of membrane proteins with a 1.7 Å reconstruction of the $\beta$3 $GABA_A$ receptor (Nakane et al. 2020).

### 4.1.2 CryoEM and ATP synthase

Recently determined EM structures also include a number of complete ATP synthase complexes from a wide range of bioenergetic systems, including the chloroplast $cF_1F_o$-ATP synthase (Hahn et al. 2018), bacterial $F_1F_o$-ATP synthases (Demmer et al. 2022; Guo et al. 2019; Sobti et al. 2019), and mitochondrial $mtF_1F_o$-ATP synthase dimers (Mühleip et al. 2020; Murphy et al. 2019; Spikes et al. 2020). Our mechanistic understanding of ATP synthase has been greatly improved by these structural studies. Studies using electron *cryo* tomography

techniques have also offered insights into the localisation and supra-molecular arrangement of ATP synthase in various energy-transducing membranes (Daum et al. 2010; Davies et al. 2014; Wietrzynski et al. 2020).

Both X-ray crystallography and *cryo*EM approaches to structural biology require the purification of the target enzyme from either natural sources or expressed in a suitable expression system. From these sources the laborious task of purification begins with careful considerations required to maintain optimal pH, temperatures and buffer conditions to obtain a highly pure and homogenous sample. Compared to soluble proteins an additional complication exists for membrane proteins such as ATP synthase, where purification requires the extraction of the enzymes from membranes by solubilisation with detergents. As with many other protein complexes, the difficulties involved in the production and purification of ATP synthases remains one of the major bottlenecks in structural biology studies (Kühlbrandt 2022).

In this study, *cryo*EM was used to confirm the change in *c*-ring stoichiometry in the F-type ATP synthase of *Synechococcus sp.* PCC 7002 caused by substituting the native *atpE* gene with the *atpE* gene from *Spirulina platensis*. The first step was to establish a robust and reliable purification protocol for the *Synechococcus* $F_1F_o$ ATP synthase. As affinity purification of other bacterial ATP synthases had previously been effective in the TM lab (Demmer et al. 2022), a 6x polyhistidine-tag was added to the N-terminus of the *atpD* gene encoding the $\beta$-subunit in *Synechococcus* by traditional cloning methods (Nixon et al. 1992). CRISPR-Cas12a genome-editing was then used to introduce point mutations or

replace the *atpE* gene in *Synechococcus sp.* PCC 7002 with the *atpE* gene from *Spirulina platensis* or *Synechococcus elongatus* SAG 89.79.

## 4.2 Materials & Methods

### 4.2.1 Purification of Synechococcus $F_1F_o$ ATP synthase

#### Solubilisation of $F_1F_o$ ATP synthase from Thylakoid Membranes

Frozen thylakoid membrane samples were thawed and added to an equal volume of solubilisation buffer (20 mM Tricine-NaOH pH = 8.0, 200 mM sucrose, 100 mM NaCl, 5 mM $MgCl_2$, 300 mM $(NH_4)_2SO_4$, 0.2 mM $Na_2$-ATP, 2 % lauryl maltose neopentyl glycol (LMNG)[1 % final]) and solubilised for 30 mins at $4^{\circ}$C with gentle rocking. Insoluble material was removed by ultracentrifugation at 55,000 rpm for 1 hour at $4^{\circ}$C (Ti70 rotor). The supernatant was collected and went onto affinity chromatography.

#### Affinity Purification of $F_1F_o$ ATP synthase

A gravity column was prepared with 2 mL bed volume of Chelating Sepharose Fast Flow resin (GE Healthcare) and charged with 5 mL of 100 mM $NiCl_2$. The column was equilibriated with 2 x column volume of Background buffer (35 mM Tricine-NaOH pH = 8.0, 50 mM NaCl, 3.5 mM $MgCl_2$, 0.1 mM $Na_2$-ATP, 0.005 % LMNG). Protein samples solubilised in 1 % LMNG were run over the column for 1 hour at $4^{\circ}$C with a peristaltic pump. The column was washed with 40

mL Background buffer + 10 mM imidazole. To elute the His-tagged sample 1 x column volume of Background buffer + 100 mM imidazole was applied to the column.

### Concentrating Protein samples

Eluted fractions containing $F_1F_o$ ATP synthase were pooled and concentrated with Amicon Ultra-15 filter concentrator 100,000 MWCO (Merck Millipore) equilibriated with Background buffer and pre-cooled to $4^{\circ}$C. Samples in concentrator were spun at 1,000 rpm for 10 mins at $4^{\circ}$C.

### Peptidisc Reconstitution of $F_1F_o$ ATP synthase

Concentrated purified samples were reconstituted into peptidiscs by adding peptidisc to the protein sample in a 2:1 (w/w) ratio. The mixture was incubated on ice for 5 mins and then centrifuged at 22,500 rpm for 10 mins at $4^{\circ}$C (Carlson et al. 2018; Demmer et al. 2022).

### Size Exclusion Chromatography

Affinity purified ATP synthase reconstituted into peptidiscs were loaded onto a Superdex 200 10/300 GL (Cytiva) column equilibriated with background buffer for gel filtration. The background buffer contained no detergent (35 mM Tricine-NaOH (pH = 8.0), 3.5 mM $MgCl_2$, 50 mM NaCl, 0.1 mM $Na_2$-ATP). Eluted fractions containing proteins were pooled and went onto electron microscopy for

structural characterisation.

### 4.2.2 Negative Stain Electron Microscopy

Purified ATP synthase samples were diluted 0.2x to an approximate protein concentration of 0.01 mg/mL and 3.5 $\mu$L was pipetted onto the carbon side of freshly glow discharged carbon film 400 mesh 25 grids (Agar Scientific). The sample was left to absorb for 60 seconds before adding 90 $\mu$ of freshly filtered 2 % uranyl acetate (w/v) and left suspended face down for 2 minutes. Filter paper was used to blot away excess uranyl acetate from the copper side of the grid and left for 5 minutes to dry. The negative stain grids were viewed using a T12 Tecnai G2 Spirit microscope (Thermo Scientific).

### 4.2.3 Electron cryo-microscopy

The freezing of grids for electron *cryo*-microscopy, operation of the Krios and Glacios microscopes and data processing were performed by Ben Phillips of the TM lab. I am extremely grateful for all the time and training Ben kindly provided me on this project. We also thank Nora Cronin and Paul Simpson for managing the EM facilities at the London Centre for Electron Microscopy (LonCEM) and the Imperial College Centre for Structural Biology (CSB) respectively.

After optimising a purification protocol for both the wild-type (*Syn* WT) and mutant (*Syn* SP) ATP synthases and checking the homogeneity of the ATP

synthase particles with SDS-PAGE and negative stain electron microscopy, the samples were freshly prepared from thylakoid membranes in one day and frozen on grids for electron *cryo*-microscopy. Lacey carbon grids with an ultrathin carbon support film (3 nm) (Agar Scientific) were glow discharged for 60 seconds before adding 3 $\mu$L of purified sample with a protein concentration of 0.05 mg/mL, using a Vitrobot IV (Thermo Scientific / Field Electron and Ion Company (FEI)). The blotting was performed in a humidity chamber held at 95 % humidity and $4^{\circ}$C. The grids were plunge frozen in liquid ethane. Images of the frozen grids were collected with either an FEI Glacios microscope at the Imperial College Centre for Structural Biology (CSB) or a Titan Krios G3 microscope at the London Centre for Electron Microscopy (LonCEM).

### 4.2.4 Cryo-EM and Data Processing

Image processing of the collected datasets was performed in CryoSPARC v3.3.2 for both *Syn* WT and *Syn* SP samples. The initial step for both samples was to correct for beam-induced motion and the dose-weighted correction images were generated from the collected movies using CryoSPARC Patch Motion Correction software. CryoSPARC Patch CTF Estimation was then used to determine contrast transfer function (CTF) parameters for each movie. ATP synthase particles were picked automatically from a trained Topaz model. Multiple rounds of two-dimensional classification were then used to clean the dataset and remove unwanted particles before *ab initio* three-dimensional reconstruction.

## 4.3 Results

### 4.3.1 Purification of Synechococcus sp. PCC 7002 ATP synthase

The purification of the F-type ATP synthase from *Synechococcus sp.* PCC 7002 was an important aspect of this project and essential for the structural characterisation of the wild-type and mutant F-type ATP synthases. As the mutations only centred around the membrane-embedded *c*-subunit it was assumed that an optimised purification protocol utilising an affinity tag on the three $\beta$-subunits in the soluble $F_1$-domain would be applicable for both the *Syn* WT and *Syn* SP enzymes. The final purification protocol included the thylakoid membrane isolation outlined in the Materials and Methods chapter and the purification starting from frozen thylakoid membranes outlined in the Materials and Methods section of this chapter.

The purification outlined in these sections is the final iteration of a lengthy process of repeated purifications and optimising different conditions. The end goal of this purification was to obtain structural evidence of a shift in *c*-ring stoichiometry of the F-type ATP synthase caused by the alteration of the *c*-subunit.

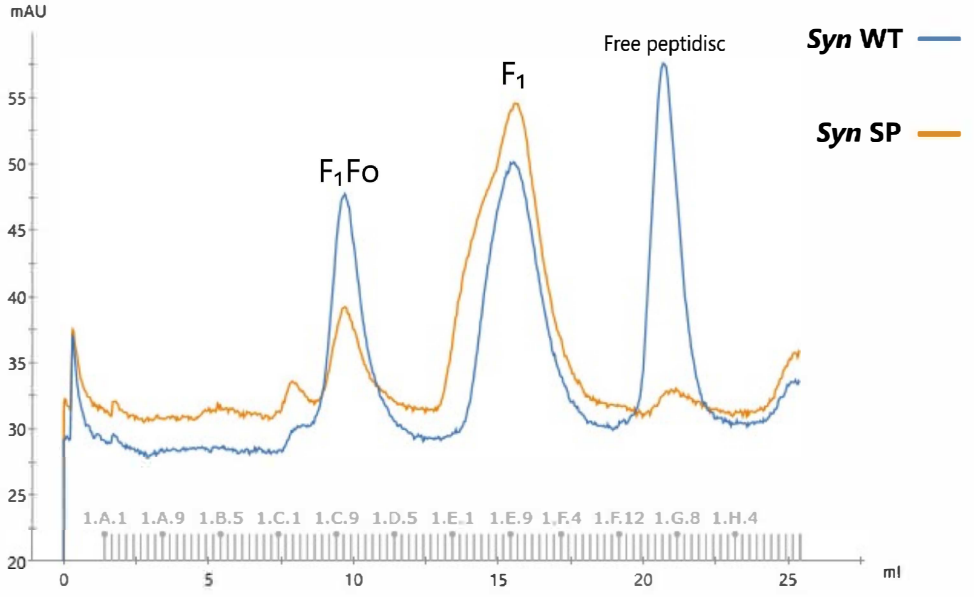


**Figure 4.1: Size exclusion chromatography**
After thylakoid membrane isolation, solubilisation, affinity chromatography and peptidisc reconstitution the final step in the purification of the $F_1F_o$-ATP synthases from both *Syn* WT and *Syn* SP was size exclusion chromatography using a Superdex 200 10/300 GL column (Cytiva) on an ÄKTA Pure system (Cytiva).

The gel filtration traces from the ÄKTA Pure 4.1 of both the *Syn* WT and *Syn* SP purifications are comparable. With three distinct peaks: the first eluted peak contained intact $F_1F_o$-ATP synthase while the second peak contained just the soluble $F_1$-domain subunits. The final peak contained free peptidiscs. A single fraction containing the $F_1F_o$ at the leading edge of the peak was selected for SDS-PAGE and clear-native PAGE analysis before electron microscopy.

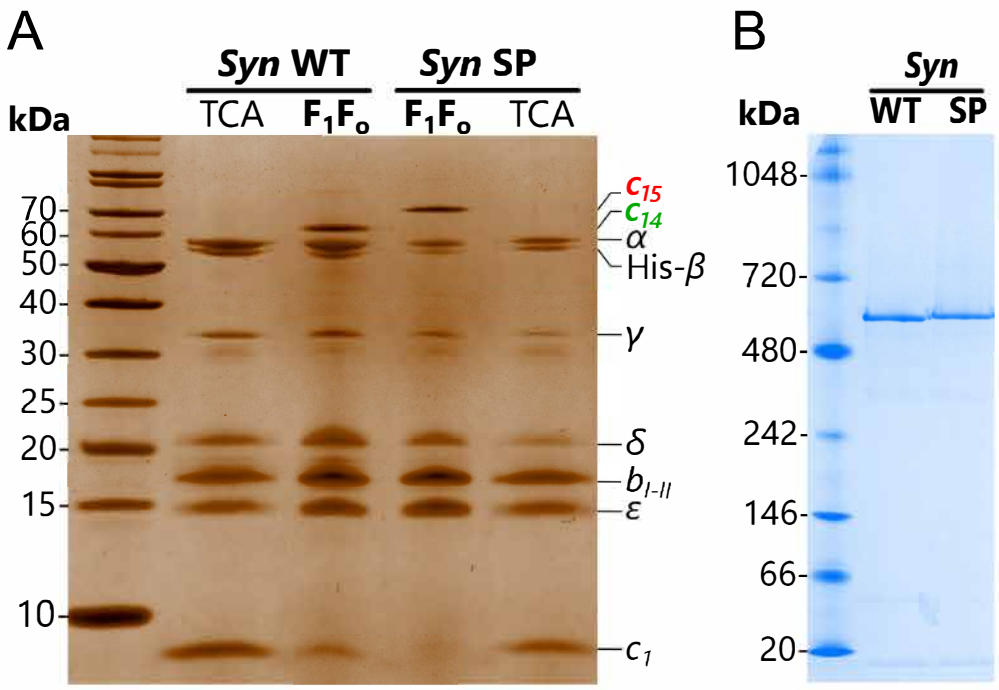


**Figure 4.2: SDS-PAGE and Clear-Native PAGE of Purified ATP synthases**

The $F_1F_o$-ATP synthases from both *Syn* WT and *Syn* SP were purified side by side and analysed by SDS-PAGE (**A**) and Native-PAGE (**B**). As some *c*-rings are SDS-stable the wild-type $c_{14}$ and the mutant $c_{15}$-rings can be seen in their oligomeric state on SDS-PAGE and this is confirmed by treating the same sample with trichloroacetic acid (TCA) which dissociates the rings into individual *c*-monomers. Native-PAGE analysis shows both enzymes are complete and intact after the purification. In both the SDS-PAGE and Native-PAGE we see the additional *c*-subunit (8 kDa) in the *Syn* SP mutant enzyme causing a slight band shift indicating a larger size.

| Subunits | Size (kDa) |
|---|---|
| $\alpha$ | 54.1 |
| His-$\beta$ | 53.0 |
| $\gamma$ | 34.7 |
| $\delta$ | 20.2 |
| $\epsilon$ | 14.4 |
| *a* | 27.1 |
| *b* | 19.0 |
| *b'* | 17.8 |
| *c* | 7.9 |
| $\alpha_3\beta_3\gamma\delta\epsilon$*abb'*$c_{14}$ | 566.5 |
| $\alpha_3\beta_3\gamma\delta\epsilon$*abb'*$c_{15}$ | 574.4 |
| $\alpha_3\beta_3\gamma\delta\epsilon$ | 390.6 |
| *abb'*$c_{14}$ | 175.9 |
| *abb'*$c_{15}$ | 183.8 |

**Table 4.1: ATP synthase Subunit and Subcomplex Sizes**
The theoretical masses of the individual subunits of *Synechococcus sp.* PCC 7002 F-type ATP synthase as well as the theoretical masses of the entire $F_1F_o$-ATP synthase and $F_1$-, $F_o$-subcomplexes.

The purified samples were run on SDS-PAGE and clear-native-PAGE gels, band shifts caused by a single additional 8 kDa *c*-subunit in the *Syn* SP mutant *c*-ring and the intact $F_1F_o$ complex are visible Fig.4.2A. After CRISPR-Cas12a genome-editing and sequencing, the SDS-PAGE and native-PAGE gels were the first indications that a chimeric F-type ATP synthase of the wild-type *Synechococcus sp.* PCC 7002 enzyme combining with the exogenous *S. platensis* $c_{15}$-ring.

### 4.3.2 Single-particle Electron Cryo-Microscopy

#### Data Collection

The *Syn* WT cryo-grids were imaged using an FEI Glacios microscope at the Imperial College Centre for Structural Biology (CSB). This microscope is equipped with a Falcon IV detector and Selectris energy filter. 4,539 images were collected using EPU EM software (Thermo Scientific / FEI) at a calibrated pixel size of 1.10 Å and a total dose of 40 $e^-/Å^2$.

For the *Syn* SP mutant sample, images were recorded at the London Centre for Electron Microscopy (LonCEM) on a Titan Krios G3 microscope (Thermo Scientific / FEI) (25th March 2022). This microscope was operated at 300 kV and used a Gatan K3 direct electron detector in electron counting mode at a calibrated pixel size of 0.412 Åin the super-resolution mode. Altogether 14,629 dose-fractionated movies were recorded using the EPU software for single-particle analysis with a total electron dose of 60 $e^-/Å^2$.

#### Data Processing

Collected datasets were processed in CryoSPARC v3.3.2 for both *Syn* WT and *Syn* SP samples. The data processing followed the schemes outlined in Fig. 4.3 and Fig. 4.4.

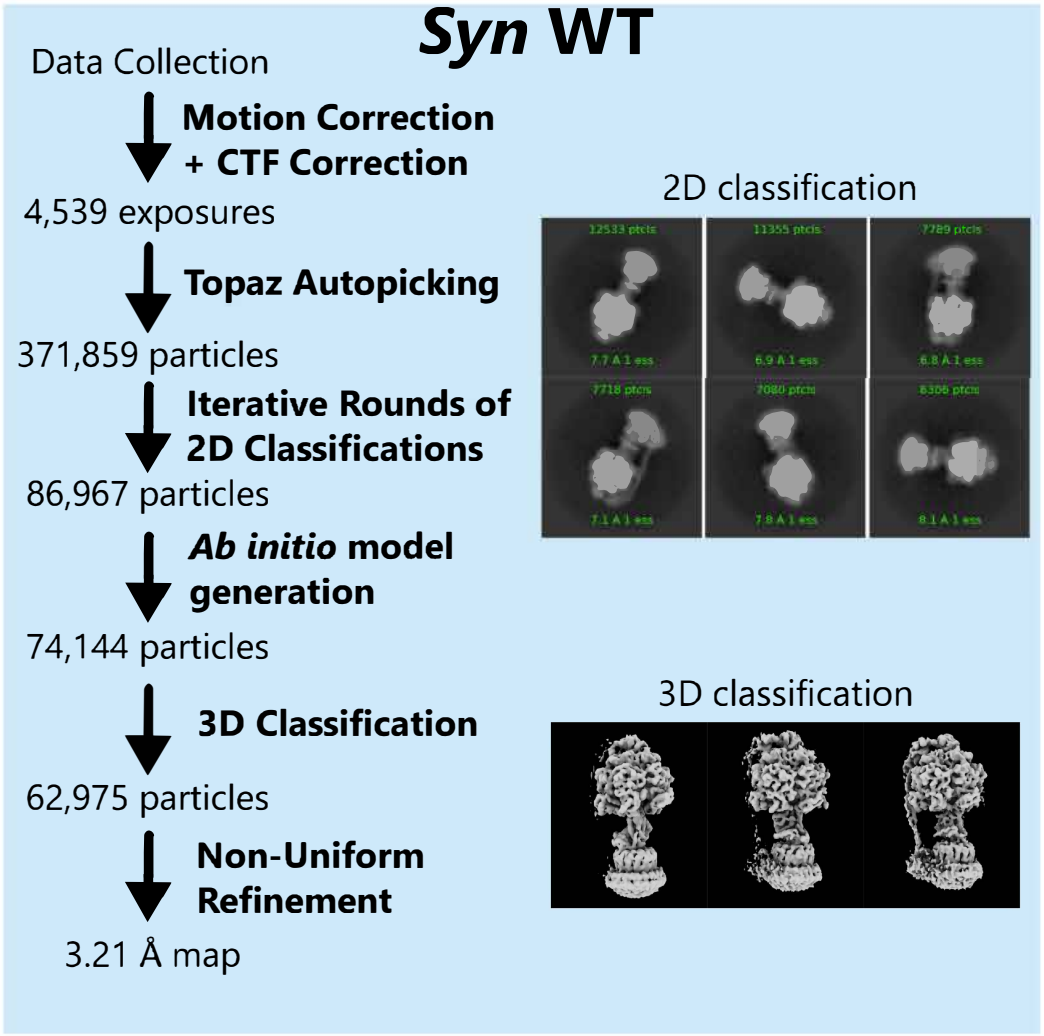


**Figure 4.3: Data processing workflow for Syn WT**

Overall workflow for processing data for single-particle analysis of *Syn* WT. 371,859 particles were picked using a trained Topaz model from 4,539 micrographs. After 2D classification and 3D classification a final 3.21 Å was obtained.

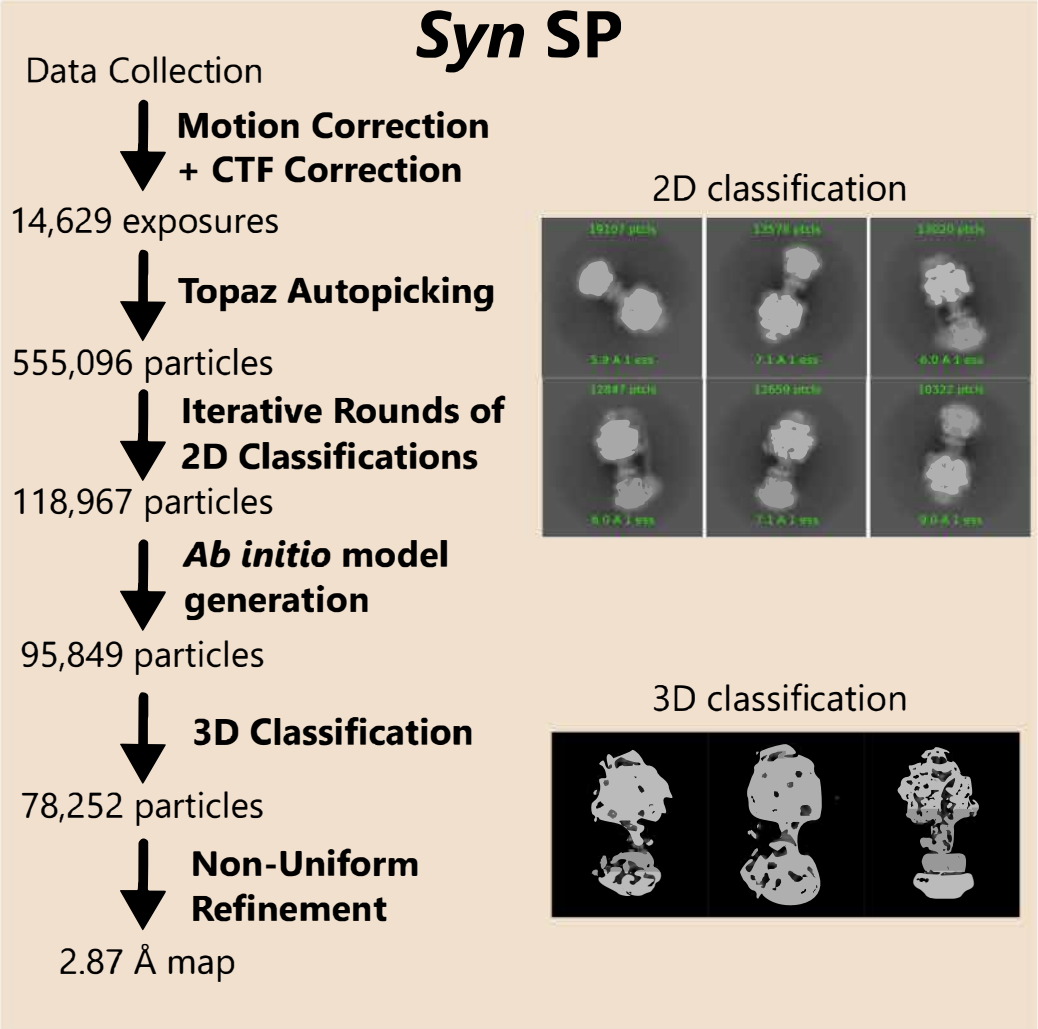


**Figure 4.4: Data processing workflow for Syn SP**

Overall workflow for processing data for single-particle analysis of *Syn* SP. 555,096 particles were picked using a trained Topaz model from 14,629 micrographs. After 2D classification and 3D classification a final 2.87 Å was obtained.

The resolution across the final maps for both *Syn* WT and *Syn* SP were not uniform and the $F_1$ soluble domains are resolved at a higher resolution than the peripheral stalks and membrane-embedded $F_o$ region.

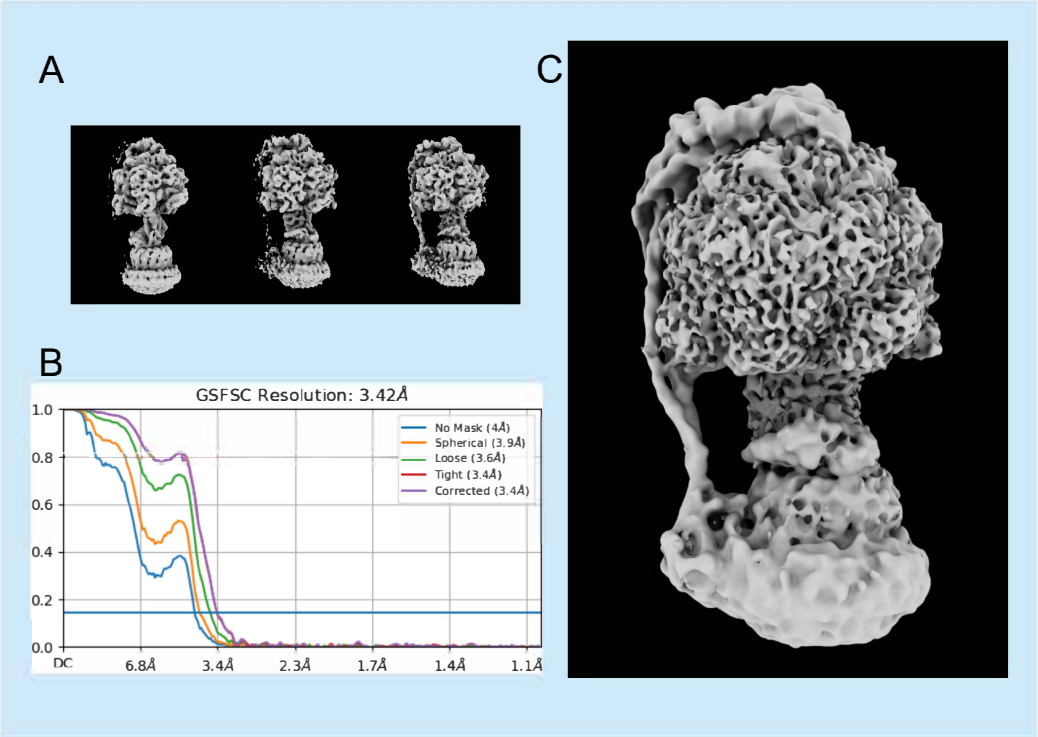


**Figure 4.5: 3D classifications and final map of Syn WT ATP synthase** (A) 3D classifications used for reconstruction. (B) The final Fourier Shell Correlation curves are also shown with and without different masks. The horizontal line shows the 0.143 threshold. (C) The final electron potential map for *Syn* WT ATP synthase.

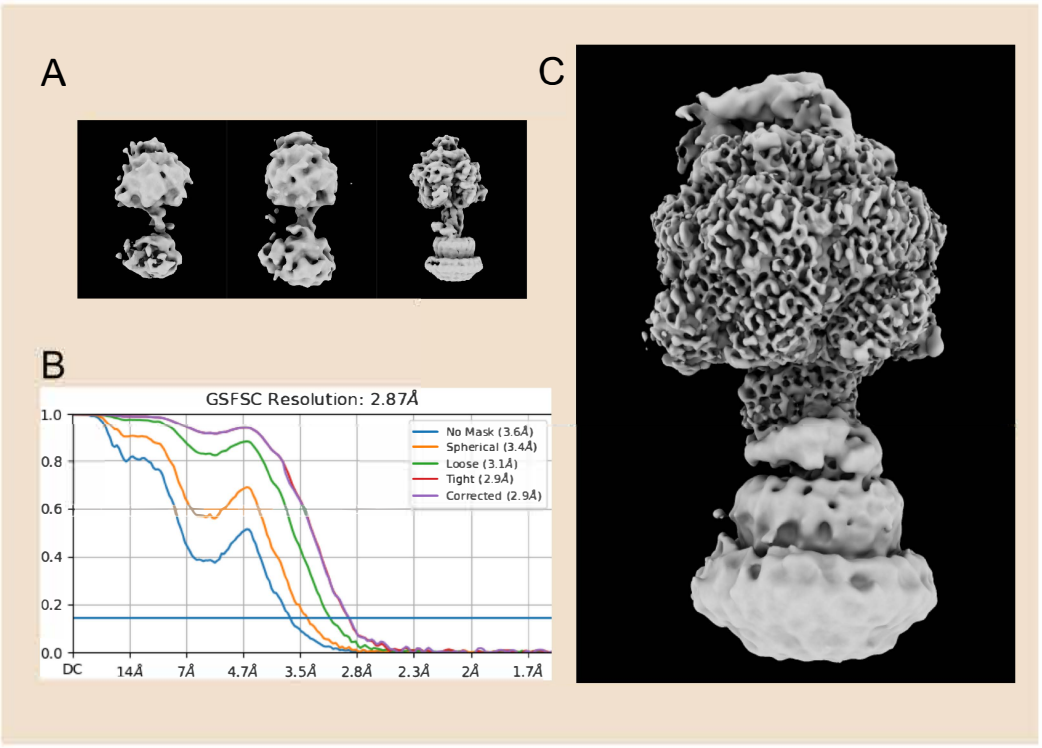


**Figure 4.6: 3D classifications and final map of Syn SP ATP synthase** (A) 3D classifications used for reconstruction. (B) The final Fourier Shell Correlation curves are also shown with and without different masks. The horizontal line shows the 0.143 threshold. (C) The final electron potential map for *Syn* SP ATP synthase.

### 4.3.3 Determination of c-ring stoichiometry

Despite the lower resolution in the $F_o$ region in both maps, the resolution was sufficient to count the stoichiometry of the *c*-rings. The cross-section through the *c*-rings 4.7 confirm a $c_{14}$-ring stoichiometry for *Syn* WT and a $c_{15}$-ring stoichiometry for *Syn* SP. This can be seen for both the inner and outer helices of each *c*-subunit.

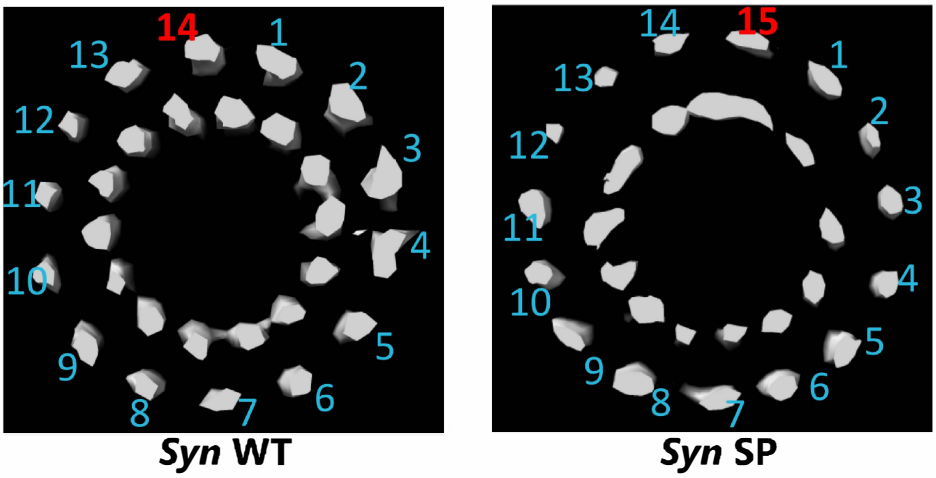


**Figure 4.7: Cross-section through c-rings from Syn WT and Syn SP**
A cross-section parallel to the membrane of the electron density close to the *c*-subunit loops facing the $\gamma$-subunit. From this the *Syn* WT can be seen to possess a $c_{14}$-ring and *Syn* SP a $c_{15}$-ring.

## 4.4 Discussion

### 4.4.1 Purification of cyanobacterial ATP synthase

The purification of the $F_1F_o$-ATP synthase from *Synechococcus sp.* PCC 7002 followed many of the fundamental principles of membrane protein purification, particularly for large membrane complexes. The notable difference between purifying membrane proteins and soluble proteins is the need to solubilise the membrane proteins in a suitable detergent. The detergents are selected to disrupt protein-lipid interactions but leave the protein undisturbed while keeping protein-protein interactions. Over the years a wide array of detergents with different chemical properties have been tested to find the best conditions for solubilising membrane proteins but it is not possible to say one detergent is universally more effective than the others. For now, it is necessary to treat each membrane protein on a case-by-case basis and screen many detergents to find the most suitable for extracting the proteins from their native membrane environments.

Drawing from existing literature, a number of solubilisation conditions and detergents were tested with parameters such as the detergent of choice, temperature and time of solubilsation being optimised. Other bacterial ATP synthase purifications had used digitonin (*E. coli*) (Sobti et al. 2020a), trans-4-(trans-4-propylcyclohexyl)cyclohexyl-$\alpha$-d-maltoside (tPCC-$\alpha$-M) *A. baumannii* (Demmer et al. 2022). A synthetic alternative to digitonin also exists, glyco-diosgenin (GDN), and has been successfully used to solubilise ATP synthase from mitochondria e.g. (Mühleip et al. 2020; Spikes et al. 2020). Previous purifications of chloroplast and cyanobacterial ATP synthases had used tPCC-$\alpha$-M (Hahn et

al. 2018) and n-Dodecyl-$\alpha$-D-maltoside (DDM) (Seelert et al. 2000). After the detergent screens, the 1 % LMNG, $4^{\circ}$C for 30 mins condition was selected for the remainder of the purifications in the project, LMNG was also the detergent used to solubilise the F-type ATP synthase from another cyanobacterium, *Synechocystis sp* 6803 (Kondo et al. 2021).

After solubilisation, the wild-type $F_1F_o$-ATP synthase from *Syn* WT and mutant $F_1F_o$-ATP synthase from *Syn* SP were purified via affinity chromatography and a final size exclusion clean up step. Reconstituting the enzymes in peptidiscs (Carlson et al. 2018) helped to remove the detergent background in micrographs taken of frozen grids and ultimately improved the signal-to-noise of the data. Peptidisc reconstitution has been successful in structural studies in another bacterial ATP synthase (Demmer et al. 2022). From the final maps we see the peptidiscs form a belt around the *c*-ring closer to the lumenal face than the stromal face.

### 4.4.2 Quality of electron potential maps

To avoid over-fitting in single particle analysis of electron *cryo*-microscopy a low-pass filter is usually applied which excludes all high-resolution frequencies beyond a pre-defined cutoff (e.g. a 10 Å filter removes any data that is less than 10 Å ). However, low-pass filtering alone does not sufficiently prevent over-fitting and further steps must be taken (Scheres and Chen 2012). The so-called "gold standard" Fourier Shell Correlation (FSC) procedure involves carrying out two independent analyses of two halves of the data (Henderson et al. 2012). As the

two half datasets were separated from the outset the electron potential maps calculated can be compared and FSC curves can be plotted to show the spatial frequencies at which the two calculated maps disagree. The calculated FSC ranges from 0 to 1, with 0 being complete disagreement of the two maps and 1 being complete agreement. Looking at FSC curves it has been generally agreed that, in the absence of over-fitting, the spatial frequency at which the FSC value drops below the threshold of 0.143 is the most comparable indicator of the resolution of the EM map to X-ray crystallographic data (Rosenthal and Henderson 2003).

Applying the gold-standard FSC procedure and 0.143 threshold to the *Syn* WT and *Syn* SP datasets we arrive at a 3.21 Å for the *Syn* WT ATP synthase and a 2.87 Å map for the *Syn* SP map, however these resolutions are not uniform throughout the whole complex. For both the wild-type and mutant enzymes the membrane-embedded regions and the peripheral stalk are less well resolved than the soluble core of the $F_1$-region. The likely cause of this is the inability to separate the three main confirmations of the ATP synthase. The conformations arise from the three most significant energy minima of the rotation during catalysis. Typically one conformation is the most populated while the other two fonromations have significantly fewer particles (Demmer et al. 2022; Hahn et al. 2018). As the three conformations are not separated during data processing in the *Syn* WT and *Syn* SP reconstructions we observe a lower resolution as all three positions of the individual subunits are averaged across the datasets. In an attempt to separate the three conformations and to improve the resolution further in the $F_o$ and peripheral stalk regions of the maps, masks were applied

to try to align particles on certain subunits and regions only. However, this was unable to separate the three conformations.

### 4.4.3 Future strategies to improve resolution

To improve resolution further, larger datasets may have to be collected as the two lesser populated conformations may not have contained enough particles to allow them to be correctly separated. However, more particles does not necessarily equate to better resolution and further improvements in sample preparation and freezing conditions can also be considered. For example, on the collected micrographs detached $F_1$ head groups could be observed even though these should have been removed by the size exclusion step immediately prior. It is likely that these $F_1$ heads become detached during the freezing step and different blotting times and blotting forces could help reduce this as well as adding different additives such as detergents at low concentrations to the sample prior to freezing.

Even though a larger dataset was collected for the *Syn* SP sample and more particles were picked (555,096 for *Syn* SP and 371,859 for *Syn* WT), the membrane-embedded region and peripheral stalk are actually less well resolved in the *Syn* SP sample. This may point to inherent instability of the chimeric *Syn* SP $F_1F_o$-ATP synthase complex. The number of particles picked is comparable to the number picked in the spinach chloroplast $cF_1F_o$-ATP synthase structure (Hahn et al. 2018) which used Relion autopicking to pick 670,614 particles and after 3D alignments had 167,171 particles in conformation 1 (the most populated confor-

mation), 15,395 particles in conformation 2 and 14,409 particles in conformation 3.

The purpose of obtaining further improvements in resolution for the cyanobacterial enzyme must also be questioned given the fact that a high-resolution map of the chloroplast enzyme already exists (Hahn et al. 2018), which has a 61 % sequence identity to the *Synechococcus sp.* PCC 7002 enzyme across all subunits. Furthermore for this particular project, resolution was only required to provide an answer to the biological question of how many *c*-subunits are in the *c*-rings of the F-type ATP synthase in *Syn* WT and *Syn* SP. Nevertheless, the two maps presented here are currently the best available for any cyanobacterial ATP synthase and also for any non-WT chimeric ATP synthase.

### 4.4.4 Confirmation of ATP synthase c-ring stoichiometries

Despite the lower resolutions in the membrane regions, both maps are sufficiently resolved to count the individual *c*-subunits in the *c*-rings. The $c_{14}$ in the *Syn* WT ATP synthase and $c_{15}$ in the *Syn* SP ATP synthase confirm the expected stoichiometries of the multiple sequence alignment against other cyanobacterial *c*-subunits with known stoichiometries and the expectation that primary structure of the *c*-subunit inherently confers *c*-ring stoichiometry (Pogoryelov et al. 2007, 2009).

The single-particle *cryo*EM analysis also shows structurally that a chimeric $F_1F_o$-

ATP synthase was formed in the *Syn* SP mutant. This supports the observed native PAGE data (Fig. 4.2) and the fact that the $c_{15}$-ring was purified alongside the other 7 ATP synthase subunits. This also adds to the previous demonstrations of chimeric ATP synthase enzymes being formed (Laubinger et al. 1990).

In summary, the cryoEM data collected on the wild-type and mutant $F_1F_o$-ATP synthases provided strong evidence for the suspected $c_{14}$-ring and $c_{15}$-ring in *Syn* WT and *Syn* SP respectively. This allowed further characterisation to investigate the effect of an increase in *c*-ring stoichiometry in ATP synthases involved in photosynthesis.

# Chapter 5

# Biochemical and Biophysical Characterisation of Synechococcus sp. PCC 7002 F-type ATP synthase

## 5.1 Introduction

### 5.1.1 The Chloroplast and Thylakoid membranes

Believed to share a common ancestor with cyanobacteria and arising from endosymbiosis, the chloroplast organelle hosts the thylakoid membrane in which the majority of membrane-embedded complexes involved in oxygenic photosynthesis are found (Kirchhoff 2019; Vries and Archibald 2017). The thylakoid membrane and inner membrane of the chloroplast define the stroma and lumen compart-

ments of chloroplasts. The thylakoids are arranged in stacks called grana of about 300-600 nm in diameter and are connected by a continuous network of stromal lamellae (Minges and Groth 2020; Staehelin and DeWit 1984). There is a lateral heterogeneity in the composition of membrane protein complexes across the thylakoid membrane, with photosystem II (PSII) and its associated light-harvesting complex II (LHCII) occupying the grana stacks and photosystem I (PSI) and ATP synthase located in the unstacked stromal lamellae (Daum et al. 2010).

Electron *cryo*-tomography studies have confirmed this lateral heterogeneity but the exact biochemical reason is not completely understood (Daum et al. 2010; Wietrzynski et al. 2020). However the steric hinderances caused by the protrusion of PSI and ATP synthase components out of the membrane, render these two complexes incompatible with tightly stacked membranes in the grana (Nevo et al. 2012). As opposed to the flatter profiles of PSII and LHCII which allow them to sit in membranes that are more tightly packed (Pribil et al. 2014). The smaller cytochrome $b_6f$ complex can be found in both appressed and non-apressed membranes.

### 5.1.2 The Chloroplast F-type ($cF_1F_o$) ATP synthase

The $cF_1F_o$ ATP synthase found in chloroplasts and the $F_1F_o$ ATP synthase found in the thylakoid membranes of cyanobacteria closely resemble the simplest form of ATP synthase, the bacterial F-type ATP synthase, in that they are monomeric

ATP synthases and have the classical $\alpha_3\beta_3\delta\gamma\epsilon$ subunits in $F_1$ and *abb'c*$_{8\text{-}15}$ composition in the membrane-embedded $F_o$ (Hahn et al. 2018). The slight difference in composition is that the $cF_1F_o$ ATP synthase has two similar but distinct *b*-subunits (*bb'*) while bacterial ATP synthase has two copies of the same *b*-subunit. Overall the $cF_1F_o$ ATP synthase is also comparable in size to the bacterial ATP synthase at approximately 540 kDa (Hahn et al. 2018; Kühlbrandt 2019). However, there are some unique aspects of the F-type ATP synthases found in photosynthetic organisms, including a redox regulation loop in the $\gamma$-subunit and a larger-than-average membrane rotor ring (Cheuk and Meier 2021; Hahn et al. 2018; Pogoryelov et al. 2007; Yang et al. 2020).

### 5.1.3 Regulation of ATP synthases

The reversible catalytic activity of the ATP synthase means that regulatory mechanisms exist to prevent wasteful hydrolysis of ATP under certain conditions. In the case of mitochondria a small peptide known as IF1 can dimerise and form an anti-parallel coiled-coil which can bind to $F_1$ to inhibit ATP hydrolysis (Cabezón et al. 2001; Cabezón et al. 2000). When a sufficient *pmf* is available the direction of rotation reverses and the IF1 dimer is ejected to allow ATP synthesis (Bason et al. 2011).

A number of different regulatory mechanisms exist in bacteria. In proteobacteria, such as *Paracoccus dentrificans*, a protein called $\zeta$-subunit acts in a similar way to IF1 to inhibit ATP hydrolysis (Morales-Rios et al. 2015). Under anoxic

conditions, some bacteria consume ATP produced from glycolysis to operate the ATP synthase in the hydrolysis direction and maintain the *pmf* for other important cellular functions such as cell motility and transmembrane transport of nutrients. In these bacteria, ATP synthase is mostly regulated by the $\epsilon$-subunit in the central stalk (Kato-Yamada et al. 1999; Laget and Smith 1979; Yagi et al. 2009). The $\epsilon$-subunit forms an N-terminal globular domain, composed mostly of $\beta$-sheets, and a C-terminal hairpin made of two $\alpha$-helices (Murakami et al. 2018; Yagi et al. 2007). The C-terminal hairpin can adopt an "up" or "down" conformation where the "up" conformation extends into the catalytic hexamer in $F_1$ and inhibits ATP hydrolysis.

### Redox Regulation of Chloroplast ATP synthase

In chloroplasts, the $\gamma$-subunit possesses an additional 40 amino acid insert (compared to all other species, Fig. 5.1), which forms an L-shape with two $\beta$-hairpins capable of inhibiting ATP hydrolysis through interaction with the $\beta$DELSEED-motif, Fig. 5.2 (Kondo et al. 2021). A disulfide bridge between two Cys residues is redox regulated by thioredoxin (Hisabori et al. 2013; Nikkanen et al. 2018; Wolosiuk and Buchanan 1977). The formation of this disulfide bridge under oxidising conditions (typically in darkness) leads to inhibition of ATP hydrolysis due to the $\gamma$- redox loop clashing with the $\beta$DELSEED motif. After the initial structure of spinach chloroplast ATP synthase (Hahn et al. 2018), the *cryo*-EM structure of the chloroplast ATP synthase was solved in both an oxidised and reduced state by locking the reduced state with the uncompetitive inhibitor, tentoxin (Yang et al. 2020).

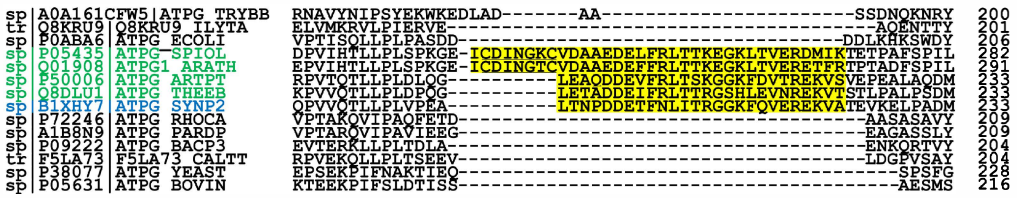


**Figure 5.1: Multiple sequence alignment of $\gamma$-subunits**

The approximately 40 amino acid insert present in the $\gamma$-subunits of the F-type ATP synthases from photosynthetic organisms are highlighted in yellow. *Synechococcus sp.* PCC 7002 is labelled in a blue font. In spinach chloroplasts the $\gamma$Cys$^{240}$ and $\gamma$Cys$^{246}$ form a redox regulated disulfide bridge.

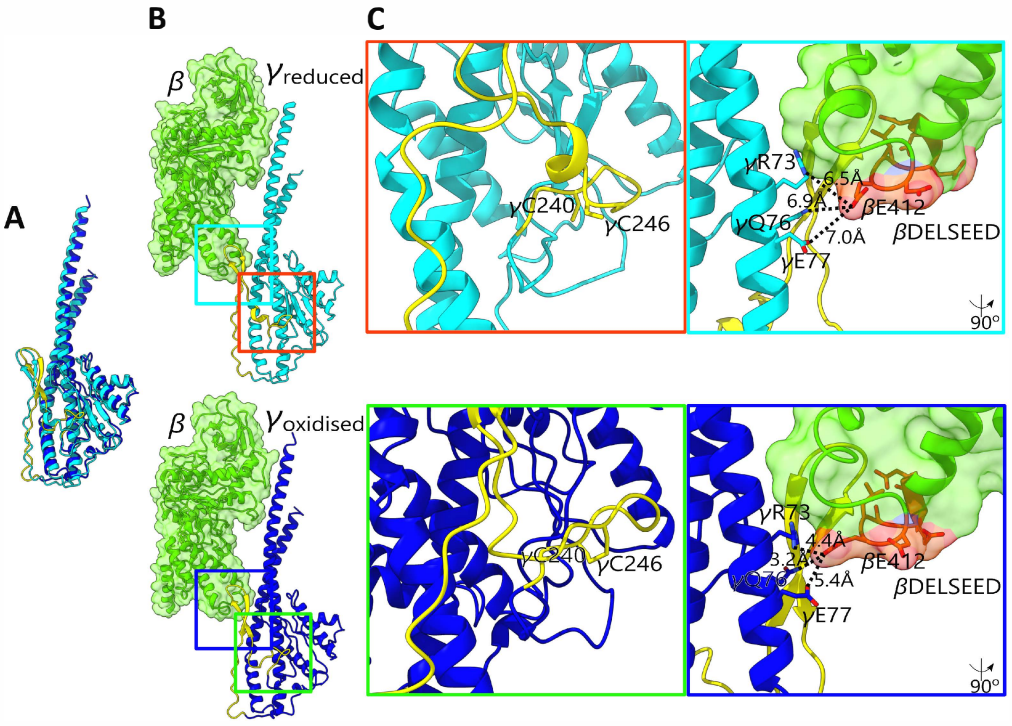


**Figure 5.2: Redox regulation of chloroplast ATP synthase by the $\gamma$-subunit**
Adapted from Figure 3 in (Cheuk and Meier 2021). (A) Overlay of the oxidised and reduced conformations in dark blue and cyan respectively. (B) The 40 amino acid insert forms an L-shape of two $\beta$ hairpins seen in yellow and interacts with the $\beta$-subunit (green). (C) In the dark, the $\gamma$Cys$^{240}$ and $\gamma$Cys$^{246}$ are oxidised (green box) forming a disulfide bridge leading to the longer $\beta$ hairpin clashing with the $\beta$-DELSEED motif when rotating in the ATP hydrolysis direction. In the light, the two Cys residues are reduced and there is no clash between the $\gamma$-subunit and the $\beta$-DELSEED motif.

### ATP synthase Regulation in Cyanobacteria

The regulation of cyanobacterial ATP synthase is less well understood than the redox regulation in chloroplast. From the multiple sequence alignment of the $\gamma$-subunits (Fig. 5.1) we see that the cyanobacterial ATP synthase $\gamma$-subunit also contain an insertion in the gloubular region of the $\gamma$-subunit like the chloro-

plast subunit. However the cyanobacterial $\gamma$-subunit is missing the two Cys residues which form the redox dependent disulfide bridge (Cozens and Walker 1987; Werner et al. 1990). In the case of cyanobacteria the concerted interaction of the $\epsilon$-subunit and $\gamma$-subunit inhibits ATP hydrolysis (Akiyama et al. 2019; Kondo et al. 2021). Truncations of parts of the C-terminal domain of $\epsilon$-subunit have shown that only the N-terminal globular domain is required inhibit ATP hydrolysis (Inabe et al. 2019).

A less well-known and recently identified form of inhibition is through a small protein highly conserved in cyanobacteria known as Atp$\theta$ (Song et al. 2022). The exact mechanism of inhibition is unknown but the ATP hydrolysis activity in isolated ATP synthases was inhibited in a dose-dependent manner. Cyanobacteria uniquely combine respiratory chain complexes and photosynthetic chain complexes on the same thylakoid membranes and the identification of Atp$\theta$ shows how not all ATP synthase regulatory mechanisms are known.

### 5.1.4 Membrane Rotor Ring Stoichiometries

Another unique aspect of the ATP synthases from photoautotrophs can be found in the membrane-embedded $F_o$ motor. The *c*-ring oligomer formed of *c*-subunits rotates against the $ab_2$ stator while protons sequentially bind to each of the *c*-subunits. The protons access the *c*-ring through two adjacent but spatially and electrochemically separated aqeous half-channels in the *a*-subunit (Vik and Antonio 1994). The positive charge from a highly conserved arginine residue ensures

dissociation of protons upon reaching the second half-channel (Hahn et al. 2018).

Currently, the available evidence strongly points towards a $c_n$-ring stoichiometry which is entirely dependent on the primary structure of the *c*-subunit and therefore remains constant within a given species but variable across different species (Meier et al. 2005a; Müller et al. 2001a; Pogoryelov et al. 2009; Preiss et al. 2010). Firstly, heterologously expressing *c*-rings from exogenous sources in *E. coli* yields non-native stoichiometries (*E. coli* = $c_{10}$) (Meier et al. 2005a, 2007; Schulz et al. 2017). Furthermore, functional chimeric ATP synthases can be formed when expressing non-native *c*-subunits (obtained through mutagenesis or from a different source organism) in place of the native *c*-subunit, the $c_n$-ring stoichiometry matches the stoichiometry of the source organism.

An individual *c*-subunit is a hairpin of two transmembrane helices connected by a short loop and is around 7-8 kDa in size. Upon oligomerisation to form the *c*-ring, the N-terminal helix arranges to face the central cavity of the ring while the C-terminal helix forms the outside surface of the ring exposed to the membrane environment (Fig.5.3). An ion-binding site is formed at the interface between two adjacent *c*-subunits about half-way up the outside of the ring with a highly conserved glutamate residue responsible for ion-binding. The arrangement and stoichiometry of the $c_n$-ring therefore determines the number of ions/protons translocated across the membrane upon completion of a full $360^\circ$ rotation because the rotational torque generated is transferred to the catalytic $F_1$-head group during ATP synthesis via the central stalk ($\gamma\epsilon$-subunits), and the number of catalytic $\beta$-subunits is fixed at three. In this way, the *c*-ring stoi-

chiometry directly dictates a parameter known as the *ion-to-ATP* ratio.

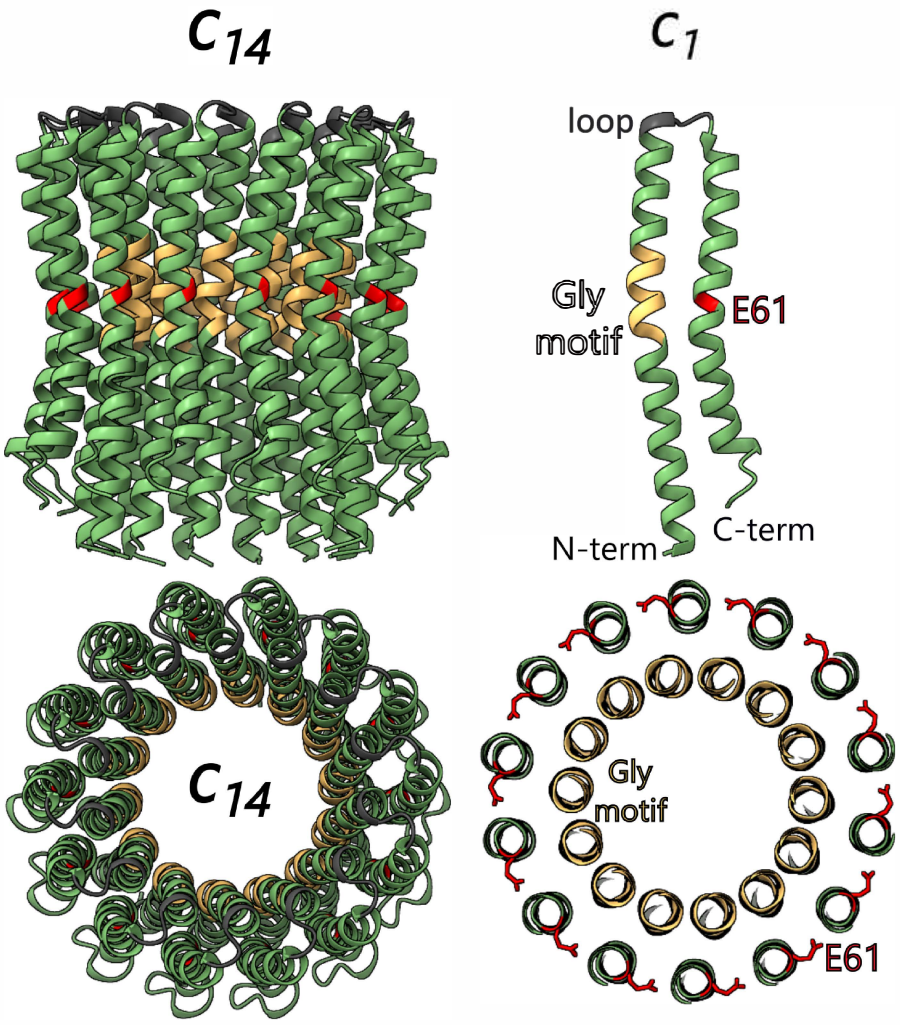


**Figure 5.3: The $c_{14}$-ring from spinach chloroplast ATP synthase**
The $c_{14}$-ring from spinach chloroplasts is shown from from the side parallel to the membrane and top view from the $F_1$ perspective. The proton-binding Glu61 is highlighted in red and is found on the outer C-terminal $\alpha$-helix while the glycine motif (highlighted in yellow) is found on the inside N-terminal $\alpha$-helix.

### 5.1.5 Rotor ring stoichiometries and the Ion/ATP Ratio

The *ion-to-ATP* ratio is essentially the number of *c*-subunits forming the *c*-ring ($n$) divided by the number of ATP molecules synthesised per turn (3) and can be calculated as $n/3$. The variable $c_n$-ring stoichiometries across different organisms means that the *ion-to-ATP* ratio is also variable. The $c_n$-ring stoichiometry and theoretical ion/ATP of a number ATP synthases from a range of organisms is given in Table 5.1.

| $c_n$ | Ion/ATP | Example Organism |
|---|---|---|
| $c_8$ | 2.7 | *Homo sapiens* |
| $c_9$ | 3.0 | *Mycobacterium phlei* |
| $c_{10}$ | 3.3 | *Escherichia coli* |
| $c_{11}$ | 3.7 | *Ilyobacter tartaricus* |
| $c_{12}$ | 4.0 | N/A |
| $c_{13}$ | 4.3 | *Bacillus pseudofirmus* OF4 |
| $c_{14}$ | 4.7 | *Spinacia oleracea* |
| $c_{15}$ | 5.0 | *Spirulina platensis* |
| $c_{16}$ | 5.3 | N/A |
| $c_{17}$ | 5.7 | *Burkholderia pseudomallei* |

**Table 5.1: c-ring stoichiometries and Ion-to-ATP ratios**
The theoretical *Ion-to-ATP* ratio of different sized *c*-rings and an example organism with the stated stoichiometry where known. *Burkholderia pseudomallei* $c_{17}$-ring comes from an N-type ATPase whilst the rest of the table belong to F-type ATP synthases. With the exception of the $c_{11}$-ring from *Ilyobacter tartaricus* which is $Na^+$-binding, the other *c*-rings are proton gradient driven.

As an important parameter with implications for the many bioenergetic processes of cellular metabolism, the diverse range of *c*-ring stoichiometries found throughout nature suggest certain ion/ATP ratios are advantageous in the different environments the organisms find themselves in. The smallest known *c*-ring

stoichiometries are found in mitochondria with between 8 and 10 *c*-subunits (Stock et al. 1999; Watt et al. 2010). The mammalian mitochondrial ATP synthase has eight *c*-subunits and is known to operate exclusively in the ATP synthesis direction. Non-photosynthetic bacteria such as *Mycobacterium phlei, Escherichia coli* and some *Bacillus* species have between nine and thirteen *c*-subunits in their ATP synthases (Preiss et al. 2010, 2015; Sobti et al. 2020b). Of these bacterial ATP synthases, those belonging to alkaliphilic bacteria have larger *c*-rings as the inverted pH gradients mean they must synthesise ATP at lower overall *pmf* (Matthies et al. 2009; Preiss et al. 2013). ATP synthases with larger *c*-rings have a lower minimum threshold of *pmf* for ATP synthesis (Ballmoos et al. 2009; Fischer and Gräber 1999).

### 5.1.6 Significance of membrane rotor ring size in photosynthesis

Photosynthetic organisms such as cyanobacteria and higher plants with chloroplasts appear to have a larger *c*-rings on average, ranging from $c_{13}$ to $c_{15}$ (Pogoryelov et al. 2007, 2009). At first sight this is a surprising feature to be selected for by natural selection as any ATP synthases with larger *c*-ring sizes would require more protons per ATP synthesised and are therefore less efficient with respect to proton consumption. However this apparent reduced efficiency assumes protons are limiting and are the only component of *pmf* that drives ATP synthesis, when in fact the transmembrane electric potential ($\Delta\psi$) and transmembrane proton gradient ($\Delta$pH) components of *pmf* contribute equally. Furthermore, the

role of ATP synthase in photosynthesis extends beyond the synthesis of ATP, playing an important role in the regulation of the light-dependent reactions and photoprotective mechanisms such as non-photochemical quenching (NPQ) and down-regulation of electron transport which are pH-dependent (Müller et al. 2001b; Nilkens et al. 2010; Tongra et al. 2014).

### The ATP/NADPH Ratio

One perspective from which to view the larger *c*-ring stoichiometries in photosynthesis is from the perspective of the ratio of ATP to NADPH produced by the light-dependent reactions, in other words, the ATP/NADPH ratio (Cheuk and Meier 2021; Davis and Kramer 2020). The ATP/NADPH ratio arises from the proton-coupled electron transfer reactions and the stoichiometry of these reactions during linear electron transport (LET). LET in the thylakoid membranes drives the light driven production of NADPH and ATP at a specific ratio due to the coupled nature of electron transport and proton translocation to build up a *pmf* (Foyer et al. 2012; Joliot and Johnson 2011). Therefore, the ATP/NADPH ratio is directly affected by the *c*-ring stoichiometry of the ATP synthase. On the other hand, cyclic electron transport cycles electrons from ferredoxin back to the plastoquinone pool and couples this with proton pumping into the lumen and ultimately leads to a net contribution of *pmf* without production of NADPH. Similarly, pseudo-cyclic electron transport transfers electrons to an alternative final electron carrier such as $O_2$ and contributes to *pmf* without producing NADPH (Shikanai and Yamamoto 2017).

| $c_n$ | $H^+$/ATP | ATP/NADPH |
|---|---|---|
| $c_8$ | 2.7 | 2.25 |
| $c_9$ | 3.0 | 2.00 |
| $c_{10}$ | 3.3 | 1.80 |
| $c_{11}$ | 3.7 | 1.64 |
| $c_{12}$ | 4.0 | 1.50 |
| $c_{13}$ | 4.3 | 1.40 |
| $c_{14}$ | 4.7 | 1.29 |
| $c_{15}$ | 5.0 | 1.20 |
| $c_{16}$ | 5.3 | 1.13 |
| $c_{17}$ | 5.7 | 1.06 |

**Table 5.2: $H^+$/ATP and ATP/NADPH ratios for different c-ring sizes** The theoretical ATP/NADPH production from linear electron transport for different *c*-ring stoichiometries and their respective $H^+$/ATP ratios. The ATP/NADPH ratio assumes perfect coupling of the electron transport reactions on the translocation of protons across the thylakoid membrane into the lumen.

Assuming a $c_{14}$-ring stoichiometry in the F-type ATP synthase and assuming that the two electrons required for reducing $NADP^+$ are coupled to the translocation of six protons across the thylakoid membrane, LET produces an ATP/NADPH ratio of 1.29. This 1.29 ratio production of ATP to NADPH is lower than the theoretical ATP/NADPH required to complete the Calvin-Benson-Bassham (CBB) cycle for carbon fixation (1.5).

Table 5.2 shows how the larger *c*-ring stoichiometries requiring more protons per ATP produced further exacerbate the deficit in ATP production relative to NADPH production in photosynthetic organisms. It is only when *c*-ring stoichiometries are less than or equal to 12 when the ATP/NADPH = 1.5 ratio for the CBB cylce is satisfied. In reality the required ATP/NADPH ratio is higher than 1.5 due to the slow kinetics and poor specificity of the carbon-fixing en-

zyme Rubisco leading to oxygenation events which necessitate the consumption of ATP to recover from. (Busch 2020; Kramer and Evans 2011).

Despite the resultant deficit in ATP/NADPH production and the requirement for cyclic electron transport pathways to compensate for this deficit, larger *c*-ring stoichiometries ($c_{13\text{-}15}$) have still been selected for in photosynthetic organisms. Clearly, a different perspective of viewing large *c*-ring stoichiometries in photosynthesis is required to understand their evolutionary advantage.

### The $\Delta\psi$ and $\Delta$pH components of pmf

The *proton motive force* (*pmf*) is composed of both a $\Delta\psi$ component and $\Delta$pH component, Eq.1.1. And these two components contribute equally to the overall *pmf*. In photosynthetic organisms light fluctuations can lead to rapid changes in *pmf*, this is particularly problematic when sudden increases in light intensity lead to rapid spikes in the electric field across the thlyakoid membrane ($\Delta\psi$). These spikes in $\Delta\psi$ increase the number of recombination events at photosystem II (PSII) leading to the production of singlet oxygen ($1O_2$), a damaging free radical (Davis et al. 2017).

The larger *c*-ring stoichiometries in photosynthesis may have been selected for as a photoprotective strategy. ATP synthesis by ATP synthases with larger *c*-rings would dissipate spikes in $\Delta\psi$ more rapidly (Johnson and Ruban 2018). Additionally, the larger rings allow ATP synthesis to be supported at a lower minimum threshold of *pmf*, avoiding both excess $\Delta\psi$ and $\Delta$pH (Davis and Kramer 2020;

Kaim and Dimroth 1999).

$$\Delta G_{\mathrm{ATP}} = n.\Delta\mu_{\mathrm{H+}} \tag{5.1}$$

**Gibbs Free Energy of ATP synthesis** Where $\Delta G_{ATP}$ = Gibbs Free Energy required for ATP synthesis; $n$ = the $H^+$/ATP ratio determined by the *c*-ring stoichiometry; and $\Delta\mu_{H+}$ is the proton motive force.

A larger $H^+$/ATP ratio (larger *c*-ring) leads to a lower minimum *pmf* threshold of ATP synthesis, Eq. 5.1.6. A $c_{14}$-ring found in the chloroplast ATP synthase has a $H^+$/ATP ratio of 4.7 and requires a lower *pmf* than a $c_8$-ring with its $H^+$/ATP ratio of 2.7. Additionally, the $\Delta$pH component of *pmf* has implications on the regulation of the light dependent reactions (Kanazawa et al. 2017). The acidification of the lumen is a signal for non-photochemical quenching and regulation of cytochrome b6f activity (Krause and Jahns 2004; Kurisu et al. 2003; Müller et al. 2001b). Both of which help to dissipate excess light energy which would otherwise lead to photodamage to the organism.

### 5.1.7 F-type ATP synthase in Syn WT and Syn SP

In this work the membrane rotor ring of the $F_1F_o$-ATP synthase in *Synechococcus sp.* PCC 7002 was replaced with the membrane rotor ring from *Spirulina platensis* (Fig 5.4). The replacement was done by substituting the *atpE* gene encoding the native *c*-subunit with the *atpE* gene from *S. platensis* by CRISPR-

Cas12a genome editing (Chapter 3). The mutation was checked by sequencing and then the formation of a chimeric ATP synthase in *Synechococcus* was verified by electron *cryo*-microscopy (Chapter 4).

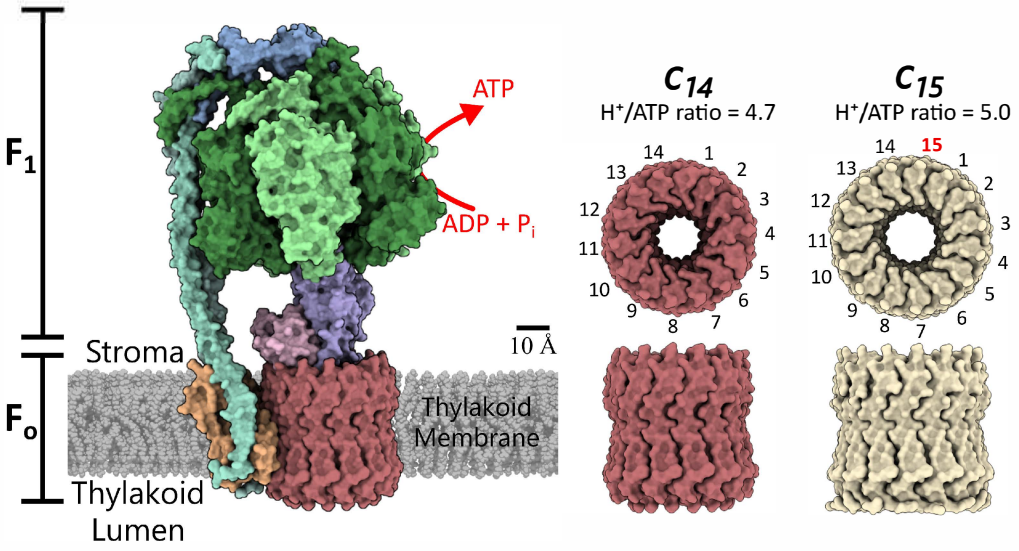


**Figure 5.4: Homology Model of F-type ATP synthase from Syn WT and Syn SP c-ring**
The homology model of the F-type ATP synthase from *Synechococcus sp.* PCC 7002 was modelled in SWISS-MODEL (Expasy) and used the spinach chloroplast structure as a template (Hahn et al. 2018). In the cream colour is the $c_{15}$-ring from *Spirulina platensis* (Pogoryelov et al. 2009) which was used to replace the native $c_{14}$.

### Comparisons of Syn WT and Syn SP

The mutant strain of *Synechococcus sp.* PCC 7002 (*Syn* SP) and wild-type strain (*Syn* WT) were compared at a cellular and biochemical level. The aim of these functional studies was to determine the differences caused by the increase in *c*-ring stoichiometry from a $c_{14}$ to a $c_{15}$-ring.

## 5.2 Materials & Methods

### 5.2.1 Chloroform-Methanol Extraction of ATP synthase c-subunits

Isolated thylakoid membrane samples were treated with 10x volume of equal methanol/chloroform mixture. After vortexing the mixture was centrifuged at 22,000 rpm for 1 min at room temperature. The chloroform phase containing *c*-monomers was extracted and SDS was added to a final concentration of 0.1 % (w/v). The chloroform was evaporated in a vacuum concentrator (Eppendorf Concentrator Plus) for 25 mins at $45^{\circ}$C. The remaining precipitate was resuspended in 1x SDS loading buffer and analysed by SDS-PAGE.

### 5.2.2 ATP Hydrolysis Assay

The ATP hydolysis activities in purified ATP synthase samples or isolated thylakoid membrane samples were assessed using an ATP-regenerating system and detecting the decrease in absorbance at 340 nm as nicotinamide adenine dinucleotide (NADH) in the reaction mixture was consumed. Assay buffer (50 mM Tris-HCl (pH $=$ 8.0), 100 mM KCl, 2 mM $MgCl_2$, 0.3 mM NADH, 2 mM phosphoenol pyruvate ($K^+$-PEP), 10 mU/mL pyruvate kinase and 6 mU/mL lactate dehydrogenase) were added to a 1 mL cuvette and the absorbance at 340 nm was measured over the course of a 20 minute reaction. Blanking against an empty cuvette the fresh buffer gives a $OD_{340}$ of $\sim$ 1.8. Then 2 mM ATP was added and the $A_{340}$ allowed to stabilise before adding ATPase-containing sam-

ples. The ATP hydrolysis rates were calculated from the steady-state decreasing slope in absorbance at 340 nm as the NADH was consumed, the slopes were allowed to decrease steadily for at least 2 minutes before any rates were calculated.

### 5.2.3 Growth Comparisons

Liquid cultures of wild-type and mutant *Synechococcus* (*Syn* WT and *Syn* SP) were grown in 25 mL of modified A-D7 media in Nunc cell culture treated flasks with filter caps (Thermo Scientific). The cultures were grown under 100 $\mu$E $m^{-2}$ $s^{-1}$ light at $31^{\circ}$C with constant shaking at 100 rpm. Cells in exponential phase (0.6 ¡ $OD_{730}$ ¡ 1.0) were harvested by centrifugation at 4,000 rpm for 20 mins and resuspended in fresh modified A-D7 media to an $OD_{730} = 0.5$. 1 mL of $OD_{730} = 0.5$ resuspended cell culture was added to 25 mL of modified A-D7 media (at varying different pH levels) in Nunc cell culture flasks. The same starter culture was used to inoculate the different pH flasks. These cultures were sampled at the time points indicated by taking up 1 mL of cell culture and measuring $Abs_{730}$ with a Cary 60 UV-Vis spectrophotometer (Agilent). The 1 mL of sampled cell culture was replaced with the same volume of $ddH_2O$.

### 5.2.4 Spheroplast Preparation

Liquid cultures of *Syn* WT and *Syn* SP were grown to an $OD_{730} = 1.0$ and harvested by centrifugation at 4,000 rpm for 20 mins at $4^{\circ}$C. Cell pellets were resuspended in spheroplast preparation buffer (500 mM mannitol, 10 mM Tricine-

NaOH (pH $=$ 8.0), 10 mM $MgCl_2$, 5 mM $K_2HPO_4$, 5 mM $NaH_2PO_4$, 100 $\mu$M phenylmethylsulfonylfluoride (PMSF)) and an additional 0.3 % lysozyme, and incubated for 1.5 hours at $37^{\circ}$C. The samples were then cooled on ice for 2 minutes and centrifuged at 4,000 rpm for 5 mins at $4^{\circ}$C. Spheroplasts in the pellet were resuspended in spheroplast suspension buffer to a final Chl *a* concentration of 0.2 mg/mL.

### 5.2.5 Luciferin/luciferase Assay

Freshly prepared spheroplast diluted to a final Chl *a* concentration of 0.2 mg/mL were pre-illuminated in 100 $\mu$E $m^{-2}$ $s^{-1}$ light at $30^{\circ}$C for 2 mins. 100 $\mu$L of spheroplasts were then added to 1 mL of Time Course Assay Buffer (20 mM Tris- $PO_4$, 5 mM $MgCl_2$) and placed under the light intensities indicated (Fig 5.7). The assay was initiated by adding 1 mM of ADP, immediately 10 $\mu$L of the reaction mix was taken and mixed into Time Course Assay Buffer $+$ 15 % (w/v) trichloroacetic acid (TCA) and placed on ice to stop the reaction, 10 $\mu$L samples were taken every 20 s up to 140 s and then a final sample taken at 240s. The ATP synthesis rates were determined by measuring the ATP concentration in the samples collected at different time points using a luciferase assay system (Promega) (Lundin 2014).

### 5.2.6 Western blot Analysis

Spheroplast samples normalised to a final Chl *a* concentration of 0.2 mg/mL were run on two identical SDS-PAGE gels. Before loading, samples were boiled at $99^{\circ}$C for 10 mins after adding SDS loading buffer. One gel was Coomassie stained and the other was blotted onto polyvinylidene fluoride (PVDF) membranes using an iBlot 2 Dry Blotting System (ThermoFisher Scientific). PVDF membranes were blocked with Blocking buffer (Tris-buffered saline (pH = 7.6) + 5 % (w/v) skimmed-milk powder) overnight at $4^{\circ}$C. The blocked membranes were incubated with anti-$\beta$ primary antibody (Agrisera) in Blocking buffer for 1 hour at room temperature followed by incubating with secondary antibody in Blocking buffer for 1 hour at room temperature. The PVDF membrane was then washed twice with TBS-T and visualised using Clarity western ECL substrate (Bio-Rad).

After imaging the blot with the anti-$\beta$-subunit antibody, the blot was washed by incubating in Stripping buffer (15 g/L glycine, 1 g/L SDS, 0.1 mL Tween 20, pH = 2.2) for 10 mins. The membrane was then washed in TBS-T three times and then incubated with the anti-*c*-subunit antibody and imaged as before. The relative abundance of ATP synthase *c*-subunits and $\beta$-subunits was determined using the ImageJ "Measure" function on selected bands to determine relative chemiluminescence intensities.

## 5.3 Results

### 5.3.1 Chloroform/Methanol Extraction of c-subunits

Thylakoid membranes of wild-type and mutant *Synechococcus sp.* PCC 7002 (*Syn* WT and *Syn* SP) were isolated as outlined in the Materials and Methods chapter. The thylakoid membranes were then treated with a chloroform and methanol 1:1 (v/v) mixture to dissociate and extract the highly hydrophobic *c*-monomers and all samples were analysed by SDS-PAGE. Figure 5.5 shows the Coomassie-stained proteins in the thylakoid membranes and the chloroform/methanol extracted samples beside each. The final two lanes show the purified *Syn* WT $F_1F_o$-ATP synthase and the same sample treated with trichloroacetic acid (TCA) which dissociates the *c*-ring into *c*-monomers. The "WT+SP mem" lane shows a mixed sample of both *Syn* WT and *Syn* SP thylakoid membranes to highlight the two distinct bands from two distinct *c*-rings . In the immunoblot we see that a higher molecular weight *c*-ring is present in the *Syn* SP thylakoid membranes.

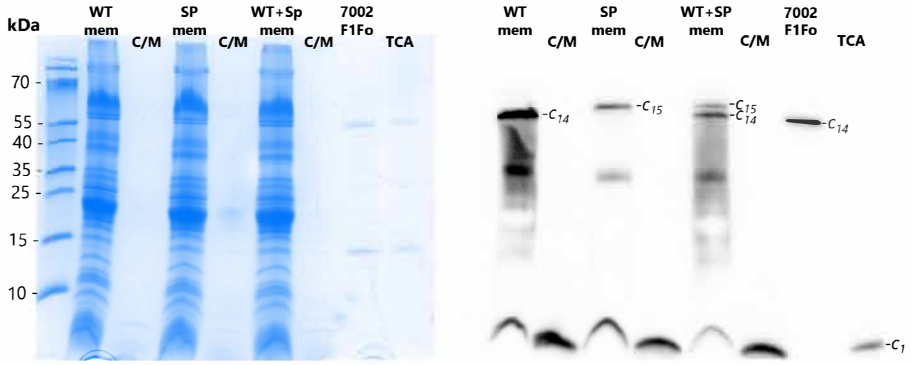


**Figure 5.5: Chloroform/Methanol extraction of Syn WT and Syn SP c-subunits**
Isolated thylakoid membrane samples were analysed by SDS-PAGE as either *Syn* WT membranes, *Syn* SP membranes or a mixed sample of both membranes. Beside each sample was the chloroform/methanol extracted *c*-subunit sample which extracts only *c*-monomers. Finally a purified sample of *Syn* WT $F_1F_o$-ATP synthase was run beside its TCA treated sample.

This immunoblot confirms the increased *c*-ring stoichiometry in the *Syn* SP mutant at the thylakoid membrane level. It supports the structural data of purified ATP synthase from *Syn* WT and *Syn* SP and allows us to confirm the mutant *Syn* SP strain was only expressing the mutant *c*-ring with an increased stoichiometry. The *cryo*-EM data shows that this increased stoichiometry is a $c_{15}$-ring and is the same as the *Spirulina platensis* stoichiometry (Pogoryelov et al. 2009).

### 5.3.2 Growth Comparisons of Syn WT and Syn SP

To assess the effect of an increased *c*-ring stoichiometry in the F-type ATP synthase of *Synechococcus sp.* PCC 7002 on a cellular level, the growth rates of *Syn* WT and *Syn* SP were compared in varying modified A-D7 media between pH = 6.8 to pH = 9.0. Three biological replicates were grown at each pH condition

with a starting culture of each replicate used to inoculate the 4 different pH conditions.

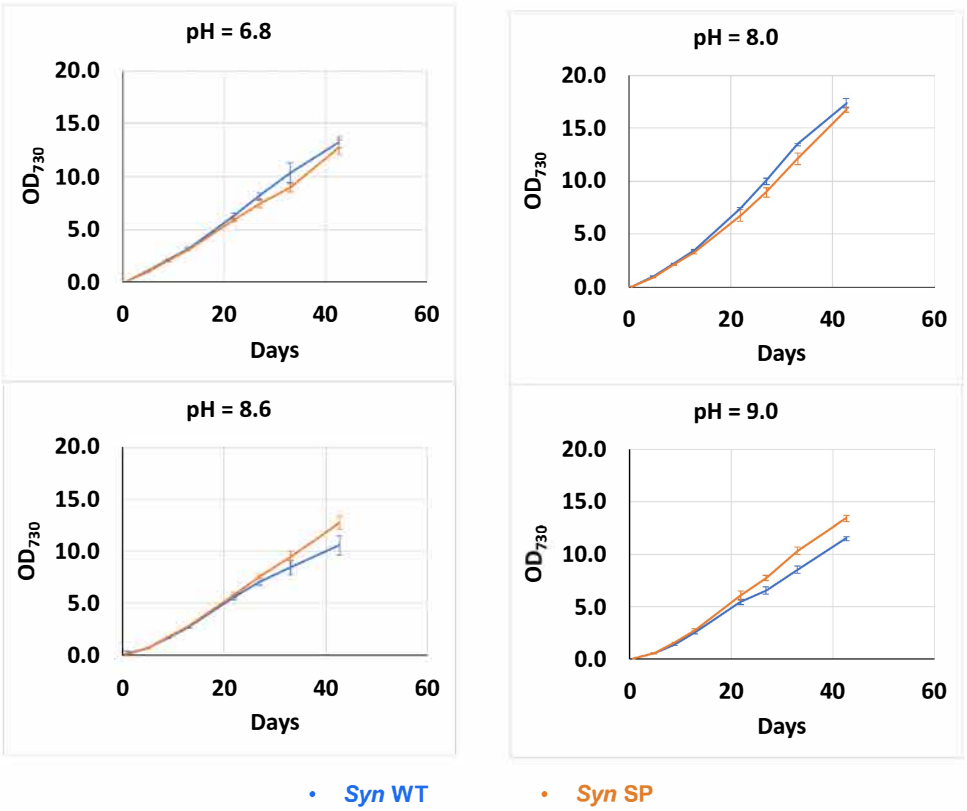


**Figure 5.6: Growth comparisons between Syn WT and Syn SP**
Growth comparisons between *Syn* WT and *Syn* SP at increasing pH levels. Normal growth of *Syn* WT is at pH = 8.0 and both *Syn* WT and *Syn* SP grow to similar optical densities at this pH. However, when increasing the growth media to pH = 8.6 and pH = 9.0 the *Syn* SP cultures outgrow *Syn* WT.

In Fig. 5.6 we see that in the regular pH = 8.0 modified A-D7 media both *Syn* WT and *Syn* SP grow at comparable rates and to similar optical densities. Similarly, at pH 6.8 both strains also grow at similar rates. However, at increasingly

alkaline pH (pH = 8.6 and 9.0) we see that *Syn* SP outgrows *Syn* WT. This difference in growth rates only appears after 20 days so may reflect the depletion of certain substrates in the growth media which the mutant *Syn* SP consumed at a lesser rate.

### 5.3.3 ATP synthesis in Syn WT and Syn SP spheroplasts

To further compare the wild-type and mutant ATP synthases, freshly prepared spheroplasts of both *Syn* WT and *Syn* SP were illuminated to initiate the generation of a *proton motive force* which can be used to drive ATP synthesis. The rates of ATP synthesis were then determined by collecting samples at stated time points and using a luciferin/luciferase assay to measure ATP concentration.

The experiment was repeated under three different light intensities 50, 100 and 250 $\mu$E $m^{-2}$ $s^{-1}$. This range is typical of the light intensities faced by cyanobacteria when growing underwater; for context direct midday sun in the tropics is approximately 1,700 $\mu$E $m^{-2}$ $s^{-1}$ (Morel and Smith 1974). At each light intensity the experiment was also repeated with three biological repeats and with 2 $\mu$M of the potent uncoupler carbonilcyanide p-triflouromethoxyphenylhydrazone (FCCP) (To et al. 2010).

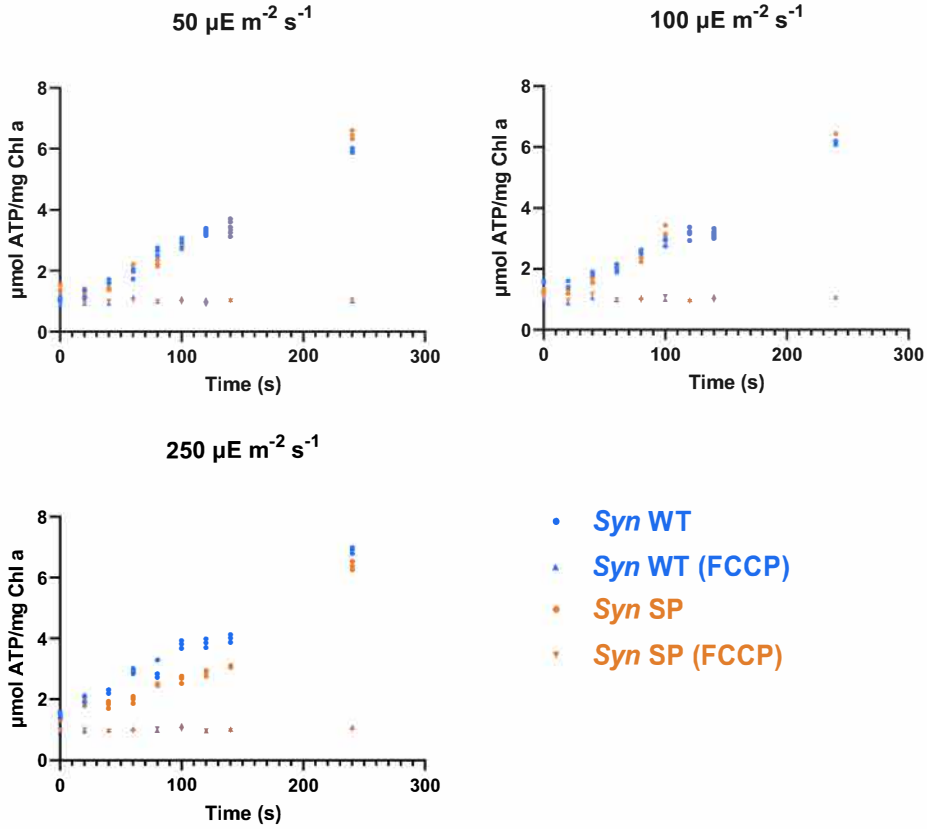


**Figure 5.7: ATP concentrations in illuminated Syn WT and Syn SP spheroplasts**
ATP concentrations were measured at given time intervals using a luciferin/luciferase assay. The experiment was repeated under three light conditions: 50, 100 and 250 $\mu$E m$^{-2}$ s$^{-1}$. No significant difference is seen at 50 or 100 $\mu$E m$^{-2}$ s$^{-1}$ light but at 250 $\mu$E m$^{-2}$ s$^{-1}$ the *Syn* WT spheroplasts produce ATP at a faster rate than the *Syn* SP spheroplasts.

In Fig. 5.7 we see similar ATP synthesis rates in both *Syn* WT and *Syn* SP spheroplasts when illuminated with 50 and 100 $\mu$E m$^{-2}$ s$^{-1}$ light. However there is an increase in ATP synthesis in *Syn* WT spheroplasts at a higher light intensity (250 $\mu$E m$^{-2}$ s$^{-1}$) compared to *Syn* SP. Under the presence of the potent uncoupler FCCP there is no ATP synthesis as the *proton motive force* is dissipated by

FCCP. Without a *pmf* there is no driving force available to the ATP synthase.

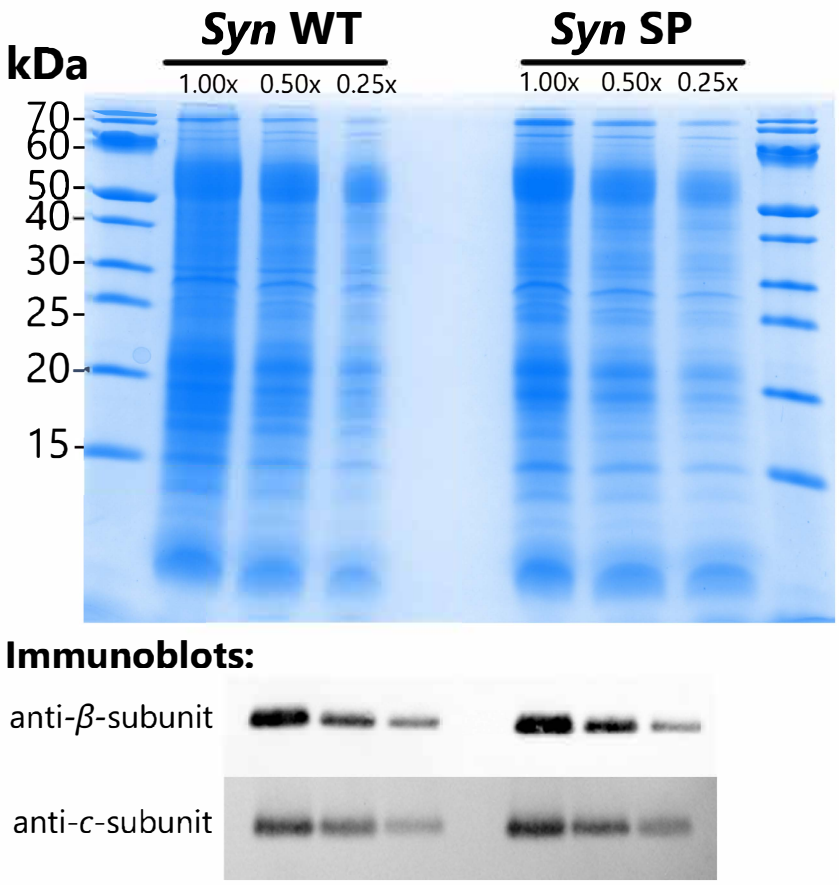


**Figure 5.8: Relative quantification of spheroplast protein**
Spheroplast samples of both *Syn* WT and *Syn* SP were normalised to a final Chl *a* concentration of 0.2 mg/mL (1.00x). A serial dilution of 1:2 was performed on each sample (0.50x and 0.25x).

Spheroplast samples, normalised to a final Chl *a* concentration of 0.2 mg/mL, were analysed by SDS-PAGE and immunoblotting to determine the relative abundance of ATP synthase in *Syn* WT and *Syn* SP. A serial dilution was used to give 0.50x and 0.25x samples. ImageJ was used to compare relative intensities

of chemiluminescent bands (Schneider et al. 2012). No significant difference was identified between the corresponding samples from *Syn* WT and *Syn* SP, suggesting similar amounts of ATP synthase complexes in both wild-type and mutant strains.

### 5.3.4 ATP hydrolysis by purified Syn WT and Syn SP ATP synthase

The ATP hydrolysis rates of purified samples of *Syn* WT and *Syn* SP $F_1F_o$-ATP synthase were determined using an ATP-regenerating system (Fig. 5.9) The assay provides phosphoenol pyruvate, NADH and ATP in excess, and the enzymes pyruvate kinase and lactate dehydrogenase, so that when ATPase in the sample hydrolyses ATP into ADP, NADH levels decrease and this can be measured as a decrease in absorbance at 340 nm.

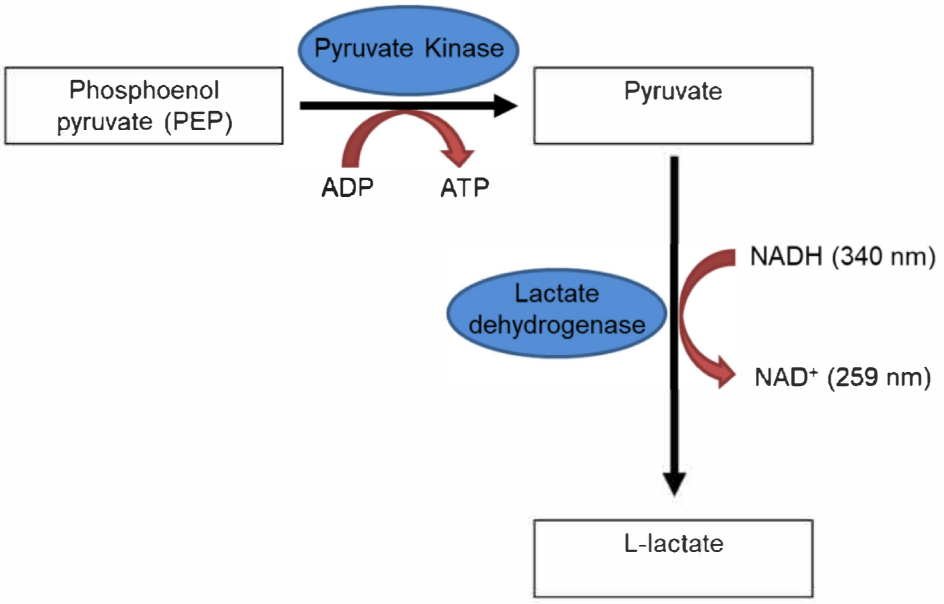


**Figure 5.9: ATP-regenerating system for ATP hydrolysis assay**
The ATP hydrolysis rate is measured indirectly through the decrease in absorption at 340 nm as NADH is consumed in the forward reaction. The phosphoenol pyruvate substrate is in excess but the reactions only proceed when ADP is available. Upon ATP hydrolysis of ATP in the assay buffer by the sample, ADP becomes available and the two enzymes, pyruvate kinase and lactate dehydrogenase, catalyse the two reactions to give pyruvate and then L-lactate. The second reactions pyruvate to L-lactate, catalysed by lactate dehydrogenase, uses NADH as a cofactor.

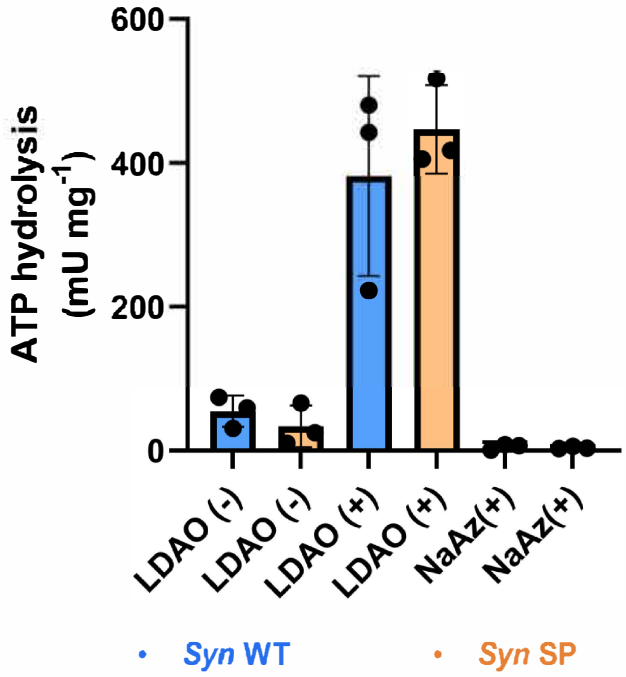


**Figure 5.10: ATP hydrolysis by purified Syn WT and Syn SP ATP synthase**
ATP hydrolysis assay of purified ATP synthase samples show no significant difference between wild-type and mutant ATP hydrolysis activities. The cyanobacterial ATP synthase is activated by the addition of N,N-Dimethyldodecylamine N-oxide (LDAO) to a final concentration of 0.1 % (v/v). Both enzymes required LDAO for activation and both can be inhibited by the addition of sodium azide at a final concentration of 0.02 % (w/v).

Both purified F-type ATP synthase samples from *Syn* WT and *Syn* SP showed ATP hydrolysis activity which was activated by the addition of LDAO and inhibited again by the addition of sodium azide. LDAO is thought to alleviate the intrinsic inhibition of ATP hydrolysis by the binding of ADP, commonly known as ADP inhibition (Sunamura et al. 2010). And sodium azide inhibits ATP hydrolysis by locking ADP molecules in the $\beta$-subunit binding sites and preventing

catalysis in both the synthesis and hydrolysis direction (Bowler et al. 2006).

## 5.4 Discussion

### 5.4.1 Improved Growth of Syn SP in alkaline media

The phosphorylation potential is the ratio of ATP to ADP present in a particular system and at thermodynamic equilibrium for ATP synthesis, the *pmf* (also referred to as $\Delta\mu H^+$) and the phosphorylation potential ($\Delta G_P$) are in balance so that $H^+/ATP$ x $\Delta\mu H^+ = \Delta G_P$. Therefore, in a given system, to maintain a certain phosphorylation potential when there is a low *pmf* available (e.g. in an alkaline environment) a strategy is to increase the *ion-to-ATP* ratio ($H^+/ATP$) (Dimroth and Cook 2004; Guffanti et al. 1984; Sturr et al. 1994).

This strategy has been observed in alkaliphilic bacteria such as *Bacillus pseudofirmus* OF4 and *Bacillus* TA2.A1 which possess a $c_{13}$-ring (Matthies et al. 2009; Preiss et al. 2013). In the *c*-subunits of these alkaliphiles the glycine motif found in the N-terminal helix is replaced by AxAxAxA. Site-directed mutagenesis of this motif with alanine-to-glycine substitutions yielded mutants with $c_{12}$-rings and a reduced growth capacity at high pH compared to the wild-type with $c_{13}$-rings.

In photosynthesis, the *pmf* used to synthesise ATP is generated by light-driven proton translocation. ATP synthase requires a minimum threshold of *pmf* to activate ATP synthesis and ATP synthases with larger *c*-ring stoichiometries have

the lowest activation threshold (Ballmoos et al. 2009; Junesch and Gräber 1987; Kaim and Dimroth 1999). Shifting to a larger *c*-ring and translocating more protons per ATP synthesised means that the torque is generated through smaller step-wise rotations as the energy for rotation is shared equally across all proton translocation steps (Ballmoos et al. 2008). This is analagous to shifting to a lower gear on a bicycle to allow travel against a steep gradient but at the cost of more rotations per distance travelled.

The *Syn* SP mutant ($c_{15}$) was grown alongside *Syn* WT ($c_{14}$) in increasingly alkaline media where the higher pH environments would have made a lower *pmf* available. At pH 6.8 and pH 8.0 there was no significant difference between wild-type and mutant growth rates. However, at pH 8.6 and pH 9.0 the *Syn* SP mutant grew at a faster rate compared to *Syn* WT. The difference in growth rates only appears after 20 days but does point towards an advantage of larger *c*-ring stoichiometries for alkaline environments and lower *pmf* availability, as seen in alkaliphilic bacteria (Preiss et al. 2013; Sturr et al. 1994). In nature, a commonly occurring condition for low *pmf* availability across thylakoid membranes is in low light settings (Davis and Kramer 2020; Huang et al. 2018). In low light, the upstream light dependent reactions involving PSII, Cyt $b_6f$ and PSI, that contribute and build up the *pmf*, have fewer excitation events and less redox potential driving force. The lower minimum *pmf* thresholds of ATP synthases with larger *c*-rings would be selected for as they allow ATP synthesis and subsequent carbon fixation to continue even under low light conditions where a lower *pmf* is generated.

### 5.4.2 Tradeoff between Photoprotection and Efficient ATP synthesis

Larger *c*-rings may also confer more photoprotective effects as the ATP synthase is able to dissipate spikes in $\Delta\psi$ more rapidly by translocating more protons per rotation. Spikes in $\Delta\psi$ have a deleterious effect as they increase the probability of charge recombination events (Davis et al. 2016; Kramer et al. 2003) which form reactive oxygen species (ROS), for example, the formation of singlet oxygen by PSII. The unpaired electron in reactive oxygen species is highly reactive and leads to photodamage (Takagi et al. 2017; Zavafer et al. 2015).

Under low $CO_2$ conditions the carbon-fixation reactions and the activity of chloroplast ATP synthase slows (Yamori and Shikanai 2016). The slowing of proton efflux from the lumen leads to a buildup of *pmf* through acidification and this activates the photoprotective mechanism called non-photochemical quenching (NPQ) (Nilkens et al. 2010; Tongra et al. 2014). NPQ dissipates excess light energy as heat to prevent damage to the photosynthetic apparatus. In *Arabidopsis*, a single point mutation at the $\gamma$-subunit of ATP synthase prevents this reduction of activity in low $CO_2$ conditions. Consequently, the mutant plant is unable to acidify the lumen and activate NPQ so photodamage is observed through loss of PSI activity (Kanazawa et al. 2017).

The reverse of this phenomena is that when $CO_2$ concentration is higher, photosynthetic organisms must de-acidify the lumen and deactivate NPQ to allow the efficient flow of electrons in the electron transport chain. Therefore, an ATP

synthase with a larger *c*-ring would be able to more quickly dissipate the buildup of protons in the lumen and more quickly have ATP and NADPH production at its most efficient. The *Syn* SP mutant with the larger *c*-ring may be better able to grow under fluctuating light conditions than the *Syn* WT $c_{14}$-ring, as the mutant would be able to more quickly reactivate the light dependent reactions and make use of lower light after a period of high light where NPQ was active.

For our wild-type and mutant strains, the amounts of ATP synthase were similar Fig.5.8, it is noted that this is not the case in the tobacco $c_{15}$ mutant where the expression of ATP synthase dropped to 25 % of wild-type levels (Yamamoto et al. 2023). In the spheroplast ATP synthesis experiments (Fig.5.7), *Syn* WT spheroplasts produce ATP at a faster rate than *Syn* SP in high light (250 $\mu$E $m^{-2}$ $s^{-1}$). At high light the smaller *c*-ring is better equipped to synthesise ATP with fewer protons and therefore improve the ATP/NADPH deficit. Whilst a larger *c*-ring helps to dissipate excess pH or transmembrane potential more quickly and also produce ATP with a lower *pmf* driving force. Overall, it seems that *c*-ring stoichiometries in photosynthesis are selected for to allow optimal ATP synthesis in a range of light conditions but must balance the need for photoprotection under high light and low $CO_2$ conditions.

### 5.4.3 Future Perspectives

Further experiments with the *Syn* SP mutant are planned. In particular, using electrochromic shift measurements (ECS) to measure the effect of the increased

*c*-ring stoichiometry on the transmembrane electric potential ($\Delta\psi$). ECS measurements make use of the fact that absorbance at certain wavelengths for some carotenoid pigments are sensitive to $\Delta\psi$ (Viola et al. 2019). These measurements will give a better understanding of how the *pmf* is partitioned into $\Delta\psi$ and $\Delta$pH in cyanobacteria under different light conditions.

More growth comparisons between *Syn* WT and *Syn* SP under fluctuating light and low light can also be conducted. This data combined with corresponding ATP synthesis rates in spheroplasts could support the idea that larger *c*-rings are less efficient in terms of proton usage and the ATP/NADPH ratio but better adapted for fluctuating light and low light due to their lower minimum *pmf* threshold for ATP synthesis.

# Bibliography


Abrahams, JP. et al. (1994). "Structure at 2.8 A resolution of F1-ATPase from bovine heart mitochondria." In: *Nature* 370.6491, pp. 621–628. DOI: 10.1038/370621a0.

Akiyama, Kentaro et al. (2019). "The -hairpin region of the cyanobacterial F1-ATPase -subunit plays a regulatory role in the enzyme activity". In: *Biochemical Journal* 476.12. Publisher: Portland Press Ltd, pp. 1771–1780. DOI: 10.1042/BCJ20190242.

Allegretti, Matteo et al. (2015). "Horizontal membrane-intrinsic -helices in the stator a-subunit of an F-type ATP synthase". In: *Nature* 521.7551, pp. 237–240. DOI: 10.1038/nature14185.

Baalen, Chase Van (1962). "Studies on Marine Blue-Green Algae". In: 4.1. Publisher: De Gruyter Section: Botanica Marina, pp. 129–139. DOI: 10.1515/botm.1962.4.1-2.129.

Ballmoos, Christoph von, Gregory M. Cook, and Peter Dimroth (2008). "Unique Rotary ATP Synthase and Its Biological Diversity". In: *Annual Review of Biophysics* 37.1. _eprint: https://doi.org/10.1146/annurev.biophys.37.032807.130018, pp. 43–64. DOI: 10.1146/annurev.biophys.37.032807.130018.

Ballmoos, Christoph von, Alexander Wiedenmann, and Peter Dimroth (2009). "Essentials for ATP synthesis by F1F0 ATP synthases". In: *Annual Review of Biochemistry* 78, pp. 649–672. DOI: 10.1146/annurev.biochem.78.081307.104803.

Barber, James (2003). "Photosystem II: the engine of life". In: *Quarterly Reviews of Biophysics* 36.1, pp. 71–89. DOI: 10.1017/s0033583502003839.

Bason, John V. et al. (2011). "Binding of the Inhibitor Protein IF1 to Bovine F1-ATPase". In: *Journal of Molecular Biology* 406.3, pp. 443–453. DOI: 10.1016/j.jmb.2010.12.025.

Bayat, Hadi, Mohammad Hossein Modarressi, and Azam Rahimpour (2018). "The Conspicuity of CRISPR-Cpf1 System as a Significant Breakthrough in Genome Editing". In: *Current Microbiology* 75.1, pp. 107–115. DOI: 10.1007/s00284-017-1406-8.

Bowler, Matthew W. et al. (2006). "How azide inhibits ATP hydrolysis by the F-ATPases". In: *Proceedings of the National Academy of Sciences* 103.23. Publisher: Proceedings of the National Academy of Sciences, pp. 8646–8649. DOI: 10.1073/pnas.0602915103.

Boyer, Paul D. (1997). "The ATP synthase - A splendid molecular machine". In: *Annual Review of Biochemistry* 66, pp. 717–749. DOI: 10.1146/annurev.biochem.66.1.717.

Busch, Florian A. (2020). "Photorespiration in the context of Rubisco biochemistry, CO2 diffusion and metabolism". In: *The Plant Journal* 101.4. _eprint: https://onlinelibrary.wiley.com/doi/pdf/10.1111/tpj.14674, pp. 919–939. DOI: 10.1111/tpj.14674.

Cabezón, E et al. (2001). "The structure of bovine IF1, the regulatory subunit of mitochondrial F-ATPase". In: *The EMBO Journal* 20.24. Publisher: John Wiley & Sons, Ltd, pp. 6990–6996. DOI: 10.1093/emboj/20.24.6990.

Cabezón, Elena et al. (2000). "Dimerization of Bovine F1-ATPase by Binding the Inhibitor Protein, IF1*". In: *Journal of Biological Chemistry* 275.37. Publisher: Elsevier, pp. 28353–28355. DOI: 10.1074/jbc.C000427200.

Carlson, Michael Luke et al. (2018). "The Peptidisc, a simple method for stabilizing membrane proteins in detergent-free solution." In: *eLife* 7. Publisher: eLife Sciences Publications, Ltd. DOI: 10.7554/eLife.34085.

Cheuk, Anthony and Thomas Meier (2021). "Rotor subunits adaptations in ATP synthases from photosynthetic organisms". In: *Biochemical Society Transactions* 49.2, pp. 541–550. DOI: 10.1042/BST20190936.

Cozens, A L and J E Walker (1987). "The organization and sequence of the genes for ATP synthase subunits in the cyanobacterium Synechococcus 6301. Support for an endosymbiotic origin of chloroplasts". In: *Journal of molecular biology* 194.3, pp. 359–383. DOI: 10.1016/0022-2836(87)90667-x.

Cross, Richard L (2000). "The rotary binding change mechanism of ATP synthases". In: *Biochimica et Biophysica Acta (BBA) - Bioenergetics* 1458.2, pp. 270–275. DOI: 10.1016/S0005-2728(00)00079-7.

Cross, Richard L. and Volker Müller (2004). "The evolution of A-, F-, and V-type ATP synthases and ATPases: Reversals in function and changes in the H+/ATP coupling ratio". In: *FEBS Letters* 576.1. Publisher: No longer published by Elsevier, pp. 1–4.

Daum, Bertram et al. (2010). "Arrangement of photosystem II and ATP synthase in chloroplast membranes of spinach and pea". In: *Plant Cell* 22.4. Publisher: American Society of Plant Biologists, pp. 1299–1312. DOI: 10.1105/tpc.109.071431.

Dautant, Alain et al. (2018). "ATP Synthase Diseases of Mitochondrial Genetic Origin". In: *Frontiers in Physiology* 9.

Davies, Koren M. et al. (2014). "Visualization of ATP synthase dimers in mitochondria by electron cryo-tomography". In: *Journal of Visualized Experiments* 91. Publisher: Journal of Visualized Experiments, p. 51228. DOI: 10.3791/51228.

Davis, Geoffry A et al. (2016). "Limitations to photosynthesis by proton motive force-induced photosystem II photodamage". In: *eLife* 5. DOI: 10.7554/eLife.16921.

Davis, Geoffry A. and David M. Kramer (2020). "Optimization of ATP Synthase c–Rings for Oxygenic Photosynthesis". In: *Frontiers in Plant Science* 10. Publisher: Frontiers Media S.A., p. 1778. DOI: 10.3389/fpls.2019.01778.

Davis, Geoffry A., A. William Rutherford, and David M. Kramer (2017). "Hacking the thylakoid proton motive force for improved photosynthesis: modulating ion flux rates that control proton motive force partitioning into  and pH". In: 372.1730. Publisher: The Royal Society, p. 20160381. DOI: 10.1098/rstb.2016.0381.

Demmer, Julius K. et al. (2022). "Structure of ATP synthase from ESKAPE pathogen Acinetobacter baumannii". In: *Science Advances* 8.7. Publisher: American Association for the Advancement of Science, eabl5966. DOI: 10.1126/sciadv.abl5966.

Dibrova, Daria V., Michael Y. Galperin, and Armen Y. Mulkidjanian (2010). "Characterization of the N-ATPase, a distinct, laterally transferred Na+-translocating form of the bacterial F-type membrane ATPase". In: *Bioinformatics* 26.12, pp. 1473–1476. DOI: 10.1093/bioinformatics/btq234.

Dimroth, Peter (1997). "Primary sodium ion translocating enzymes". In: *Biochimica et Biophysica Acta - Bioenergetics* 1318.1. Publisher: Elsevier, pp. 11–51. DOI: 10.1016/S0005-2728(96)00127-2.

Dimroth, Peter and Gregory M. Cook (2004). "Bacterial Na+ - or H+ -coupled ATP synthases operating at low electrochemical potential". In: *Advances in Microbial Physiology* 49, pp. 175–218. DOI: 10.1016/S0065-2911(04)49004-3.

Dubochet, J. et al. (1982). "Electron microscopy of frozen water and aqueous solutions". In: *Journal of Microscopy* 128.3. Publisher: Wiley/Blackwell (10.1111), pp. 219–237. DOI: 10.1111/j.1365-2818.1982.tb04625.x.

Ducat, Daniel C., Jeffrey C. Way, and Pamela A. Silver (2011). "Engineering cyanobacteria to generate high-value products". In: *Trends in Biotechnology* 29.2, pp. 95–103. DOI: 10.1016/j.tibtech.2010.12.003.

Duncan, T. M. et al. (1995). "Probing interactions of the Escherichia coli F0F1 ATP synthase beta and gamma subunits with disulphide cross-links". In: *Biochemical Society Transactions* 23.4, pp. 736–741. DOI: 10.1042/bst0230736.

Elmlund, Dominika and Hans Elmlund (2015). "Cryogenic Electron Microscopy and Single-Particle Analysis". In: *Annual Review of Biochemistry* 84.1. Pub-

lisher: Annual Reviews, pp. 499–517. DOI: 10.1146/annurev-biochem-060614-034226.

Englund, Elias, Feiyan Liang, and Pia Lindberg (2016). "Evaluation of promoters and ribosome binding sites for biotechnological applications in the unicellular cyanobacterium Synechocystis sp. PCC 6803". In: *Scientific Reports* 6, p. 36640. DOI: 10.1038/srep36640.

Ferreira, Kristina N. et al. (2004). "Architecture of the Photosynthetic Oxygen-Evolving Center". In: *Science* 303.5665. Publisher: American Association for the Advancement of Science, pp. 1831–1838. DOI: 10.1126/science.1093087.

Fischer, Susanne and Peter Gräber (1999). "Comparison of pH- and -driven ATP synthesis catalyzed by the $H^+$-ATPases from *Escherichia coli* or chloroplasts reconstituted into liposomes". In: *FEBS Letters* 457.3, pp. 327–332. DOI: 10.1016/S0014-5793(99)01060-1.

Foyer, Christine H. et al. (2012). "Photosynthetic control of electron transport and the regulation of gene expression". In: *Journal of Experimental Botany* 63.4, pp. 1637–1661. DOI: 10.1093/jxb/ers013.

Frain, Kelly M., Colin Robinson, and Jan Maarten van Dijl (2019). "Transport of Folded Proteins by the Tat System". In: *The Protein Journal* 38.4, pp. 377–388. DOI: 10.1007/s10930-019-09859-y.

Futai, Masamitsu et al. (2019). "Vacuolar-type ATPase: A proton pump to lysosomal trafficking". In: *Proceedings of the Japan Academy. Series B, Physical and Biological Sciences* 95.6, pp. 261–277. DOI: 10.2183/pjab.95.018.

Gresser, M. J., J. A. Myers, and P. D. Boyer (1982). "Catalytic site cooperativity of beef heart mitochondrial F1 adenosine triphosphatase. Correlations of initial velocity, bound intermediate, and oxygen exchange measurements with an alternating three-site model". In: *The Journal of Biological Chemistry* 257.20, pp. 12030–12038.

Grüber, Gerhard et al. (2014). "ATP synthases from archaea: The beauty of a molecular motor". In: *Biochimica et Biophysica Acta - Bioenergetics* 1837.6. Publisher: Elsevier B.V., pp. 940–952. DOI: 10.1016/j.bbabio.2014.03.004.

Gu, Jinke et al. (2019). "Cryo-EM structure of the mammalian ATP synthase tetramer bound with inhibitory protein IF1". In: *Science* 364.6445. Publisher: American Association for the Advancement of Science, pp. 1068–1075. DOI: 10.1126/science.aaw4852.

Guffanti, A A et al. (1984). "A transmembrane electrical potential generated by respiration is not equivalent to a diffusion potential of the same magnitude for ATP synthesis by Bacillus firmus RAB." In: *Journal of Biological Chemistry* 259.5, pp. 2971–2975. DOI: 10.1016/S0021-9258(17)43244-3.

Guo, Hui, Stephanie A. Bueler, and John L. Rubinstein (2017). "Atomic model for the dimeric FO region of mitochondrial ATP synthase". In: *Science* 358.6365. Publisher: American Association for the Advancement of Science, pp. 936–940. DOI: 10.1126/science.aao4815.

Guo, Hui, Toshiharu Suzuki, and John L. Rubinstein (2019). "Structure of a bacterial atp synthase". In: *eLife* 8. Publisher: eLife Sciences Publications Ltd. DOI: 10.7554/eLife.43128.

Hahn, Alexander et al. (2016). "Structure of a Complete ATP Synthase Dimer Reveals the Molecular Basis of Inner Mitochondrial Membrane Morphology". In: *Molecular Cell* 63.3. Publisher: Cell Press, pp. 445–456. DOI: 10.1016/j.molcel.2016.05.037.

Hahn, Alexander et al. (2018). "Structure, mechanism, and regulation of the chloroplast ATP synthase." In: *Science* 360.6389. Publisher: American Association for the Advancement of Science, eaat4318. DOI: 10.1126/science.aat4318.

Henderson, Richard et al. (2012). "Outcome of the First Electron Microscopy Validation Task Force Meeting". In: *Structure* 20.2. Publisher: Elsevier, pp. 205–214. DOI: 10.1016/j.str.2011.12.014.

Hisabori, Toru et al. (2013). "The Chloroplast ATP Synthase Features the Characteristic Redox Regulation Machinery". In: *Antioxidants & Redox Signaling* 19.15, pp. 1846–1854. DOI: 10.1089/ars.2012.5044.

Huang, Wei et al. (2018). "Chloroplastic ATP synthase plays an important role in the regulation of proton motive force in fluctuating light". In: *Journal of Plant Physiology* 226, pp. 40–47. DOI: 10.1016/j.jplph.2018.03.020.

Inabe, Kosuke et al. (2019). "The N-terminal region of the  subunit from cyanobacterial ATP synthase alone can inhibit ATPase activity". In: *The Journal of Biological Chemistry* 294.26, pp. 10094–10103. DOI: 10.1074/jbc.RA118.007131.

Jinek, Martin et al. (2012). "A programmable dual-RNA-guided DNA endonuclease in adaptive bacterial immunity". In: *Science* 337.6096. Publisher: American Association for the Advancement of Science, pp. 816–821. DOI: 10.1126/science.1225829.

Johnson, Matthew P. and Alexander V. Ruban (2018). "Rethinking the existence of a steady-state  component of the proton motive force across plant thylakoid membranes". In: *Photosynthesis Research* 119.1 (), pp. 233–242. DOI: 10.1007/s11120-013-9817-2.

Joliot, Pierre and Giles N. Johnson (2011). "Regulation of cyclic and linear electron flow in higher plants". In: *Proceedings of the National Academy of Sciences* 108.32. Publisher: Proceedings of the National Academy of Sciences, pp. 13317–13322. DOI: 10.1073/pnas.1110189108.

Jordan, Patrick et al. (2001). "Three-dimensional structure of cyanobaoterial photosystem I at 2.5 Å resolution". In: *Nature* 411.6840. Publisher: Nature Publishing Group, pp. 909–917. DOI: 10.1038/35082000.

Junesch, Ulrike and Peter Gräber (1987). "Influence of the redox state and the activation of the chloroplast ATP synthase on proton-transport-coupled ATP synthesis/hydrolysis". In: *BBA - Bioenergetics* 893.2. Publisher: Elsevier, pp. 275–288. DOI: 10.1016/0005-2728(87)90049-1.

Junge, Wolfgang and Nathan Nelson (2015). "ATP Synthase". In: *Annual Review of Biochemistry* 84.1. Publisher: Annual Reviews, pp. 631–657. DOI: 10.1146/annurev-biochem-060614-034124.

Kagawa, Y. and E. Racker (1966). "Partial resolution of the enzymes catalyzing oxidative phosphorylation. 8. Properties of a factor conferring oligomycin sensitivity on mitochondrial adenosine triphosphatase". In: *The Journal of Biological Chemistry* 241.10, pp. 2461–2466.

Kaibara, Chitose et al. (1996). "Structural Asymmetry of F1-ATPase Caused by the  Subunit Generates a High Affinity Nucleotide Binding Site". In: *Journal of Biological Chemistry* 271.5, pp. 2433–2438. DOI: 10.1074/jbc.271.5.2433.

Kaim, G. and P Dimroth (1999). "ATP synthesis by F-type ATP synthase is obligatorily dependent on the transmembrane voltage". In: *The EMBO Journal* 18.15, pp. 4118–4127. DOI: 10.1093/emboj/18.15.4118.

Kampjut, Domen and Leonid A. Sazanov (2020). "The coupling mechanism of mammalian respiratory complex I". In: *Science (New York, N.Y.)* 370.6516, eabc4209. DOI: 10.1126/science.abc4209.

Kanazawa, Atsuko et al. (2017). "Chloroplast ATP Synthase Modulation of the Thylakoid Proton Motive Force: Implications for Photosystem I and Photosystem II Photoprotection". In: *Frontiers in Plant Science* 8, p. 719. DOI: 10.3389/fpls.2017.00719.

Kato-Yamada, Y. et al. (1999). "Epsilon subunit, an endogenous inhibitor of bacterial F(1)-ATPase, also inhibits F(0)F(1)-ATPase". In: *The Journal of Biological Chemistry* 274.48, pp. 33991–33994. DOI: 10.1074/jbc.274.48.33991.

Kendrew, J. C. et al. (1958). "A three-dimensional model of the myoglobin molecule obtained by x-ray analysis". In: *Nature* 181.4610. Publisher: Nature Publishing Group, pp. 662–666. DOI: 10.1038/181662a0.

Khoshouei, Maryam et al. (2017). "Revisiting the Structure of Hemoglobin and Myoglobin with Cryo-Electron Microscopy". In: *Journal of Molecular Biology* 429.17, pp. 2611–2618. DOI: 10.1016/j.jmb.2017.07.004.

Kirchhoff, Helmut (2019). "Chloroplast ultrastructure in plants". In: *New Phytologist* 223.2, pp. 565–574. DOI: 10.1111/nph.15730.

Kondo, Kumiko et al. (2021). "The phototroph-specific -hairpin structure of the subunit of FoF1-ATP synthase is important for efficient ATP synthesis of cyanobacteria". In: *Journal of Biological Chemistry* 297.3, p. 101027. DOI: 10.1016/j.jbc.2021.101027.

Koonin, Eugene V., Kira S. Makarova, and Feng Zhang (2017). "Diversity, classification and evolution of CRISPR-Cas systems". In: *Current Opinion in Microbiology* 37, pp. 67–78. DOI: 10.1016/j.mib.2017.05.008.

Kramer, David M, Jeffrey A Cruz, and Atsuko Kanazawa (2003). "Balancing the central roles of the thylakoid proton gradient." In: *Trends in plant science* 8.1, pp. 27–32.

Kramer, David M and John R Evans (2011). "The importance of energy balance in improving photosynthetic productivity." In: *Plant physiology* 155.1. Publisher: American Society of Plant Biologists, pp. 70–8. DOI: 10.1104/pp.110.166652.

Krause, G. Heinrich and Peter Jahns (2004). "Non-photochemical Energy Dissipation Determined by Chlorophyll Fluorescence Quenching: Characterization and Function". In: *Chlorophyll a Fluorescence*. Dordrecht: Springer Netherlands, pp. 463–495. DOI: 10.1007/978-1-4020-3218-9_18.

Kufryk, Galyna I et al. (2002). "Transformation of the cyanobacterium Synechocystis sp. PCC 6803 as a tool for genetic mapping: optimization of efficiency". In: *FEMS Microbiology Letters* 206.2, pp. 215–219. DOI: 10.1111/j.1574-6968.2002.tb11012.x.

Kühlbrandt, Werner (2014). "The Resolution Revolution". In: *Science* 343.6178, pp. 1443–1444. DOI: 10.1126/science.1251652.

— (2019). "Structure and Mechanisms of F-Type ATP Synthases". In: *Annual Review of Biochemistry* 88.1. Publisher: Annual Reviews, pp. 515–549. DOI: 10.1146/annurev-biochem-013118-110903.

— (2022). "Forty years in cryoEM of membrane proteins". In: *Microscopy (Oxford, England)* 71 (Supplement_1), pp. i30–i50. DOI: 10.1093/jmicro/dfab041.

Kurisu, Genji et al. (2003). "Structure of the Cytochrome b6f Complex of Oxygenic Photosynthesis: Tuning the Cavity". In: *Science* 302.5647, pp. 1009–1014. DOI: 10.1126/science.1090165.

Laget, Patrice P. and Jeffrey B. Smith (1979). "Inhibitory properties of endogenous subunit  in the Escherichia coli F1 ATPase". In: *Archives of Biochemistry and Biophysics* 197.1, pp. 83–89. DOI: 10.1016/0003-9861(79)90222-4.

Larsson, Anders (2014). "AliView: a fast and lightweight alignment viewer and editor for large datasets". In: *Bioinformatics* 30.22, pp. 3276–3278. DOI: 10.1093/bioinformatics/btu531.

Laubinger, Werner et al. (1990). "A Hybrid Adenosinetriphosphatase Composed of F1 of Escherichia coli and F0 of Propionigenium modestum Is a Functional

Sodium Ion Pump". In: *Biochemistry* 29.23. Publisher: American Chemical Society, pp. 5458–5463. DOI: 10.1021/bi00475a008.

Laughlin, Thomas G. et al. (2019). "Structure of the complex I-like molecule NDH of oxygenic photosynthesis". In: *Nature* 566.7744. Publisher: Nature Publishing Group, pp. 411–414. DOI: 10.1038/s41586-019-0921-0.

Ludwig, Marcus and Donald A. Bryant (2011). "Transcription Profiling of the Model Cyanobacterium Synechococcus sp. Strain PCC 7002 by Next-Gen (SOLiD™) Sequencing of cDNA". In: *Frontiers in Microbiology* 2, p. 41. DOI: 10.3389/fmicb.2011.00041.

Lundin, Arne (2014). "Optimization of the firefly luciferase reaction for analytical purposes". In: *Advances in Biochemical Engineering/Biotechnology* 145, pp. 31–62. DOI: 10.1007/978-3-662-43619-6_2.

Lyumkis, Dmitry et al. (2013). "Likelihood-based classification of cryo-EM images using FREALIGN". In: *Journal of Structural Biology* 183.3. Publisher: Academic Press, pp. 377–388. DOI: 10.1016/J.JSB.2013.07.005.

Matthies, Doreen et al. (2009). "The c13 ring from a thermoalkaliphilic ATP synthase reveals an extended diameter due to a special structural region". In: *Journal of Molecular Biology* 388.3, pp. 611–618. DOI: 10.1016/j.jmb.2009.03.052.

Matzke, Nicholas J. et al. (2021). "Flagellar export apparatus and ATP synthetase: Homology evidenced by synteny predating the Last Universal Common Ancestor". In: *BioEssays* 43.7, p. 2100004. DOI: 10.1002/bies.202100004.

Meier, Thomas and Peter Dimroth (2002). "Intersubunit bridging by Na+ ions as a rationale for the unusual stability of the c-rings of Na+-translocating F1F0 ATP synthases". In: *EMBO reports* 3.11. Publisher: John Wiley & Sons, Ltd, pp. 1094–1098. DOI: 10.1093/embo-reports/kvf216.

Meier, Thomas, José Faraldo-Gómez, and Michael Börsch (2011). "ATP synthase – A paradigmatic molecular machine". In: *Molecular Machines in Biology: Workshop of the Cell*. Ed. by Joachim Frank. Cambridge: Cambridge University Press, pp. 208–238. DOI: 10.1017/CBO9781139003704.013.

Meier, Thomas et al. (2005a). "Structural evidence for a constant c11 ring stoichiometry in the sodium F-ATP synthase". In: *The FEBS journal* 272.21, pp. 5474–5483. DOI: 10.1111/j.1742-4658.2005.04940.x.

Meier, Thomas et al. (2005b). "Structure of the Rotor Ring of F-Type Na+-ATPase from Ilyobacter tartaricus". In: *Science* 308.5722, pp. 659–662. DOI: 10.1126/science.1111199.

Meier, Thomas et al. (2007). "A tridecameric c ring of the adenosine triphosphate (ATP) synthase from the thermoalkaliphilic Bacillus sp. strain TA2.A1 facilitates ATP synthesis at low electrochemical proton potential". In: *Molec-*

*ular Microbiology* 65.5. Publisher: John Wiley & Sons, Ltd, pp. 1181–1192. DOI: 10.1111/j.1365-2958.2007.05857.x.

Merk, Alan et al. (2016). "Breaking Cryo-EM Resolution Barriers to Facilitate Drug Discovery". In: *Cell* 165.7. Publisher: Cell Press, pp. 1698–1707.

Minges, Alexander and Georg Groth (2020). "Chapter Two - Structure and supramolecular architecture of chloroplast ATP synthase". In: *Advances in Botanical Research*. Ed. by Toru Hisabori. Vol. 96. ATP Synthase in Photosynthetic Organisms. Academic Press, pp. 27–74. DOI: 10.1016/bs.abr.2020.07.004.

Mitchell, Peter (1961). "Coupling of Phosphorylation to Electron and Hydrogen Transfer by a Chemi-Osmotic type of Mechanism". In: *Nature* 191.4784. Publisher: Nature Publishing Group, pp. 144–148. DOI: 10.1038/191144a0.

Morales-Rios, Edgar et al. (2015). "Structure of ATP synthase from Paracoccus denitrificans determined by X-ray crystallography at 4.0 Å resolution". In: *Proceedings of the National Academy of Sciences of the United States of America* 112.43. Publisher: National Academy of Sciences, pp. 13231–13236. DOI: 10.1073/pnas.1517542112.

Morel, André and Raymond C. Smith (1974). "Relation between total quanta and total energy for aquatic photosynthesis1: Total quanta and total energy relations". In: *Limnology and Oceanography* 19.4, pp. 591–600. DOI: 10.4319/lo.1974.19.4.0591.

Mühleip, Alexander, Sarah E McComas, and Alexey Amunts (2020). "Structure of a mitochondrial ATP synthase with bound native cardiolipin". In: *eLife* 8, e51179. DOI: 10.7554/eLife.51179.

Mühleip, Alexander et al. (2021). "ATP synthase hexamer assemblies shape cristae of Toxoplasma mitochondria". In: *Nature Communications* 12.1. Publisher: Nature Research. DOI: 10.1038/s41467-020-20381-z.

Müller, Daniel et al. (2001a). "ATP synthase: constrained stoichiometry of the transmembrane rotor". In: *FEBS Letters* 504.3. Publisher: John Wiley & Sons, Ltd, pp. 219–222. DOI: 10.1016/S0014-5793(01)02708-9.

Müller, Patricia, Xiao-Ping Li, and Krishna Niyogi (2001b). "Non-photochemical quenching. A response to excess light energy." In: *Plant physiology* 125.4. Publisher: American Society of Plant Biologists, pp. 1558–66.

Murakami, Satoshi et al. (2018). "Structure of the – complex of cyanobacterial F 1 -ATPase reveals a suppression mechanism of the  subunit on ATP hydrolysis in phototrophs". In: *Biochemical Journal* 475.18. Publisher: Portland Press Ltd, pp. 2925–2939. DOI: 10.1042/BCJ20180481.

Murphy, Bonnie J. et al. (2019). "Rotary substates of mitochondrial ATP synthase reveal the basis of flexible F1-Fo coupling". In: *Science* 364.6446. Publisher: American Association for the Advancement of Science. DOI: 10.1126/science.aaw9128.

Nakahira, Yoichi et al. (2013). "Theophylline-dependent riboswitch as a novel genetic tool for strict regulation of protein expression in Cyanobacterium Synechococcus elongatus PCC 7942". In: *Plant & Cell Physiology* 54.10, pp. 1724–1735. DOI: 10.1093/pcp/pct115.

Nakane, Takanori et al. (2020). "Single-particle cryo-EM at atomic resolution". In: *Nature* 587.7832. Number: 7832 Publisher: Nature Publishing Group, pp. 152–156. DOI: 10.1038/s41586-020-2829-0.

Nakano, Atsuki et al. (2023). "Mechanism of ATP hydrolysis dependent rotation of bacterial ATP synthase". In: *Nature Communications* 14.1. Number: 1 Publisher: Nature Publishing Group, p. 4090. DOI: 10.1038/s41467-023-39742-5.

Naschberger, Andreas et al. (2022). "Algal photosystem I dimer and high-resolution model of PSI-plastocyanin complex". In: *Nature Plants* 8.10. Number: 10 Publisher: Nature Publishing Group, pp. 1191–1201. DOI: 10.1038/s41477-022-01253-4.

Nesterenko, Michael V., Michael Tilley, and Steve J. Upton (1994). "A simple modification of Blum's silver stain method allows for 30 minite detection of proteins in polyacrylamide gels". In: *Journal of Biochemical and Biophysical Methods* 28.3. Publisher: J Biochem Biophys Methods, pp. 239–242. DOI: 10.1016/0165-022X(94)90020-5.

Neumann, Sandra et al. (1998). "Purification and Properties of the F1Fo ATPase of Ilyobacter tartaricus, a Sodium Ion Pump". In: *Journal of Bacteriology* 180.13, pp. 3312–3316.

Nevo, Reinat et al. (2012). "Composition, architecture and dynamics of the photosynthetic apparatus in higher plants". In: *The Plant Journal* 70.1, pp. 157–176. DOI: 10.1111/j.1365-313X.2011.04876.x.

Nikkanen, Lauri et al. (2018). "Regulation of cyclic electron flow by chloroplast NADPH-dependent thioredoxin system". In: *Plant Direct* 2.11, e00093. DOI: 10.1002/pld3.93.

Nilkens, Manuela et al. (2010). "Identification of a slowly inducible zeaxanthin-dependent component of non-photochemical quenching of chlorophyll fluorescence generated under steady-state conditions in Arabidopsis". In: *Biochimica et Biophysica Acta (BBA) - Bioenergetics* 1797.4, pp. 466–475. DOI: 10.1016/j.bbabio.2010.01.001.

Nixon, Peter J., Jeffrey T. Trost, and Bruce A. Diner (1992). "Role of the Carboxy Terminus of Polypeptide D1 in the Assembly of a Functional Water-Oxidizing Manganese Cluster in Photosystem II of the Cyanobacterium Synechocystis sp. PCC 6803: Assembly Requires a Free Carboxyl Group at C-Terminal Position 344". In: *Biochemistry* 31.44. Publisher: American Chemical Society, pp. 10859–10871. DOI: 10.1021/bi00159a029.

Nixon, Peter J. et al. (2010). "Recent advances in understanding the assembly and repair of photosystem II". In: *Annals of Botany* 106.1, pp. 1–16. DOI: 10.1093/aob/mcq059.

Noji, Hiroyuki et al. (1997). "Direct observation of the rotation of F1-ATPase". In: *Nature* 386.6622. Publisher: Nature Publishing Group, pp. 299–302. DOI: 10.1038/386299a0.

Pan, Xiaowei et al. (2020). "Structural basis for electron transport mechanism of complex I-like photosynthetic NAD(P)H dehydrogenase". In: *Nature Communications* 11.1. Number: 1 Publisher: Nature Publishing Group, p. 610. DOI: 10.1038/s41467-020-14456-0.

Phillips, Rob and Ron Milo (2009). "A feeling for the numbers in biology". In: *Proceedings of the National Academy of Sciences of the United States of America* 106.51. Publisher: National Academy of Sciences, pp. 21465–21471. DOI: 10.1073/pnas.0907732106.

Pogoryelov, Denys et al. (2007). "The oligomeric state of c rings from cyanobacterial F-ATP synthases varies from 13 to 15". In: *Journal of Bacteriology* 189.16. Publisher: American Society for Microbiology (ASM) ISBN: 0021-9193 (Print), pp. 5895–5902. DOI: 10.1128/JB.00581-07.

Pogoryelov, Denys et al. (2009). "High-resolution structure of the rotor ring of a proton-dependent ATP synthase". In: *Nature Structural & Molecular Biology* 16.10. Publisher: Nature Publishing Group, pp. 1068–1073. DOI: 10.1038/nsmb.1678.

Pogoryelov, Denys et al. (2012). "Engineering rotor ring stoichiometries in the ATP synthase". In: *Proceedings of the National Academy of Sciences of the United States of America* 109.25. Publisher: National Academy of Sciences, E1599–608. DOI: 10.1073/pnas.1120027109.

Pope, Matthew A., Josh A. Hodge, and Peter J. Nixon (2020). "An Improved Natural Transformation Protocol for the Cyanobacterium Synechocystis sp. PCC 6803". In: *Frontiers in Plant Science* 11.

Preiss, L. et al. (2013). "The c-ring stoichiometry of ATP synthase is adapted to cell physiological requirements of alkaliphilic Bacillus pseudofirmus OF4". In: *Proceedings of the National Academy of Sciences* 110.19, pp. 7874–7879. DOI: 10.1073/pnas.1303333110.

Preiss, Laura et al. (2010). "A new type of proton coordination in an F1Fo-ATP synthase rotor ring". In: *PLoS Biology* 8.8. Publisher: Public Library of Science, pp. 57–58. DOI: 10.1371/journal.pbio.1000443.

Preiss, Laura et al. (2015). "Structure of the mycobacterial ATP synthase Fo rotor ring in complex with the anti-TB drug bedaquiline". In: *Science Advances* 1.4. Publisher: American Association for the Advancement of Science, e1500106. DOI: 10.1126/sciadv.1500106.

Pribil, Mathias, Mathias Labs, and Dario Leister (2014). "Structure and dynamics of thylakoids in land plants". In: *Journal of Experimental Botany* 65.8, pp. 1955–1972. DOI: 10.1093/jxb/eru090.

Rawson, Shaun et al. (2015). "Structure of the vacuolar H+-ATPase rotary motor reveals new mechanistic insights". In: *Structure* 23.3. Publisher: Cell Press, pp. 461–471. DOI: 10.1016/j.str.2014.12.016.

Rosenthal, Peter B. and Richard Henderson (2003). "Optimal Determination of Particle Orientation, Absolute Hand, and Contrast Loss in Single-particle Electron Cryomicroscopy". In: *Journal of Molecular Biology* 333.4, pp. 721–745. DOI: 10.1016/j.jmb.2003.07.013.

Ruffing, Anne M., Travis J. Jensen, and Lucas M. Strickland (2016). "Genetic tools for advancement of Synechococcus sp. PCC 7002 as a cyanobacterial chassis". In: *Microbial Cell Factories* 15.1, p. 190. DOI: 10.1186/s12934-016-0584-6.

Russo, David A. and Julie A. Z. Zedler (2020). "Genomic insights into cyanobacterial protein translocation systems". In: *Biological Chemistry* 402.1, pp. 39–54. DOI: 10.1515/hsz-2020-0247.

Safari, Fatemeh et al. (2019). "CRISPR Cpf1 proteins: structure, function and implications for genome editing". In: *Cell & Bioscience* 9, p. 36. DOI: 10.1186/s13578-019-0298-7.

Saito, Keisuke et al. (2011). "Short hydrogen bond between redox-active tyrosine Y(Z) and D1-His190 in the photosystem II crystal structure". In: *Biochemistry* 50.45, pp. 9836–9844. DOI: 10.1021/bi201366j.

Saroussi, Shai et al. (2012). "Structure and Flexibility of the C-Ring in the Electromotor of Rotary FoF1-ATPase of Pea Chloroplasts". In: *PLoS ONE* 7.9. Publisher: Public Library of Science, e43045. DOI: 10.1371/journal.pone.0043045.

Schägger, Hermann (2006). "Tricine–SDS-PAGE". In: *Nature Protocols* 1.1, pp. 16–22. DOI: 10.1038/nprot.2006.4.

Scheres, Sjors H. W. and Shaoxia Chen (2012). "Prevention of overfitting in cryo-EM structure determination". In: *Nature Methods* 9.9. Number: 9 Publisher: Nature Publishing Group, pp. 853–854. DOI: 10.1038/nmeth.2115.

Schneider, Caroline A., Wayne S. Rasband, and Kevin W. Eliceiri (2012). "NIH Image to ImageJ: 25 years of image analysis". In: *Nature Methods* 9.7, pp. 671–675. DOI: 10.1038/nmeth.2089.

Schulz, Sarah et al. (2017). "Molecular architecture of the N-type ATPase rotor ring from Burkholderia pseudomallei". In: *EMBO reports* 18.4, pp. 526–535. DOI: 10.15252/embr.201643374.

Seelert, H et al. (2000). "Dye-ligand chromatographic purification of intact multisubunit membrane protein complexes: application to the chloroplast H+-FoF1-ATP synthase." In: *The Biochemical journal* 346 Pt 1, pp. 41–4.

Shibato, Junko, Munehiko Asayama, and Makoto Shirai (1998). "Specific recognition of the cyanobacterial psbA promoter by RNA polymerases containing principal sigma factors". In: *Biochimica et Biophysica Acta (BBA) - Gene Structure and Expression* 1442.2, pp. 296–303. DOI: 10.1016/S0167-4781(98)00149-3.

Shikanai, Toshiharu (2016). "Chloroplast NDH: A different enzyme with a structure similar to that of respiratory NADH dehydrogenase". In: *Biochimica et Biophysica Acta (BBA) - Bioenergetics*. SI: Respiratory Complex I 1857.7, pp. 1015–1022. DOI: 10.1016/j.bbabio.2015.10.013.

Shikanai, Toshiharu and Hiroshi Yamamoto (2017). "Contribution of Cyclic and Pseudo-cyclic Electron Transport to the Formation of Proton Motive Force in Chloroplasts". In: *Molecular Plant* 10.1. Publisher: Cell Press, pp. 20–29. DOI: 10.1016/J.MOLP.2016.08.004.

Shmakov, Sergey et al. (2017). "Diversity and evolution of class 2 CRISPR-Cas systems". In: *Nature Reviews. Microbiology* 15.3, pp. 169–182. DOI: 10.1038/nrmicro.2016.184.

Sigworth, F.J. (1998). "A Maximum-Likelihood Approach to Single-Particle Image Refinement". In: *Journal of Structural Biology* 122.3, pp. 328–339. DOI: 10.1006/jsbi.1998.4014.

Silverstein, Todd P. (2014). "An exploration of how the thermodynamic efficiency of bioenergetic membrane systems varies with c-subunit stoichiometry of F1F0 ATP synthases". In: *Journal of Bioenergetics and Biomembranes* 46.3. Publisher: Springer New York LLC, pp. 229–241. DOI: 10.1007/s10863-014-9547-y.

Smith, P K et al. (1985). "Measurement of protein using bicinchoninic acid". In: *Analytical Biochemistry* 150.1, pp. 76–85. DOI: 10.1016/0003-2697(85)90442-7.

Sobti, Meghna, Robert Ishmukhametov, and Alastair G. Stewart (2020a). "ATP Synthase: Expression, Purification, and Function". In: *Protein Nanotechnology: Protocols, Instrumentation, and Applications*. Ed. by Juliet A. Gerrard and Laura J. Domigan. Methods in Molecular Biology. New York, NY: Springer US, pp. 73–84. DOI: 10.1007/978-1-4939-9869-2_5.

Sobti, Meghna et al. (2019). "Cryo-EM reveals distinct conformations of E. coli ATP synthase on exposure to ATP". In: *eLife* 8. Publisher: eLife Sciences Publications Ltd. DOI: 10.7554/eLife.43864.

Sobti, Meghna et al. (2020b). "Cryo-EM structures provide insight into how E. coli F1Fo ATP synthase accommodates symmetry mismatch". In: *Nature Communications* 11.1. Number: 1 Publisher: Nature Publishing Group, p. 2615. DOI: 10.1038/s41467-020-16387-2.

Song, Kuo et al. (2022). "Atp is an inhibitor of F0F1 ATP synthase to arrest ATP hydrolysis during low-energy conditions in cyanobacteria". In: *Current biology: CB* 32.1, 136–148.e5. DOI: 10.1016/j.cub.2021.10.051.

Spikes, Tobias E., Martin G. Montgomery, and John E. Walker (2020). "Structure of the dimeric ATP synthase from bovine mitochondria". In: *Proceedings of the National Academy of Sciences of the United States of America* 117.38. Publisher: National Academy of Sciences, pp. 23519–23526. DOI: 10.1073/pnas.2013998117.

Staehelin, L. Andrew and Marcia DeWit (1984). "Correlation of structure and function of chloroplast membranes at the supramolecular level". In: *Journal of Cellular Biochemistry* 24.3, pp. 261–269. DOI: 10.1002/jcb.240240307.

Stewart, Alastair G et al. (2013). "Rotary ATPases: models, machine elements and technical specifications." In: *Bioarchitecture* 3.1. Publisher: Taylor & Francis, pp. 2–12. DOI: 10.4161/bioa.23301.

Stock, Daniela, Andrew G.W. Leslie, and John E Walker (1999). "Molecular architecture of the rotary motor in ATP synthase". In: *Science* 286.5445. Publisher: American Association for the Advancement of Science, pp. 1700–1705. DOI: 10.1126/science.286.5445.1700.

Sturr, M. G., A. A. Guffanti, and T. A. Krulwich (1994). "Growth and bioenergetics of alkaliphilic Bacillus firmus OF4 in continuous culture at high pH". In: *Journal of Bacteriology* 176.11, pp. 3111–3116. DOI: 10.1128/jb.176.11.3111-3116.1994.

Sunamura, Ei-Ichiro et al. (2010). "Physiological impact of intrinsic ADP inhibition of cyanobacterial FoF1 conferred by the inherent sequence inserted into the gammasubunit". In: *Plant & Cell Physiology* 51.6, pp. 855–865. DOI: 10.1093/pcp/pcq061.

Suzuki, Toshiharu et al. (2007). "The product of uncI gene in F1Fo-ATP synthase operon plays a chaperone-like role to assist c-ring assembly". In: *Proceedings of the National Academy of Sciences of the United States of America* 104.52. Publisher: National Academy of Sciences, pp. 20776–20781. DOI: 10.1073/pnas.0708075105.

Swarts, Daan C. and Martin Jinek (2019). "Mechanistic Insights into the cis- and trans-Acting DNase Activities of Cas12a". In: *Molecular Cell* 73.3, 589–600.e4. DOI: 10.1016/j.molcel.2018.11.021.

Tabita, F. Robert (1994). "The Biochemistry and Molecular Regulation of Carbon Dioxide Metabolism in Cyanobacteria". In: *The Molecular Biology of Cyanobacteria*. Ed. by Donald A. Bryant. Advances in Photosynthesis. Dordrecht: Springer Netherlands, pp. 437–467. DOI: 10.1007/978-94-011-0227-8_14.

Takagi, Daisuke et al. (2017). "Chloroplastic ATP synthase builds up a proton motive force preventing production of reactive oxygen species in photosystem

I". In: *The Plant Journal: For Cell and Molecular Biology* 91.2, pp. 306–324. DOI: 10.1111/tpj.13566.

Tan, Yong Zi et al. (2022). "Structure of V-ATPase from citrus fruit". In: *Structure* 30.10. Publisher: Elsevier, 1403–1410.e4. DOI: 10.1016/j.str.2022.07.006.

To, Minh-Son et al. (2010). "Mitochondrial uncoupler FCCP activates proton conductance but does not block store-operated Ca(2+) current in liver cells". In: *Archives of Biochemistry and Biophysics* 495.2, pp. 152–158. DOI: 10.1016/j.abb.2010.01.004.

Tongra, Teena, Sudhakar Bharti, and Anjana Jajoo (2014). "Cyclic electron flow around photosystem I is enhanced at low pH". In: *Plant Physiology and Biochemistry* 83. Publisher: Elsevier Masson, pp. 194–199. DOI: 10.1016/J.PLAPHY.2014.08.002.

Tsirigotaki, Alexandra et al. (2017). "Protein export through the bacterial Sec pathway". In: *Nature Reviews. Microbiology* 15.1, pp. 21–36. DOI: 10.1038/nrmicro.2016.161.

Ungerer, Justin and Himadri B. Pakrasi (2016). "Cpf1 Is A Versatile Tool for CRISPR Genome Editing Across Diverse Species of Cyanobacteria". In: *Scientific Reports* 6.1. Publisher: Nature Publishing Group, p. 39681. DOI: 10.1038/srep39681.

Vik, S. B. and B. J. Antonio (1994). "A mechanism of proton translocation by F1F0 ATP synthases suggested by double mutants of the a subunit". In: *The Journal of Biological Chemistry* 269.48, pp. 30364–30369.

Viola, Stefania et al. (2019). "Probing the electric field across thylakoid membranes in cyanobacteria". In: *Proceedings of the National Academy of Sciences of the United States of America* 116.43. Publisher: National Academy of Sciences, pp. 21900–21906. DOI: 10.1073/pnas.1913099116.

Vlasov, A. V. et al. (2019). "Unusual features of the c-ring of F1FO ATP synthases". In: *Scientific Reports* 9.1, p. 18547. DOI: 10.1038/s41598-019-55092-z.

Vonck, Janet et al. (2009). "Three-dimensional structure of A1A0 ATP synthase from the hyperthermophilic archaeon Pyrococcus furiosus by electron microscopy". In: *Journal of Biological Chemistry* 284.15. Publisher: Elsevier, pp. 10110–10119. DOI: 10.1074/jbc.M808498200.

Vries, Jan de and John M. Archibald (2017). "Endosymbiosis: Did Plastids Evolve from a Freshwater Cyanobacterium?" In: *Current Biology* 27.3, R103–R105. DOI: 10.1016/j.cub.2016.12.006.

Walker, J.E. et al. (1982). "Distantly related sequences in the alpha- and beta-subunits of ATP synthase, myosin, kinases and other ATP-requiring enzymes and a common nucleotide binding fold." In: *The EMBO Journal* 1.8. Pub-

lisher: John Wiley & Sons, Ltd, pp. 945–951. DOI: 10.1002/j.1460-2075.1982.tb01276.x.

Walker, John E. (2013). "The ATP synthase: The understood, the uncertain and the unknown". In: *Biochemical Society Transactions* 41.1, pp. 1–16. DOI: 10.1042/BST20110773.

Watt, Ian N et al. (2010). "Bioenergetic cost of making an adenosine triphosphate molecule in animal mitochondria". In: *Proceedings of the National Academy of Sciences of the United States of America* 107.39. Publisher: National Academy of Sciences, pp. 16823–16827. DOI: 10.1073/pnas.1011099107.

Wendt, Kristen E. et al. (2016). "CRISPR/Cas9 mediated targeted mutagenesis of the fast growing cyanobacterium Synechococcus elongatus UTEX 2973". In: *Microbial Cell Factories* 15.1. Publisher: BioMed Central, p. 115. DOI: 10.1186/s12934-016-0514-7.

Werner, Sabine, Jürgen Schumann, and Heinrich Strotmann (1990). "The primary structure of the -subunit of the ATPase from Synechocystis 6803". In: *FEBS Letters* 261.1. _eprint: https://onlinelibrary.wiley.com/doi/pdf/10.1016/0014-5793%2890%2980671-5, pp. 204–208. DOI: 10.1016/0014-5793(90)80671-5.

Wietrzynski, Wojciech et al. (2020). "Charting the native architecture of chlamydomonas thylakoid membranes with single-molecule precision". In: *eLife* 9. Publisher: eLife Sciences Publications Ltd. DOI: 10.7554/eLife.53740.

Włodarczyk, Artur et al. (2020). "Newly discovered Synechococcus sp. PCC 11901 is a robust cyanobacterial strain for high biomass production". In: *Communications Biology* 3.1. Publisher: Nature Research, pp. 1–14. DOI: 10.1038/s42003-020-0910-8.

Wolosiuk, Ricardo A. and Bob B. Buchanan (1977). "Thioredoxin and glutathione regulate photosynthesis in chloroplasts". In: *Nature* 266.5602. Number: 5602 Publisher: Nature Publishing Group, pp. 565–567. DOI: 10.1038/266565a0.

Wu, Shenping, Jean Paul Armache, and Yifan Cheng (2016). "Single-particle cryo-EM data acquisition by using direct electron detection camera". In: *Microscopy* 65.1. Publisher: Oxford University Press, pp. 35–41. DOI: 10.1093/jmicro/dfv355.

Yagi, Hiromasa et al. (2007). "Structures of the thermophilic F1-ATPase subunit suggesting ATP-regulated arm motion of its C-terminal domain in F1". In: *Proceedings of the National Academy of Sciences* 104.27. Publisher: Proceedings of the National Academy of Sciences, pp. 11233–11238. DOI: 10.1073/pnas.0701045104.

Yagi, Hiromasa et al. (2009). "Structural and functional analysis of the intrinsic inhibitor subunit of F1-ATPase from photosynthetic organisms". In: *Biochemical Journal* 425.1, pp. 85–98. DOI: 10.1042/BJ20091247.

Yamamoto, Hiroshi et al. (2023). "Impact of engineering the ATP synthase rotor ring on photosynthesis in tobacco chloroplasts". In: *Plant Physiology*, kiad043. DOI: 10.1093/plphys/kiad043.

Yamori, Wataru and Toshiharu Shikanai (2016). "Physiological Functions of Cyclic Electron Transport Around Photosystem I in Sustaining Photosynthesis and Plant Growth". In: *Annual Review of Plant Biology* 67.1. Publisher: Annual Reviews, pp. 81–106. DOI: 10.1146/annurev-arplant-043015-112002.

Yang, Jay-How et al. (2020). "Structural basis of redox modulation on chloroplast ATP synthase". In: *Communications Biology* 3.1. Publisher: Nature Publishing Group, p. 482. DOI: 10.1038/s42003-020-01221-8.

Yoshida, M. et al. (1975). "A highly stable adenosine triphosphatase from a thermophillie bacterium. Purification, properties, and reconstitution". In: *The Journal of Biological Chemistry* 250.19, pp. 7910–7916.

Yoshida, M. et al. (1979). "Subunit structure of adenosine triphosphatase. Comparison of the structure in thermophilic bacterium PS3 with those in mitochondria, chloroplasts, and Escherichia coli". In: *The Journal of Biological Chemistry* 254.19, pp. 9525–9533.

Zavafer, Alonso et al. (2015). "Photodamage to the oxygen evolving complex of photosystem II by visible light". In: *Scientific Reports* 5.1. Number: 1 Publisher: Nature Publishing Group, p. 16363. DOI: 10.1038/srep16363.

Zetsche, Bernd et al. (2015). "Cpf1 Is a Single RNA-Guided Endonuclease of a Class 2 CRISPR-Cas System". In: *Cell* 163.3, pp. 759–771. DOI: 10.1016/j.cell.2015.09.038.

Zhang, Heng et al. (2019). "Structural Basis for the Inhibition of CRISPR-Cas12a by Anti-CRISPR Proteins". In: *Cell Host & Microbe* 25.6. Publisher: Elsevier, 815–826.e4. DOI: 10.1016/j.chom.2019.05.004.

Zhang, Wei et al. (2008). "Heterogeneity of Large Macromolecular Complexes Revealed by 3D Cryo-EM Variance Analysis". In: *Structure* 16.12, pp. 1770–1776. DOI: 10.1016/j.str.2008.10.011.

Zhao, Jianhua, Samir Benlekbir, and John L. Rubinstein (2015). "Electron cryomicroscopy observation of rotational states in a eukaryotic V-ATPase". In: *Nature* 521.7551. Publisher: Nature Publishing Group, pp. 241–245. DOI: 10.1038/nature14365.

Zhu, Jiapeng, Kutti R. Vinothkumar, and Judy Hirst (2016). "Structure of mammalian respiratory complex I". In: *Nature* 536.7616. Number: 7616 Publisher: Nature Publishing Group, pp. 354–358. DOI: 10.1038/nature19095.